

UC Santa Barbara

UC Santa Barbara Electronic Theses and Dissertations

Title

Synthesis and Application of Photochromic Organic Small Molecules

Permalink

<https://escholarship.org/uc/item/8ct8n9zk>

Author

Hemmer, James

Publication Date

2017

Peer reviewed|Thesis/dissertation

UNIVERSITY OF CALIFORNIA

Santa Barbara

Synthesis and Application of Photochromic Organic Small Molecules

A dissertation submitted in partial satisfaction of the
requirements for the degree Doctor of Philosophy
in Chemistry

by

James Robert Hemmer

Committee in charge:

Professor Javier Read de Alaniz, Chair

Professor Craig J. Hawker

Professor Trevor Hayton

Professor Armen Zakarian

December 2017

The dissertation of James Robert Hemmer is approved.

Craig J. Hawker

Trevor Hayton

Armen Zakarian

Javier Read de Alaniz, Committee Chair

December 2017

Synthesis and Application of Photochromic Organic Small Molecules

Copyright © 2017

by

James Robert Hemmer

ACKNOWLEDGEMENTS

First and foremost I would like to thank my advisor, Javier Read de Alaniz. He has taught me so much about how to be a better scientist, how to be optimistic, and especially how to make presentations. He has always been available to talk when I want to discuss my research. He has also been very adaptable by allowing for me to take on a research project that was far outside the scope of his background of synthetic methodology. He was able to offer excellent insight into problems far outside of his field.

I would also like to thank my mentors from the DOD research labs, Brian Mason and Joe Hooper. They funded at least three years of my graduate school, and we have co-authored several papers together. They have both been mentors for me throughout my graduate school career. Brian even flew to UCSB to work directly with me several times in the beginning of graduate school to help me in the lab. Joe's family has been a second family to me in California, and I have spent several Thanksgivings there. They have also greatly assisted me in getting a post-doc, and in fact I'll be working for Brian directly. The support from both of them has been phenomenal.

The senior group members, Chuck Fraiser, Don Wenz, Gesine Viets, Leoni Palmer, Sam Helmy, David Sandoval, Nic Treat, and Robert Lewis greatly assisted me in my early years and helped to improve my lab technique. Senior group member and post-docs Nic Treat and Zak Paige pushed me to publish my results and greatly helped think about how to develop a paper. They also greatly assisted me with my experiments. The other group members my year, David Fisher and Saemi Oh, have been great friends both in and out of lab and have helped me in lab and in class. Also, for the new students, Jamie, Kyle, Andre, Meghan, Yvonne, for being good friends after everyone else had graduated. Especially to Kyle Clark, for his help with the acceptor project.

We have had a few foreign students rotate through our lab, and they have all been both great friends and collaborators. First, Søren Broman, the Danish exchange student who was both a great friend and mentor. He helped me through my first year in graduate school and show me many lab techniques. Sebastian Ulrich, the German exchange student from EMPA, who collaborated with me directly on the polymer DASA project. He was extremely helpful when I went to Switzerland, and he fostered many great discussions about our research. Fritz Stricker, an exchange student from Mainz, Germany. He is a great scientist and friend, and an incredibly dedicated hard worker. He greatly assisted me in the acceptor project.

Other graduate students in the have been great friends, including Bi Nguyen, Tracy Chuong, Ryan Barnes, Zack Jones, Annie Lamontagne, and Mareike Adams. They are responsible for most of the good times outside of the lab.

Finally, my parents have been extremely supportive. My mother, Anne Hemmer, and father Philip Hemmer. My father, a PhD in physics, has always pushed me to go to graduate school. They both have pushed me to do well in school throughout my life, and they are the reason I'm here.

VITA OF JAMES ROBERT HEMMER

August 2017

EDUCATION

Bachelor of Science in Chemistry, Texas A&M University, May 2012 (Magna Cum Laude)
Doctor of Philosophy in Chemistry, University of California, Santa Barbara, September 2017
(expected)

PROFESSIONAL EMPLOYMENT

Graduate Student Assistant, University of California, Santa Barbara, CA.
August 2012 - September 2017

Visiting Researcher, EMPA, St. Gallen, Switzerland.
June 2016- July 2016

Research Assistant, Naval Post-Graduate School, Monterey, CA.
June 2012 – July 2012

Intern, Naval Research Enterprise Internship Program (NREIP), Indian Head, MD.
June 2010 – August 2010, June 2011 – August 2011

Undergraduate Researcher, Texas A&M University, College Station, TX.
January 2009 – December 2011

PUBLICATIONS

Ulrich, S.; **Hemmer, J. R.**; Page, Z. A.; Dolinski, N. D.; Rifaie-Graham, O.; Bruns, N.; Hawker, C. J.; Boesel, L. F.; Read de Alaniz, J. “*Visible Light-Responsive DASA-Polymer Conjugates.*” *ACS Macro Letters*, **2017**, 6, 738–742.

Diaz, Y. J.; Page, Z. A.; Knight, A. S.; Treat, N. J.; **Hemmer, J. R.**; Hawker, C. J.; Read de Alaniz, J. “*A Versatile and Highly Selective Colorimetric Sensor for the Detection of Amines*” *Chem. Eur. J.* **2017**, 23, 3562.

Hemmer, J. R.; Poelma, S. O.; Treat, N.; Page, Z. A.; Dolinski, N. D.; Diaz, Y. J.; Tomlinson, W.; Clark, K. D.; Hooper, J. P.; Hawker, C.; Read de Alaniz, J. “*Tunable Visible and Near Infrared Photoswitches.*” *J. Am. Chem. Soc.* **2016**, 138, 13960–13966.

Mason, B. P.; Wittaker, M.; **Hemmer, J. R.**; Arora, S.; Harper, A.; Alnemrat, S.; McEachen, A.; Helmy, S.; Read de Alaniz, J.; Hooper, J. P. “*A temperature-mapping molecular sensor for polyurethane-based elastomers*” *Appl. Phys. Lett.* **2016**, 108, 041906

van Horn, M.; Smith, P.; Mason, B. P.; **Hemmer, J. R.**; Read de Alaniz, J.; Hooper, J. P.; Osswald, S. “*Optical characterization and confocal fluorescence imaging of mechanochromic acrylate polymers*” *J. Appl. Phys.*, **2015**, 117, 43103.

Hemmer, J. R., Smith, P. D., van Horn, M., Alnemrat, S., Mason, B. P., de Alaniz, J. R., Osswald, S. and Hooper, J. P. “*High Strain-Rate Response of Spiropyran Mechanophores in PMMA*” *J. Polym. Sci. Part B Polym. Phys.* **2014**, 52, 1347-6.

Durán-Galván, M.; **Hemmer, J. R.**; Connell, B. T. “*Synthesis of tertiary 1,3-butadien-2-ylcarbinols from chromium-catalyzed addition of (4-bromobut-2-ynyl)trimethylsilane to ketones*” *Tetrahedron Lett.*, **2010**, 51, 5080–5082.

AWARDS

Poster, Materials Research Outreach Program Symposium 2015
High Strain-Rate Response of Spiropyran Mechanophores in PMMA

ABSTRACT

Synthesis and Application of Color Changing Organic Small Molecules

by

James Robert Hemmer

Photochromic small molecules have long been of interest for their ability to translate small changes at the atomic level into an easily identified visual color change. These compounds allow the use of stimuli such as light or heat to cause a change in the conformation and thus the size and polarity of a molecule. In the reverse, they allow for changes such as heat and mechanical stress to be easily visualized at the macroscopic level through a color change. The general concept and background of these photo- and thermochromic molecules will be introduced. The synthesis and properties of two privileged classes of photochromic molecules, spiropyrans and donor-acceptor Stenhouse adducts (DASAs) will be discussed. These two compounds will be used extensively in the research in this dissertation. Next, the use of these compounds for sensing stress at high strain rates will be examined. Then the synthesis of novel DASAs with highly tunable absorption profiles will be discussed, along with their properties. This will be followed by a highly modular approach to the incorporation of DASAs into acrylate polymers.

TABLE OF CONTENTS

Chapter 1: Introduction	1
1.1 History and definitions.....	1
1.2 Common classes of photochromic molecules.....	2
1.3 Visible light activated azobenzenes	6
1.4 DASAs	10
1.5 Work by Read de Alaniz.....	12
1.6 References.....	17
Chapter 2: Small molecule sensors for high strain rate events	21
2.1 Introduction.....	21
2.2 Synthesis	24
2.3 High strain rate testing	29
2.4 Thermochromic compounds for high strain rate studies.....	33
2.5 DASA-HTPB thermochromic polymer synthesis.....	35
2.6 Testing of DASA-HTPB thermochromic polymer	37
2.7 Experimental.....	40
2.8 References.....	48
Chapter 3: DASAs with aniline based donors	51
3.1 Introduction.....	51
3.2 Synthesis	54
3.3 Properties	57
3.4 Wavelength tunability.....	57
3.5 DASA photoswitching properties.....	59

3.6 Solvent and polymer photoswitching.....	61
3.7 Conclusion	67
3.8 Tables of Aniline DASA properties:.....	67
3.9 Experimental	70
3.10 References.....	84
Chapter 4: DASAs covalently bound to polymers	87
4.1 Introduction.....	87
4.2 DASA polymer synthetic approach.....	90
4.3 Small molecule synthesis	91
4.4 Polymer functionalization	92
4.5 DASA polymer photoswitching properties	94
4.6 Experimental	99
4.7 References.....	105
Chapter 5: Novel acceptors for DASAs	108
5.1 Introduction.....	108
5.2 Carbon acid acceptor design	112
5.3 Functional carbon acids	114
5.3 Characterization	116
5.4 Experimental	119
5.4 References.....	125

Figure 1.1: Nitro-spiropyran photoswitch, with its highly polar open form shown on the right.	2
Figure 1.2: Diarylethene photoswitch. These are very thermally stable, and able to exist in either state for years at room temperature.....	3
Figure 1.3: Azobenzene photoswitch.....	4
Figure 1.4: Light penetration of tissue by wavelength.....	5
Figure 1.5: Visible light photoswitching BF ₂ azobenzene	6
Figure 1.6: BF ₂ azobenzene with electron donating substituents.	7
Figure 1.7 <i>Ortho</i> fluoro azobenzenes.....	8
Figure 1.8: <i>Ortho</i> -amino azobenzenes.....	9
Figure 1.9: <i>Ortho</i> methoxy azobenzenes that absorb in the visible.	9
Figure 1.10: Basic Structure of DASA. The open triene form on the left can cyclize to the closed cyclopentenone form in the presence of light, and reverts to its original composition thermodynamically.	10
Figure 1.11: Synthesis of Stenhouse salts. Two equivalents of aniline are combined with furfural and an equivalent of Bronstead acid.	11
Figure 1.12: Synthesis of DASA by Safar.	11
Figure 1.13: Methods of cyclizing the triene to the cyclopentenone.	12
Figure 1.14: Synthesis of furan adducts in water from furfural and a carbon acid.	13
Figure 1.15: Synthesis of DASAs with various secondary amines.....	14
Figure 1.16: Absorption spectra of DASAs with different acceptors. Reprinted with permission from (44). Copyright (2014) American Chemical Society."	15
Figure 2.1: Upon application of mechanical force to the polymer chains, the mechanophore changes its structure.....	21

Figure 2.2: (a) Spiropyran, a photoswitch which can transform between yellow and red colored states. (b) Spiropyran mechanophore, with a spiropyran polymer attachment points. These allow the mechanical force to be transferred across the spiro C-O bond, and the molecule to go into its open form using mechanical force. (c) Bulk polymer embedded with spiropyran mechanophore changes color after force is applied..22

Figure 2.3: General scheme of spiropyran mechanophore synthesis. The appropriate hydroxyl functionalized indolenine and benzaldehyde are condensed to form a spiropyran. The spiropyran is then acylated with a group to provide polymer attachment.....24

Figure 2.4: Hydroxy benzaldehyde synthesis from *o*-Vanillin.25

Figure 2.5: Indolenine fragment synthesis from methoxy phenylhydrazine.25

Figure 2.6: Synthesis of difunctional spiropyran.26

Figure 2.7: Synthesis of the monofunctional control. (a) Moore's original control. (b) Failed attempt at making an acyl protected control. (c) The pivyl group proved to be more robust and gave the desired spiropyran.27

Figure 2.8: Synthesis of a linear acrylate polymer to create spiropyran mechanophore at center of a polymer chain.....28

Figure 2.9: Spiroyrans used in testing.....29

Figure 2.10: Hopkinson bar, an instrument which allows for high strain rate testing of materials.....30

Figure 2.11: Results of impact testing on spiropyran mechanophores and controls embedded in PMMA. (a) Activation occurs in active mechanophore and monofunctional control. (b) Static testing shows that both the active mechanophore and monofunctional control are thermally active, while the difunctional control is not.....31

Figure 2.12: Fluorescence microscopy of the surface of a fragment of a monofunctional control sample (left) and an active mechanophore sample (right). The colors correspond to fluorescence intensity. Though widespread activation is seen both samples, the mechanophore sample seems to show enhanced activation in microcracks. Reprinted with permission from (14). Copyright (2014) Wiley.32

Figure 2.13: HTPB pre-polymer, left, is cured with a diisocyanate to form an elastomer. 34

Figure 2.14: Attempts of using thermochromic molecules in HTPB. (a) spirooxazine, which quickly reconverts to its closed form at room temperature. (b) A Diels-Alder adduct that was inactive at high strain rates.34

Figure 2.15: Basic structure of DASA. It is thermodynamically stable in the open colored form, and visible light can cause it to cyclized into a colorless form.35

Figure 2.16: Synthesis of the closed form of dioctylamine DASA.....36

Figure 2.17: Static testing of HTPB DASA. (a) DASA activates when heated in an oven. (b) Kinetics of DASA activation in HTPB. Reprinted with permission from (19). Copyright (2016) Applied Physics Letters.37

Figure 2.18: High strain rate testing of HTPB with embedded DASA. (a) Frames from a high speed camera, showing activation at the edges of the material forced out. (b) View of the sample before and after the test, showing localized activation.38

Figure 2.19: Bullet impact of DASA/HTPB. (a) Moment before bullet impact. (b) Sample post impact. (c) Larger sample post impact, showing bullet path. (d) Cross section of sample, showing approximate temperatures reached. Reprinted with permission from (19). Copyright (2016) Applied Physics Letters.39

Figure 3.1: Upon light irradiation, the triene form of the DASA undergoes an *E/Z* isomerization. The *Z* triene can then undergo a 4π electrocyclization to yield the closed cyclopentenone form.52

Figure 3.2: General structure of the second generation of DASAs. The open triene form is shown on the left, and the cyclized cyclopentenone form on the right. The various colors shown on the left are dependent on the donor aniline used. Reprinted with permission from (22). Copyright (2016) American Chemical Society.53

Figure 3.3: General synthesis scheme for aniline based DASAs with Meldrum’s or barbituric acid acceptors. Reagents and conditions; (i) H₂O (ii) aniline derivative, neat, THF, DCM, or MeOH. Reprinted with permission from (22). Copyright (2016) American Chemical Society.54

Figure 3.4: Normalized absorption profile for DASAs with barbituric acid acceptor and a range of aniline donors. Reprinted with permission from (22). Copyright (2016) American Chemical Society.....57

Figure 3.5: Comparing dihedral angles (from DFT calculations) of NMA to indoline donors. The relatively large dihedral angle present in DASAs with the NMA donor reduces the absorption wavelength and reduces the effect of electron donating groups have on the absorption. Reprinted with permission from (22). Copyright (2016) American Chemical Society.....58

Figure 3.6: Closing kinetics of *N*-methylaniline donor barbituric acid acceptor DASAs at 4 different temperatures. The Arrhenius plot is shown in the insert. Reprinted with permission from (22). Copyright (2016) American Chemical Society.60

Figure 3.7: Left: sample of a single switching cycle. The light irradiation period is shaded yellow. Right: Cycling study show up to 200 cycles. Reprinted with permission from (22). Copyright (2016) American Chemical Society.	61
Figure 3.8: Comparison of photoswitching of dialkyl DASAs to aniline DASAs in a range of four solvents. Diethylamine DASA (top) only exhibits photoswitching only in toluene, while aniline DASA photoswitches in toluene, THF, methylene chloride, and acetonitrile. Reprinted with permission from (22). Copyright (2016) American Chemical Society.....	62
Figure 3.9: Photoswitching of three barbituric acid aniline DASAs drop cast each with three different acrylate polymers. Reprinted with permission from (22). Copyright (2016) American Chemical Society.....	63
Figure 3.10: Selective photoswitching of two mixed DASAs, <i>N</i> -methylaniline Meldrum's acid 13 and indoline barbituric acid 11 using filtered broadband white LED. Compounds 11 and 13 were mixed in toluene followed by photoswitching through a 514 nm bandpass filter to cyclize 13 or a 650 nm long-pass filter to cyclize 11. Reprinted with permission from (22). Copyright (2016) American Chemical Society.	64
Figure 3.11: Selective switching of DASA in dropcast PMMA film. Reprinted with permission from (22). Copyright (2016) American Chemical Society.	66
Figure 4.1: Acrylate functionalization of azobenzene and spiropyran photoswitches. The acrylate group is highlighted with a red box.	87
Figure 4.2: Attempts to co-polymerize DASA with acrylates. (a) Unstable triene degrades in radical conditions. (b) Unstable alkene degrades in polymerization conditions..	88
Figure 4.3: Pentafluorophenyl ester conjugation chemistry. The reaction is highly selective to primary amines.....	89

Figure 4.4: General scheme of polymer bound DASA synthesis. First, primary amine functionalized aniline is reacted with the polymer. The aniline functionalized polymer then reacts with a furan adduct to yield DASA.....90

Figure 4.5: Synthesis of primary amine functionalized anilines: a) solvent free Buchwald coupling to give MPDP b) triethylsilane reduction of tryptamine91

Figure 4.6: Monitoring the displacement of pentafluoropenol by ¹⁹F NMR. Adapted with permission from (21). Copyright (2017) American Chemical Society.92

Figure 4.7: Poly methylacrylate functionalized with four different DASAs. a) UV/Vis absorption spectrum. b) Samples spun coat onto glass slides, showing both open and closed states. Adapted with permission from (21). Copyright (2017) American Chemical Society.....95

Figure 4.8: Matrix T_g effects on DASA switching. (a) Structures of the open and closed DASA functionalized polymers. (b) Thermal equilibrium at 40°C, showing faster equilibration for DASAs with polymer T_g below 40°C. (c) DASA/poly(ethyl methacrylate) (parent T_g=65°C) being heated to 60°C, showing a rapid absorption increase on heating. (d) Effect of T_g on photocyclization. DASA polymers at temperatures below their parent T_g are slower to photocyclize. Adapted with permission from (21). Copyright (2017) American Chemical Society.96

Figure 4.9: (a) Selective cyclization of rTryp/barbituric acid polymer with 617 nm light. (b) Selective switching of rTryp/barbituric, then both rTryp/barbituric and MPDP/Meldrum's polymer with spatial control using a photomask. Adapted with permission from (21). Copyright (2017) American Chemical Society.98

Figure 5.1: Basic structure and properties of the Donor Acceptor Stenhouse Adduct (DASA).

Visible light causes the DASA to isomerize, which is followed by a cyclization to the closed form.....108

Figure 5.2. Carbazole and indole donors are unable to ring open the furan adduct...110

Figure 5.3: (a) A carbon acid (Meldrums acid) is condensed with furfural to create a furan adduct. This is reacted with an amine to yield a DASA. (b) Early failed attempts at using other carbon acids.113

Figure 5.4: Left, Meldrum's and barbituric acid. Right, acidic acceptors that fail to produce DASAs.114

Figure 5.5: Carbon acids that can be used as acceptors to make DASAs.114

Figure 5.6: Carbon acids chosen for the acceptor study. From left to right, methyl isoxazolone, CF₃ isoxazolone, CF₃ pyrazolone, pyrazolidinedione, hydroxypyridone, and indanedione.115

Figure 5.7: Absorption spectra of various acceptors with 2-methylindoline donor...117

Figure 5.8: Percent open DASAs of various acceptors with 2-methylindoline donors.118

Chapter 1: Introduction

1.1 History and definitions

The history of organic photochromic compounds dates back to 1867 when Fritzsche¹ observed that an orange solution of tetracene became colorless during the day, and that the color would return upon standing in the dark overnight. Other early reports included the change of dinitroethane from red to orange in 1899.² Although other photochromic molecules were reported, it was not until the 1960's when good spectroscopic analytical techniques became readily available that the study of organic photochromic molecules took off. Since then there have been thousands of papers describing the synthesis, properties, and applications of photochromic organic molecules.³

In a simple sense, photochromism is the changing of color upon exposure to light. Formally, photochromism is defined as a “reversible transformation of a chemical species induced in one or both directions by absorption of electromagnetic radiation between two forms, **A** and **B**, having different absorption spectra”.⁴ Here, the **A** form is the thermodynamically stable form, and it is converted into the metastable **B** form with light irradiation. Generally, photochromic compounds absorb blue or UV light in a colorless or yellow **A** form to yield red, purple, or blue **B** form. Upon visible light irradiation (**P** type photochromism) or thermal relaxation (**T** type photochromism), they revert from the **B** form back to the **A** form. When the **A** form has a longer wavelength than the **B** form, the resulting system is known as an “inverse” or “negative” photochrome.⁴

As a photochromic compound changes from one isomer to another a number of its properties can change, including size, shape, polarity, absorption, and fluorescence. Due to

the ability to externally control microscopic properties with spatial and temporal control, photoswitches have been an area of prolific study. Research into photoswitches has explored applications such as delivering drugs⁵⁻⁷, memory storage⁸⁻¹⁰, sensors¹¹⁻¹³, and logic gates¹⁴ to name a few.

1.2 Common classes of photochromic molecules

While numerous types of photoswitches have been developed over the years, a privileged few have been studied and applied more than any of the others. These classes of compounds have become well known because of their robustness, ease of synthesis, bright color change, or simply that they have been around a long time. The three most widely used photochromic compounds that will be discussed here are: spiropyran, diarylethene, and azobenzene.

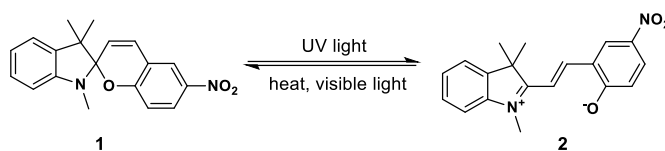


Figure 1.1: Nitro-spiropyran photoswitch, with its highly polar open form shown on the right.

Spiroyrans are a popular class of photochromic compounds. Countless derivatives with different substituents have been synthesized.¹⁵ The basic structure common in the most widely used spiropyran is shown in figure 1.1. The thermodynamically stable spiropyran form, shown on the left, can undergo photoisomerization into the merocyanine form, shown on the right. The merocyanine form absorbs strongly in the visible, creating a bright color ranging from red through purple to blue, depending on the spiropyran derivative and the solvent environment. Due to the very visible color change, change in size, and change in

polarity, the spiropyran follows the azobenzene as one of the most widely used photoswitching compounds.¹⁶

One property of spiropyran that is often utilized is the large polarity change between the open and closed form. The closed form is a non-polar organic molecule. The open form, on the other hand, is far more polar compound and can even exist in a zwitterionic form.¹⁷ In the most simple application, the polarity and water contact angle of surfaces has been altered by irradiating a spiropyran functionalized polymer.^{18,19} Here, UV light irradiation causes the formation of the more polar merocyanine form which in turn reduces the water contact angle of water droplets on the surface of a polymer. In other cases, spiropyrans containing polymers or dendrimers can be used to create micelles in water. Here, the spiropyran makes up the non-polar part of the micelle. When the solution is irradiated with UV light, the spiropyran becomes highly polar, and the micelle is disrupted.^{20,21}

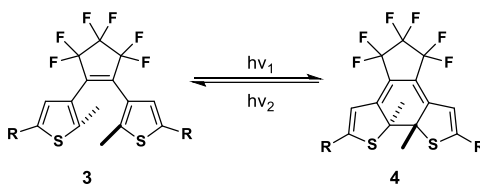


Figure 1.2: Diarylethene photoswitch. These are very thermally stable, and able to exist in either state for years at room temperature.

Diarylethenes are another class of photochromic material (Figure 1.2). They have highly desirable properties not often found in other photoswitches. They can be easily designed so that they are thermally stable in either form. A sample can be irradiated to induce cyclization, and the cyclized form will be stable for months even at elevated temperature in the dark. Upon light irradiation, the reverse reaction will occur.²² Almost all other photochromic compounds exhibit at least some thermochromatic behavior. Second, diarylethenes have very

high fatigue resistance. Normally photoswitches degrade after cycling 20 or 30 times between open and closed forms. However, diarylethenes have been made that can last thousand of cycles. These two features have made diarylethenes very attractive candidates for data storage, where information can be recorded read by using only light. Much of the work of with diarylethenes has focused in this area.^{23,24}

Azobenzenes (Figure 1.3) are photoswitches which are able to undergo an *E-Z* isomerization under light irradiation, with the reverse isomerization happening with a second wavelength or under thermodynamic control. They were discovered in the 19th century and are among the oldest photoswitches. Initially azobenzene derivatives were widely studied for their use as dyes.²⁵ It would take nearly another century after their first synthesis before their photochromic properties were observed.^{26,27} The photochromism of azobenzene was first discovered in 1937 by Hartley²⁸, and since then it has become the most widely studied photochromic system.

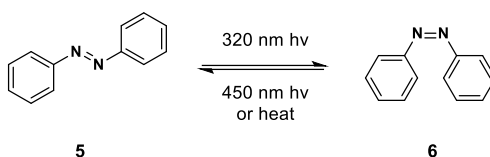


Figure 1.3: Azobenzene photoswitch.

Under UV light irradiation, the *trans* form of azobenzene isomerizes to the *cis* form (Figure 1.3). *Trans* azobenzene typically has a strong absorption from the π - π^* transition in the UV part of the spectrum, and a weak n - π^* absorption in the visible. When the π - π^* is irradiated, the molecule converts into the *cis* form. The *cis* form has a weaker π - π^* transition and a stronger n - π^* , at similar wavelengths. The increase in the absorbance of the visible light n - π^* causes the color to change. Since the π - π^* transition still exists in the *cis* form, it is

not normally possible to drive the azobenzene completely into the *cis* form, as UV irradiation also converts the *cis* back into the *trans*. Typically, 80% of the *cis* form can be obtained with irradiation. This amount of the photoswitch that can isomerize under light is known as the photostationary state.²⁹

Because they are well studied, are relatively chemically stable, and photoswitch in a variety of solvents, azobenzenes have been used applications too numerous to be fully discuss here. There are several reviews^{6,30,31} and books^{32,33} that cover some of the applications of azobenzenes. Some examples will be given to demonstrate the versatility of azobenzenes. Azobenzenes can be incorporated into thin liquid crystal polymer networks. When light hits these thin strips of polymer, the contraction from the isomerization causes one side of the polymer to contract. This in bends the polymer, and in this way light can be converted to mechanical work.^{34,35} Azobenzenes can also be attached to drugs and antibodies to modulate their activity in the body.⁵ This can allow for drugs that only activate in a specific part of an organism, and to only activate when irradiated with light.

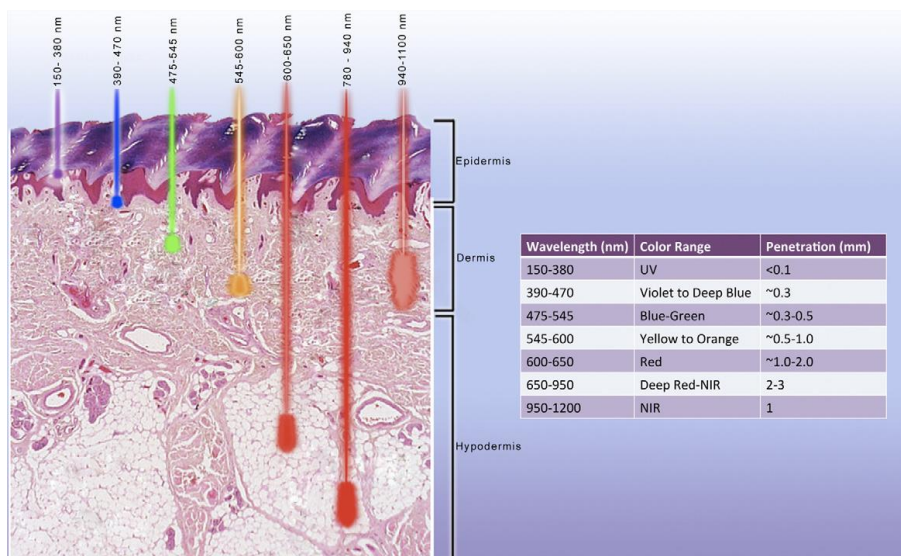


Figure 1.4: Light penetration of tissue by wavelength

1.3 Visible light activated azobenzenes

One major limitation of the use of azobenzenes and any other photoswitch in biological systems is that they generally require UV light to photoisomerize. This is problematic, as the penetration depth of UV light through tissue is very low (< 1.0 mm) (Figure 1.4). Visible light (1-2 mm penetration) or near IR (2-3 mm penetration) are far more suitable to use in a biological setting.³⁶ Because of this, efforts have been made to synthesize azobenzenes that will isomerize with visible or near IR light.³⁷ Early approaches made donor-acceptor azobenzenes, where an electron donating group is placed on one ring of the azobenzene, and an electron withdrawing group is placed on the other ring. These gave visible light absorbing azobenzenes, but the isomerization rates become very high, and the half-life drops to less than microseconds.²⁹ Such a short half-life requires very intense light to get an appreciable amount of the photoswitch into the photostationary state. Several other approaches to red-shifting the absorption wavelength have yielded more success and retained the desirable characteristics of azobenzene. Some of these synthetic approaches include: boron coordination, *ortho* withdrawing substituents, *ortho* donating substituents.

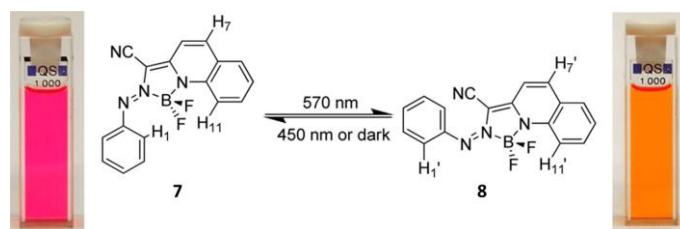


Figure 1.5: Visible light photoswitching BF₂ azobenzene

Aprahamian found that azobenzene coordinated with boron was thermodynamically stable in the *cis* isomer (Figure 1.5).³⁸ It absorbs light at 530 nm, and upon 570 nm irradiation it photosomerizes to the *cis* isomer to the *trans* isomer, which gives an orange color with a

480 nm λ_{\max} . DFT calculations showed that coordination of the BF_2 with the azo lone pairs raised the energy for the $\pi\text{-}\pi^*$ transition and lowers it for the $n\text{-}\pi^*$. This is a reversal of the energy levels typical in azobenzene. The result is that the $\pi\text{-}\pi^*$ transitions now occur at energies that correspond to visible light. Additionally, the half-life of the *trans* isomer was found to be 12.5 hours, which was a significant improvement over the microseconds observed in push pull systems.

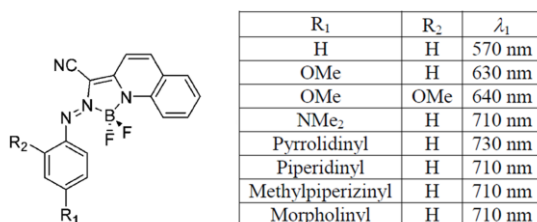


Figure 1.6: BF_2 azobenzene with electron donating substituents.

Encouraged by these preliminary azobenzene BF_2 compounds, Aprahamian set out to investigate a variety of azobenzene BF_2 derivatives.³⁹ These kept the same basic structure as the previously reported BF_2 azobenzene, but incorporated electron donating functionalization on the phenyl ring (Figure 1.6). These gave photoswitches with very long absorbing wavelengths, even passing 700 nm λ_{\max} , and have good half lives in the range of minutes to hours. Less appealing is that the absorption wavelengths for both the *cis* and *trans* forms are quite similar, meaning that for the blue compounds both forms have the same blue color. Additionally, these compounds hydrolyze in water over a few hours, which limits their application in biological settings.

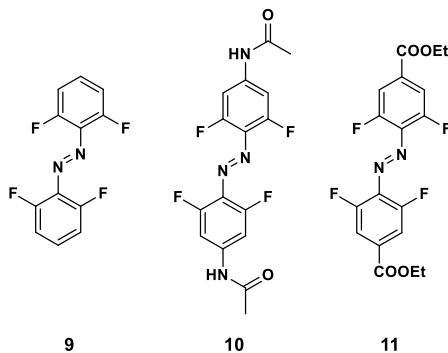


Figure 1.7 *Ortho* fluoro azobenzenes.

Another approach explored by Hecht is the use of electron withdrawing fluoro atoms at the ortho positions.⁴⁰ The strategy was to reduce the electron density of the N=N bond to separate the $n\text{-}\pi^*$ transitions. With distinct $n\text{-}\pi^*$ transitions, visible light photoswitching could be achieved. Indeed they discovered that they could synthesize ortho fluoroazobenzene (**9**), and that the $n\text{-}\pi^*$ bands were sufficiently separated (44 nm) to allow for visible light photoswitching in the region of 450 nm. Further, this compound had a very thermally stable *Z* form with a half-life of over 300 days. Derivatives **10** and **11** were also synthesized. The electron withdrawing group's role in separating the $n\text{-}\pi^*$ transitions was confirmed by these derivatives. Electron donating **2** showed a $n\text{-}\pi^*$ separation of only 22 nm, while the additional electron donating groups in **3** gave separation of 50 nm. However, since the $n\text{-}\pi^*$ are being used, they are much weaker than the $\pi\text{-}\pi^*$ transitions, which means that the ortho fluoro azobenzenes have low molar absorptivities of around 2-3000 $\epsilon(\text{M}^{-1}\text{cm}^{-1})$.

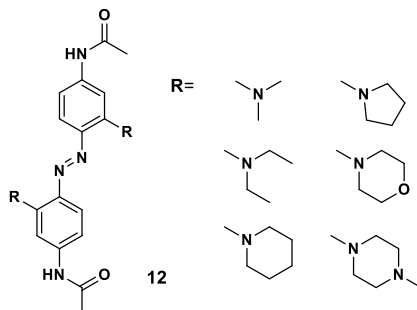


Figure 1.8: *Ortho*-amino azobenzenes.

The Woolley lab achieved visible light switching azobenzenes through another route: use of ortho donating groups. Initially, a number of ortho amino azobenzene derivatives were synthesized (Figure 1.8).⁴¹ The addition of these ortho donating groups gave absorptions with maxima from 435 to 513 nm. The longest wavelength absorbing compounds were those R groups that had a nitrogen most ready to donate electrons. The piperidyl derivative gave the longest wavelength, and the piperizyl gave the shortest wavelength. The stability of the *trans* form followed the opposite trend: the less electron rich amines gave the most stable *trans* forms. The half-lives on these compounds ranged from a few seconds for the electron rich amines, to a few minutes for the electron poor amines.

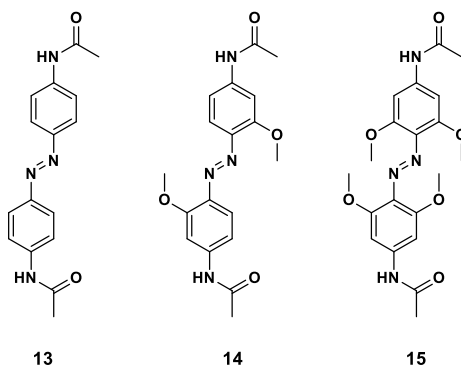


Figure 1.9: Ortho methoxy azobenzenes that absorb in the visible.

Looking to improve the ortho amino azobenzenes, the Woolley group set out to synthesize electron donating azobenzenes with other substituents. The addition of two methoxy groups on each ring lead to red-shifting of the trans $n-\pi^*$ bands and a blue shifting of the cis $n-\pi^*$ bands, giving a 36 nm separation between the two.⁴² This allowed for an 80% conversion into the cis form with 540 nm irradiation. This compound displayed a respectable half life of 1.5 hours.

While there have been great advances with azobenzene, there are still a number of drawbacks. For example, they require very careful control of the wavelength of light used, they often have low molar absorptivities, and they can be difficult to synthesize. Therefore, there is reason to develop new visible light photoswitches. One novel class of photochromic compounds that exhibits long wavelength absorption are Donor Acceptor Stenhouse Adducts (DASAs).

1.4 DASAs

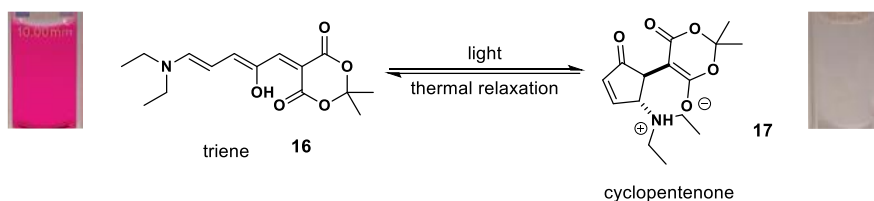


Figure 1.10: Basic Structure of DASA. The open triene form on the left can cyclize to the closed cyclopentenone form in the presence of light, and reverts to its original composition thermodynamically.

DASAs as photoswitches were discovered in group of Read de Alaniz in 2014.^{43,44} The basic structure of this photoswitch is shown in figure 1.10. DASAs have a brightly

colored, highly conjugated open triene form, and a colorless cyclopentenone form. The closed form is far more polar than the open form and exists as a zwitterion when basic secondary amines are used. Light can be used to drive the triene form into the closed cyclopentenone form, and this can thermally relax back into the triene form. Since only one wavelength of light can control this process, DASAs are exclusively T-type photochromic systems.

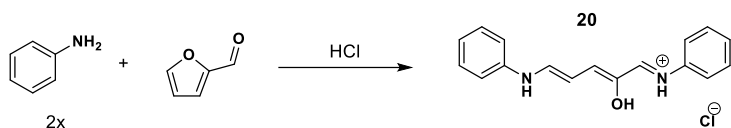


Figure 1.11: Synthesis of Stenhouse salts. Two equivalents of aniline are combined with furfural and an equivalent of Bronstead acid.

While the DASA is a newly discovered photochromic system, its origins date back into the 18th century. In 1870, John Stenhouse discovered that a brightly colored dye could be made by mixing two equivalents of aniline with one equivalent of furfural and one equivalent of acid (Figure 1.11).⁴⁵ Stenhouse salts were studied extensively as dyes, and early on it was noticed that there were difficulties in measuring a good absorption spectrum.⁴⁶ However, it was not until 1980 that Honda discovered that Stenhouse salts were photochromic.⁴⁷ Honda showed that several aniline Stenhouse salts exhibited reverse photochromic behavior in alcoholic solvents. Despite this initial discovery, no additional work on the photochromic nature of Stenhouse salts was performed by Honda or any other group.

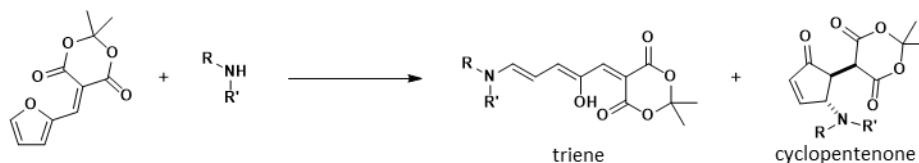


Figure 1.12: Synthesis of DASA by Safar.

In 1999, Safar demonstrated that the Knoevenagel adduct of furfural and Meldrum's acid would react with secondary amines to form a highly conjugated product.⁴⁸ The product of the reaction was dependent on the amine used (Figure 1.12). If pyrrolidine or hexahydroazepine were used, exclusively the triene was formed. However, if piperidine or morpholine are used, a mixture of the triene and cyclopentenone are formed. This occurred regardless of reaction temperature or solvent. The authors noted that selectivity for the product formed may be a “function of the basicity of the amine used”, with more basic amines giving exclusively the triene.

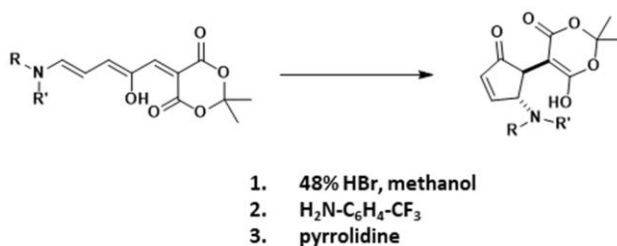


Figure 1.13: Methods of cyclizing the triene to the cyclopentenone.

In examining the reactivity of the triene, Safar noticed that there were a number of conditions that could cyclize the triene to the cyclopentenone form (Figure 1.13). First, heating in methanol with strong mineral acid would bring about rapid cyclization. Second, heating with an electron deficient aniline or with pyrrolidine would bring about cyclization. Though Safar studied the chemistry and reactivity of these compounds, he paid little attention to the color changing properties, and did not make any mention of any photoswitching properties.

1.5 Work by Read de Alaniz

In 2014 our group reported in two papers the synthesis and photoswitching properties of these DASA compounds. First, it was shown that the starting furan adducts could be made

from either Meldrum's or Barbituric acid in furfural in water by adapting a method pioneered by Sartori (Figure 1.14).⁴⁹ In both of these syntheses, it is possible to isolate the product in good yield through simple filtration, and without additional purification steps.

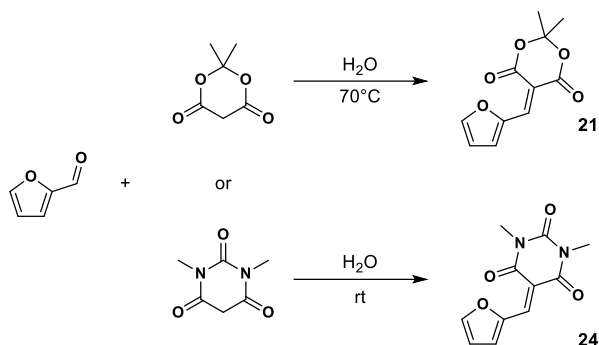


Figure 1.14: Synthesis of furan adducts in water from furfural and a carbon acid.

Next, the Meldrum's or barbituric acid furan adducts could be combined with a range of secondary amines in good yield (Figure 1.15). To run the reaction, the furan adduct is dissolved in THF, then the second amine is added. The reaction immediately turns deep red in the case of Meldrum's acid, or deep purple in the case of barbituric acid. Soon after the addition of the amine, a solid begins to precipitate out, and is isolated by filtration. In the cases where the product is not a solid, purification is performed with column chromatography, eluting with methylene chloride, then methylene chloride and methanol. The chromatography is simplified due to the fact that both the furan adduct starting material and product DASA are easily visualized on the silica as bright yellow and bright red bands, respectively.

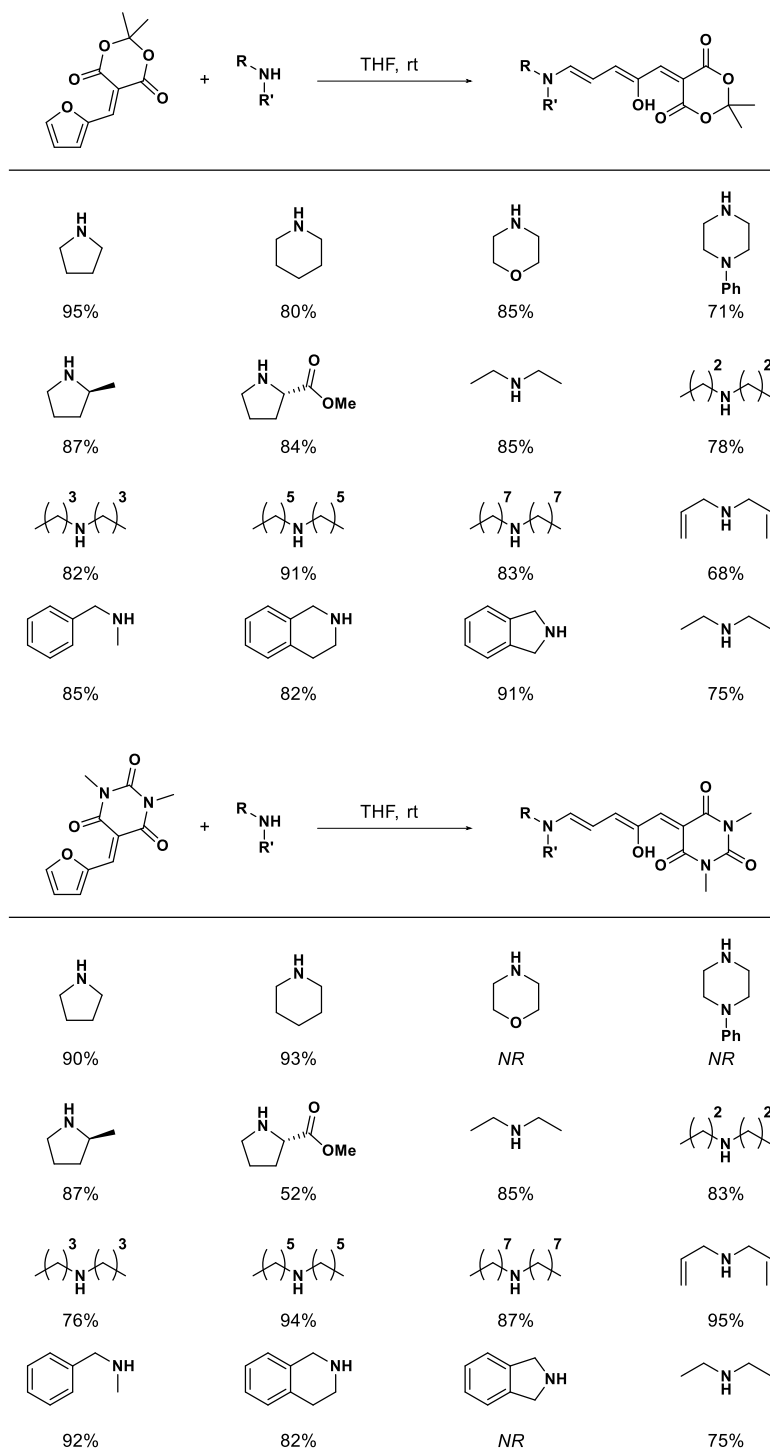


Figure 1.15: Synthesis of DASAs with various secondary amines.

In addition to the open triene form, the cyclized cyclopentenone form can be isolated as crystalline solid for some derivatives. This is achieved by running the reaction in methanol

overnight, and then filtering the resulting solid. The open DASAs can also be transformed into the closed form by stirring in methanol under light, or heating in a polar solvent such as acetonitrile with a nucleophilic catalyst, such as triphenyl phosphine. These closed form DASAs are essential to the thermochromic systems that will be discussed later.

DASA's generally reside in the open form in relatively polar solvents that are not miscible with water, such as methylene chloride and chloroform. They are also largely in the open form in solvents such as acetone, ethyl acetate, and THF. In polar solvents such as methanol, ethanol, or water, the DASAs convert over a period of hours into the closed, zwitterionic form. In non-polar solvents, such as toluene, benzene, or hexanes, the DASAs exist in what is most likely a mixture of open and closed. The open closed ration of secondary amine DASAs in these solvents has not been yet measured. Most importantly, in these non-polar solvents, photoswitching can be observed.

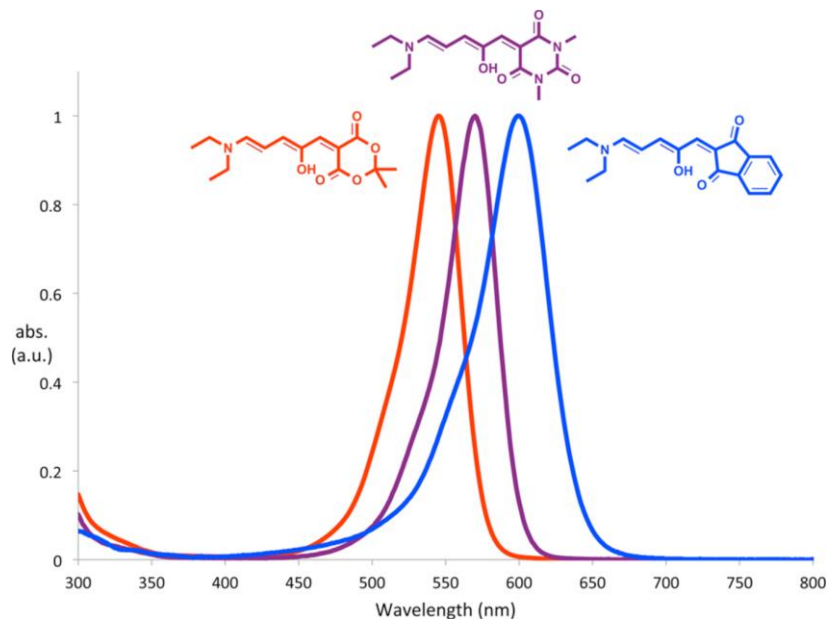


Figure 1.16: Absorption spectra of DASAs with different acceptors. Reprinted with permission from (44). Copyright (2014) American Chemical Society."

The absorption profile of DASA compounds can be tuned by altering the acceptor moiety (Figure 1.16). In methylene chloride, Meldrum's acid based DASAs absorb at 538 nm, barbituric acid at 568 nm, and indanedione at 600 nm. However, to date there has been no evidence of photoswitching with the indanedione derivative. Thus, the wavelengths of a photoswitching for alkyl DASAs are limited to ~540 nm and ~ 570 nm, depending on which acceptor is used. Using any of the different donor amines in figure 1.15 has no effect on the absorption wavelength. This severely limits the wavelength tunability of dialkyl DASAs.

DASAs provide a novel platform for visible light photochromism. They are easy to synthesize, have large changes in polarity from open to closed, and have high molar absorptivities. Despite these advantageous properties, they are not without limitations. For example, they have only reversibly switch in non-polar aromatic solvents, they are unable to reversible switch in polymer or solid matrix, and have limited absorption wavelength tunability. These limitations are addressed with the second generation of DASAs (Chapter 3).

1.6 References

- (1) Fritzsche, J. *Sci. Paris* **1867**, 69 (1035), 78.
- (2) ter Meer, E. *Justus Liebigs Ann. Chem.* **1876**, 181 (1), 1.
- (3) *Photomechanical Materials, Composites, and Systems*; White, T. J., Ed.; John Wiley & Sons, Ltd, 2017.
- (4) BOUAS-LAURENT, H.; DÜRR, H. **2001**, 73 (4), 639.
- (5) Velema, W. A.; Szymanski, W.; Feringa, B. L. *J. Am. Chem. Soc.* **2014**, 136 (6), 2178.
- (6) Broichhagen, J.; Frank, J. A.; Trauner, D. *Acc. Chem. Res.* **2015**, 48 (7), 1947.
- (7) Petriashvili, G.; Devadze, L.; Zurabishvili, T.; Sepashvili, N.; Chubinidze, K. *Biomed. Opt. Express* **2016**, 7 (2), 442.
- (8) Fukaminato, T.; Doi, T.; Tamaoki, N.; Okuno, K.; Ishibashi, Y.; Miyasaka, H.; Irie, M. *J. Am. Chem. Soc.* **2011**, 133 (13), 4984.
- (9) Majumdar, D.; Lee, H. M.; Kim, J.; Kim, K. S.; Mhin, B. J. *J. Chem. Phys.* **1999**, 111 (13), 5866.
- (10) Feringa, B. L.; Jager, W. F.; de Lange, B. *Tetrahedron* **1993**, 49 (37), 8267.
- (11) Xie, X.; Mistlberger, G.; Bakker, E. *J. Am. Chem. Soc.* **2012**, 134 (41), 16929.
- (12) Qin, M.; Huang, Y.; Li, F.; Song, Y. *J. Mater. Chem. C* **2015**, 3 (36), 9265.
- (13) Abdollahi, A.; Alinejad, Z.; Mahdavian, A. R. *J. Mater. Chem. C* **2017**, 5 (26), 6588.
- (14) Andréasson, J.; Pischel, U. *Chem. Soc. Rev.* **2015**, 44 (5), 1053.
- (15) Zakhs, É. R.; Martynova, V. M.; Éfros, L. S. *Chem. Heterocycl. Compd.* **1979**, 15 (4), 351.
- (16) Klajn, R. *Chem. Soc. Rev.* **2014**, 43 (1), 148.
- (17) Burke, K.; Riccardi, C.; Buthelezi, T. *J. Phys. Chem. B* **2012**, 116 (8), 2483.

- (18) Hayashida, S.; Sato, H.; Sugawara, S. *Polymer Journal*. 1986, pp 227–235.
- (19) Rosario, R.; Gust, D.; Hayes, M.; Jahnke, F.; Springer, J.; Garcia, A. A. *Langmuir* **2002**, *18* (21), 8062.
- (20) Son, S.; Shin, E.; Kim, B. *Biomacromolecules* **2014**, *15*, 628.
- (21) Niu, Y.; Li, Y.; Lu, Y.; Xu, W.; Xia, X. N.; Lu, Y. B.; Ji, J.; Cheng, J. J.; Ren, J.; Cheng, J. J. *RSC Adv.* **2014**, *4* (102), 58432.
- (22) Irie, M. *Diarylethenes for Memories and Switches*; 2000; Vol. 100.
- (23) Irie, M.; Fukaminato, T.; Matsuda, K.; Kobatake, S. *Chem. Rev.* **2014**, *114* (24), 12174.
- (24) Tsujioka, T.; Kondo, H. *Appl. Phys. Lett.* **2003**, *83* (5), 937.
- (25) Venkataraman, K. (Krishnasami). *The chemistry of synthetic dyes.*; Academic Press, 1952.
- (26) Mitscherlich. *Ann. der Pharm.* **1834**, *12* (2–3), 311.
- (27) Noble, A. *Justus Liebigs Ann. Chem.* **1856**, *98* (2), 253.
- (28) Hartley, G. S. *Nature* **1937**, *140* (3537), 281.
- (29) Bandara, H. M. D.; Burdette, S. C. *Chem. Soc. Rev.* **2012**, *41* (5), 1809.
- (30) Mart, R. J.; Allemann, R. K. *Chem. Commun.* **2016**, *52* (83), 12262.
- (31) Sudesh, G.; Road, T. B.; Sciences, P.; Green, B. **1989**, No. 48, 1915.
- (32) *Smart Light-Responsive Materials: Azobenzene-Containing Polymers and Liquid Crystals*; Wiley-Interscience, 2009.
- (33) Watson, L. E. *Azobenzene: Aspects, Applications and Research (Chemistry Research and Applications)*; Nova Science Publishers, Inc., 2017.
- (34) Lee, K. M.; Smith, M. L.; Koerner, H.; Tabiryan, N.; Vaia, R. A.; Bunning, T. J.; White, T. J. *Adv. Funct. Mater.* **2011**, *21* (15), 2913.

- (35) Iamsaard, S.; Abhoff, S. J.; Matt, B.; Kudernac, T.; Cornelissen, J. J. L. M.; Fletcher, S. P.; Katsonis, N. *Nat. Chem.* **2014**, *6* (3), 229.
- (36) Avci, P.; Gupta, A.; Sadasivam, M.; Vecchio, D.; Pam, Z.; Pam, N.; Hamblin, M. R. *Semin. Cutan. Med. Surg.* **2013**, *32* (1), 41.
- (37) Wegner, H. A. *Angew. Chemie - Int. Ed.* **2012**, *51* (20), 4787.
- (38) Yang, Y.; Hughes, R. P.; Aprahamian, I. *J. Am. Chem. Soc.* **2012**, *134* (37), 15221.
- (39) Yang, Y.; Hughes, R. P.; Aprahamian, I. *J. Am. Chem. Soc.* **2014**, *136*, 13190.
- (40) Bléger, D.; Schwarz, J.; Brouwer, A. M.; Hecht, S. *J. Am. Chem. Soc.* **2012**, *134* (51), 20597.
- (41) Sadovski, O.; Beharry, A. A.; Zhang, F.; Woolley, G. A. *Angew. Chemie - Int. Ed.* **2009**, *48* (8), 1484.
- (42) Beharry, A. A.; Sadovski, O.; Woolley, G. A. *J. Am. Chem. Soc.* **2011**, *133* (49), 19684.
- (43) Helmy, S.; Leibfarth, F. A.; Oh, S.; Poelma, J. E.; Hawker, C. J.; Read De Alaniz, J. J. *J. Am. Chem. Soc.* **2014**, *136* (23), 8169.
- (44) Helmy, S.; Oh, S.; Leibfarth, F. A.; Hawker, C. J.; Read De Alaniz, J. J. *Org. Chem.* **2014**, *79* (23), 11316.
- (45) Stenhouse, J. *Justus Liebigs Ann. Chem.* **1870**, *156* (2), 197.
- (46) Lewis, K. G.; Mulquiney, C. E. *Tetrahedron* **1977**, *33* (5), 463.
- (47) Honda, K.; Komizu, H.; Kawasaki, M. *J. Chem. Soc. Chem. Commun.* **1982**, No. 4, 253.
- (48) ŠAFÁŘ, P.; POVAŽANEC, F.; PRÓNAYOVÁ, N.; BARAN, P.; KICKELBICK, G.; KOŽÍŠEK, J.; BREZA, M. *Collect. Czech. Chem. Commun.* **2000**, *65*, 1911.
- (49) Bigi, F.; Carloni, S.; Ferrari, L.; Maggi, R.; Mazzacani, A.; Sartori, G. *Tetrahedron*

Lett. **2001**, 42 (31), 5203.

Chapter 2: Small molecule sensors for high strain rate events

2.1 Introduction

Strain and temperature sensing in polymers is of great importance in materials such as solid rocket motors, armor, and explosive formulations. Impact events can lead to small scale temperature rises that can cause catastrophic failure.^{1,2} Understanding how shock affects both the structure and local temperature of materials is critical to engineering better materials. Unfortunately, these events are difficult or even impossible to observe due to the short (microseconds) time scale involved at the event.³ We believe that small molecular sensors embedded in the materials could be used to better understand how high strain rate events affect them. They could give detailed information about what is happening on the microscale in terms of strain and temperature through an easy to visualize color change. The implications of such a sensor could have effects on fields ranging from impact monitoring on helmets to improved explosive safety testing techniques.

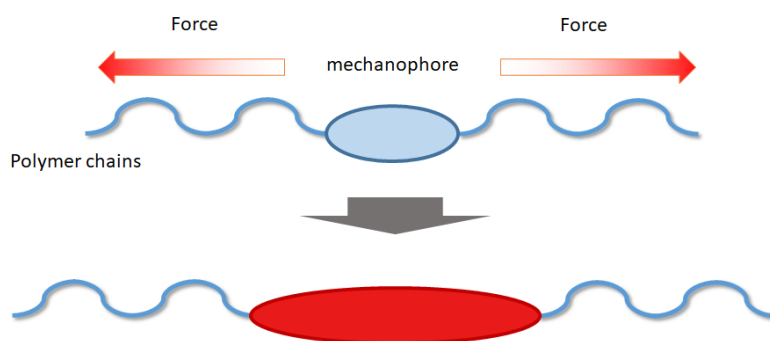


Figure 2.1: Upon application of mechanical force to the polymer chains, the mechanophore changes its structure.

When we began this investigation, no small molecule high-strain rate sensors existed. However, there has been a recent interest in the study of mechanophores, which are small

molecules that transform in response to mechanical force. Mechanophores are connected to a polymer at two points, and when mechanical force is applied to the polymer backbone, a weak bond selectively breaks to cause a change in molecular structure (Figure 2.1).⁴ This concept has been applied to allow the use of mechanical force to activate catalysts,^{5,6} cause classically forbidden chemical transformations,⁷ and generate reactive intermediates such as radicals⁸ and acids.⁹ Initially, these mechanophores were activated by dissolving them in solution and exposing them to high energy ultrasound. In 2009 this changed when the Moore group showed that mechanical force could activate a mechanophore in a bulk polymer.¹⁰

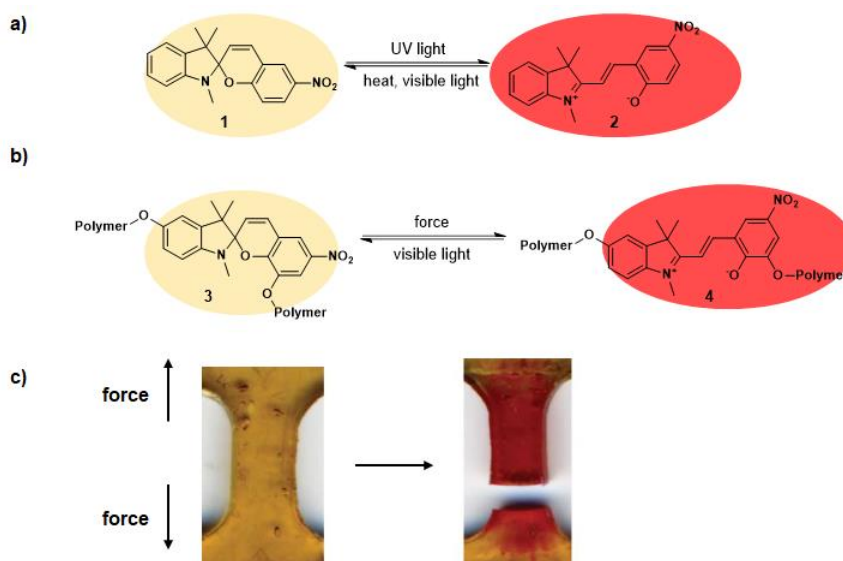


Figure 2.2: (a) Spiropyran, a photoswitch which can transform between yellow and red colored states. (b) Spiropyran mechanophore, with a spiropyran polymer attachment points. These allow the mechanical force to be transferred across the spiro C-O bond, and the molecule to go into its open form using mechanical force. (c) Bulk polymer embedded with spiropyran mechanophore changes color after force is applied.

For their solid matrix studies, the Moore group chose the spiropyran as their mechanophore. Spiropyran is a well known photoswitch, with a yellow closed spiropyran

form that can convert into a purple merocyanine form with UV light (Figure 2.2a). With proper polymer attachment, mechanical force can be transferred across the C-O spiro bond, causing it to rupture (Figure 2.2b). This converts the spiropyran into the brightly colored merocyanine, but with force rather than UV light. The Moore group synthesized spiropyran in the middle of a PMA chain as well as a cross-linker in PMMA beads. In both cases, mechanical force on the bulk polymer caused a visible color change in the bulk material (Figure 2.2c).

With the ability to sense mechanical strain to give a visible color change, the spiropyran mechanophore seemed like a potentially useful tool for gaining information about microscale strain in a bulk polymer. The Moore group has studied the spiropyran mechanophore extensively. They have found that in order to activate as a mechanophore, the spiropyran must to be properly aligned on the axis of force.¹¹ They also found that the glassiness of the matrix played an important role, as very glassy polymer would break before mechanophore alignment could occur, and there is no activation.¹² Additionally, strain rate was shown to be important, as lower strain rate gives the molecules more chance to align and leads to higher levels of activation.¹³

We had initial doubts as to whether or not the spiropyran mechanophore would activate at all at high strain rates. The short time scales did not give time for the polymers to orient in the direction of applied force, which is important for activation. Still, we thought that the overwhelming force of a high strain rate event could show some activation. In order to investigate whether a mechanophore would function at all in a high strain rate environment, we set out to reproduce Moore's spiropyran, but to subject it to impact testing.¹⁴

2.2 Synthesis

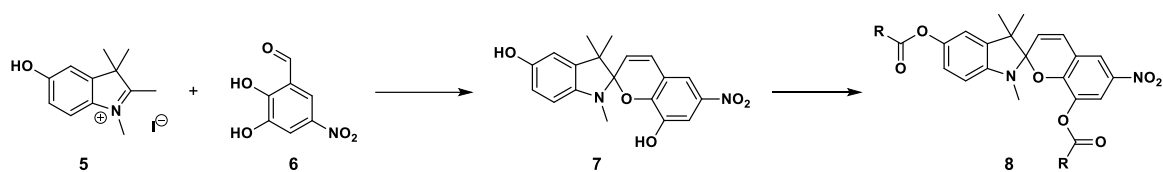


Figure 2.3: General scheme of spiropyran mechanophore synthesis. The appropriate hydroxyl functionalized indolenine and benzaldehyde are condensed to form a spiropyran. The spiropyran is then acylated with a group to provide polymer attachment points.

In order to fully test the mechanophore, we would need to synthesize several spiropyrans. First, we would need the active mechanophore spiropyrans. These would have either di-arylates for use as a cross-linker, or di- α -bromoisobutyryl groups that could be used to initiate polymer growth with ATRP conditions. In addition to the active mechanophores, we would need at least control molecules. These would be spiropyrans with polymer attached to only one point on the molecule, or two points on the molecule that would not allow for mechanical force to be transferred across the C–O bond. These controls are essential to prove that the color change is from mechanical force, and not some type of localized heating.

The synthesis of the difunctional spiropyran mechanophore closely followed Moore's work,^{10,15} but some modifications were made to increase yield or reduce the amount of purification necessary. The general scheme of the spiropyran mechanophore is shown in figure 2.3. A hydroxyl functionalized indolenine and a hydroxyl functionalized hydroxybenzaldehyde are condensed to give a di-hydroxy spiropyran. This spiropyran is then acylated to provide for two polymer attachment points. For monofunctional control spiropyrans, one of the hydroxyl groups is protected.

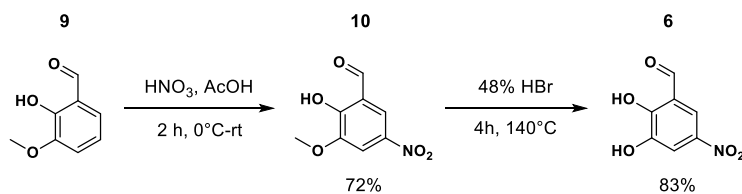


Figure 2.4: Hydroxy benzaldehyde synthesis from *o*-Vanillin.

Synthesis of the benzaldehyde fragment is shown in figure 2.4. First, *o*-vanillin is dissolved in acetic acid, cooled to with an ice bath and nitrated with concentrated nitric acid. This is transferred into excess water to afford yellow, fluffy crystals. These crystals are filtered and rinsed with water to give the nitro-*o*-vanillin in good yield. Demethylation is achieved through heating in a concentrated 48% solution of HBr. The reaction is then cooled and filtered to a black solid. This was then dissolved in minimal hot ethyl acetate, and decolorizing carbon was added. The hot mixture was then pushed through a plug of silica. The solution is then cooled in the freezer to give crystals which can be filtered. Though the literature procedure calls for simple recrystallization, this can often lead to dark colored product. The addition of decolorizing carbon and the short silica plug remove the dark impurities, leaving the product as bright yellow solid. Overall, the benzaldehyde fragment synthesis is fast and scalable, and requires no chromatography.

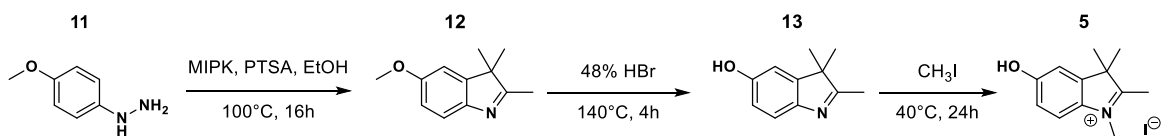


Figure 2.5: Indolenine fragment synthesis from methoxy phenylhydrazine.

The indolenine fragment could be synthesized in 3 steps from *p*-methoxy phenylhydrazine. First, a Fischer indole synthesis with methyl isopropyl ketone and *p*-methoxy phenylhydrazine HCl catalyzed with *p*-toluenesulfonic acid was carried out.

Although the literature procedure called for column chromatography, we found this could be avoided with an extractive work-up. The crude reaction mixture had solvent removed under reduced pressure, followed by addition of 1N HCl to dissolve the indolenine. The aqueous layer was then extracted with hexanes and ethyl acetate to remove organic impurities. The isolated aqueous layer could be neutralized with sodium bicarbonate and extracted with methylene chloride to give a clean product.

In a manner similar to the benzaldehyde synthesis, the demethylation was accomplished by heating in 48% HBr. The reaction mixture is quenched, neutralized, and then extracted with methylene chloride. Solvent removal under reduced pressure gives the product in high yield and good purity. *N*-Methylation was achieved by neat reaction in refluxing methyl iodide overnight, followed by filtration and recrystallization from an alcoholic solvent.

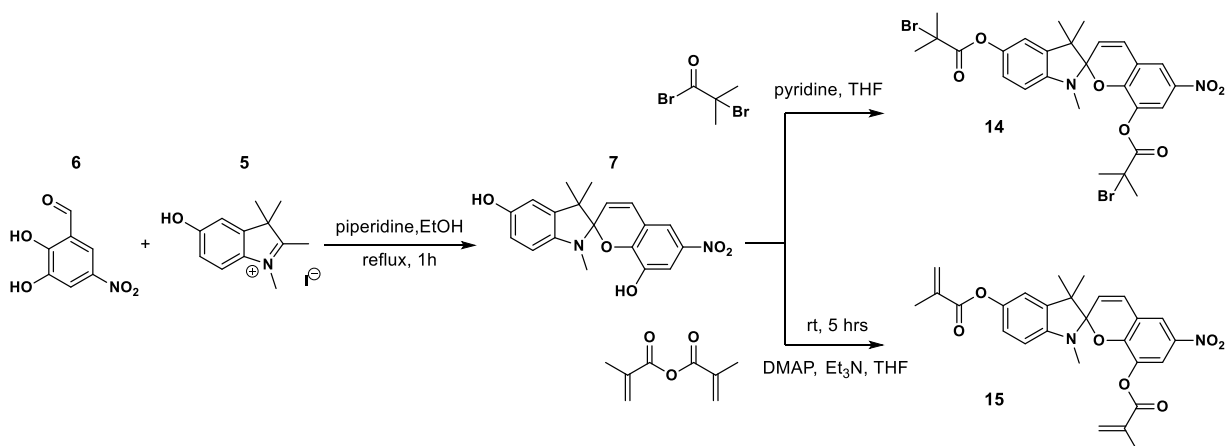


Figure 2.6: Synthesis of difunctional spiropyran.

In figure 2.6, synthesis of spiropyran mechanophore is shown. First, the indolenine iodide and dihydroxy nitrobenzaldehyde are combined in ethanol and refluxed with piperidine. This gives a black mass of insoluble dihydroxyl spiropyran which can be isolated

through filtration. This can then be acylated with α -bromoisobutyryl bromide to give a spiropyran that can be used as an ATRP initiator. Conversely, methacrylic anhydride in the presence of trimethylamine with DMAP as a catalyst can be used to give a dimethacrylate functionalized spiropyran. The use of pyridine or DMAP greatly enhances the yields of these reactions. Purification is accomplished by chromatography, but must be done quickly as the spiropyran isomerizes on silica.

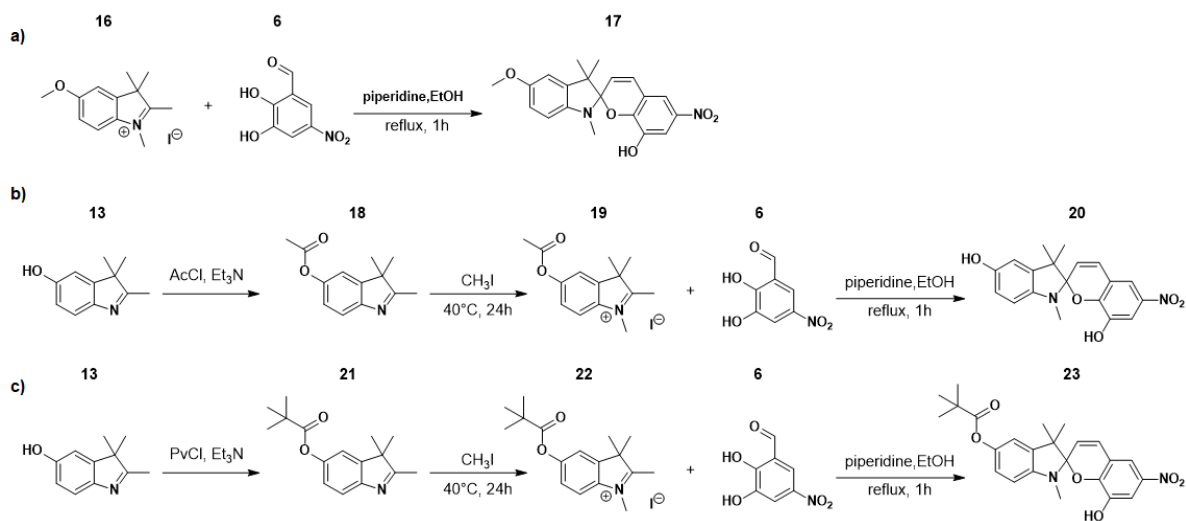


Figure 2.7: Synthesis of the monofunctional control. (a) Moore's original control. (b) Failed attempt at making an acyl protected control. (c) The pivyl group proved to be more robust and gave the desired spiropyran.

To make the monofunctional control used by the Moore group, the synthesis was kept the same but the indolenine was not demethylated (Figure 2.7a). However, we found that when we incorporated this control molecule into a polymer, the spiropyran would activate at ambient conditions. We theorized that this was due to the electron rich nature of the methoxy group donating into the spiropyran. To synthesize a control with functionality as similar as possible to the actual mechanophore, an *O*-acyl derivative was designed. This was made from the acylation of indolenine, followed by methylation with methyl iodide. Surprisingly, the

product of the condensation with benzaldehyde was the di-hydroxyl spiropyran (Figure 2.7b). The acyl group had been inadvertently deprotected during the spiropyran synthesis. To address this problem, the same procedure was repeated but with a pivyl group. The increased stability of the pivyl group allowed for the successful synthesis of a monofunctional control spiropyran (Figure 2.7c). The pivyl protected control molecule also behaved thermally similar to the difunctional mechanophore in the polymer.

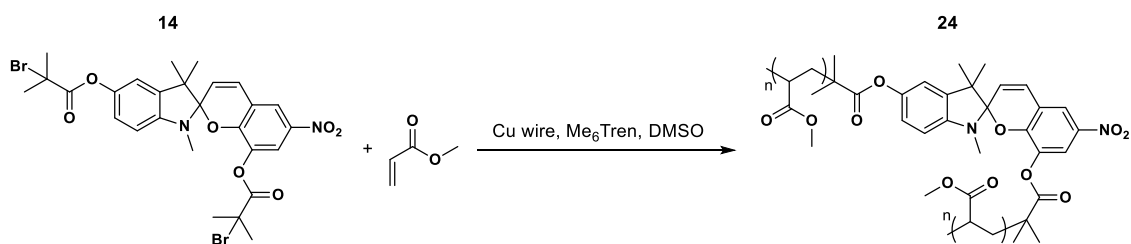


Figure 2.8: Synthesis of a linear acrylate polymer to create spiropyra mechanophore at center of a polymer chain.

ATRP polymerization was carried out with methyl acrylate as a monomer, and copper wire wrapped around the stir bar as the copper source (Figure 2.8). The polymerization was run, diluted with THF upon completion, then run through a plug of silica to remove copper. This was then dripped into methanol to yield a very gummy substance. Precipitation into a Teflon beaker aided greatly with handling of the polymer. Finally, the polymer was dried under vacuum to yield a tar like substance that would turn color when mechanical force was applied.

The cross-linked PMMA samples were made by taking the acrylate functionalized spiropyran, dissolving it methyl methacrylate, then placing this in a 1 dram vial. Then benzoyl peroxide and *N-N*-dimethylaniline were added to the solution degassed. These vials

were allowed to stand in a shallow water bath overnight. The next day, the vials were placed inside of a nitrile glove and broken with a hammer. The glass was carefully removed to give a transparent polymer disk.

2.3 High strain rate testing

Initially, testing was performed with linear PMA samples. However, several limitations were discovered when using PMA. First, PMA had to be molded into disk shape from small chunks of polymer. This gave less than consistent samples. The samples also had very rough ends, which was not ideal for contact with the rods of the Hopkinson bar. Finally, PMA had a tendency to soften, so it was difficult to analyze the samples after impact testing.

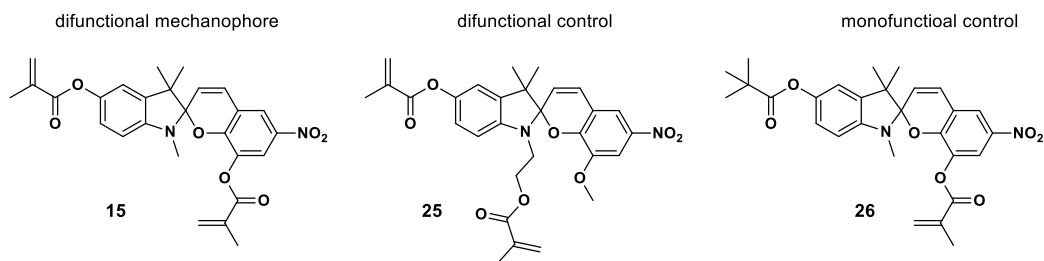


Figure 2.9: Spiroyrans used in testing.

The PMMA disks, on the other hand, gave consistent sized samples. These could be sanded on both sides to give a flat edge for good contact with the Hopkinson bar. Additionally, the fragments held their shape well, as they were cross-linked polymers. Because of these advantages, all of the testing performed used PMMA disks from an early stage. The spiropyran's tested in PMMA are show in figure 2.9. They consist of a spiropyran mechanophore, a difunctional control molecule where mechanical force does not go across the liable C-O bond, and a monofunctional control that closely mimics the structure of the mechanophore but is only attached to the polymer at a single point.

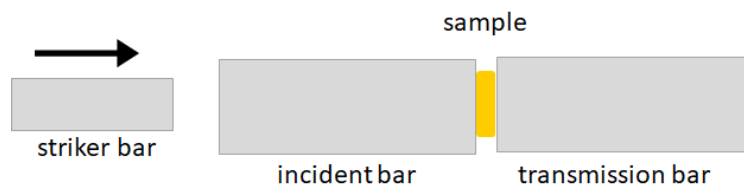


Figure 2.10: Hopkinson bar, an instrument which allows for high strain rate testing of materials.

High strain rate testing was carried out using a Hopkinson bar. The basic structure of Hopkinson bar is shown in figure 2.10. A sample is placed between two long rods, and one end of one of the rods is hit with a gas powered striker. This sends a compression wave down the bar, crushing the sample. The strain rates achieved are on the order of $>10^3 \text{ s}^{-1}$. Sensors can be added to determine the stress strain properties of the material, but in our case the instrument was simply used as an convenient method to achieve high strain rates.

Difunctional spiropyran PMMA samples were shot, along with the difunctional control and monofunctional control. The Hopkinson bar completely destroyed the PMMA samples, sending small pieces of PMMA flying in all directions. By enclosing the impact zone with a plastic cylinder, the fragments could be collected and sorted. Spiropyran activation was highly heterogeneous, with some fragments showing no activation and some samples showing extensive activation. Activation seemed to be more intense around the edges of samples. Fragments showing activation were examined using fluorescence microscopy.

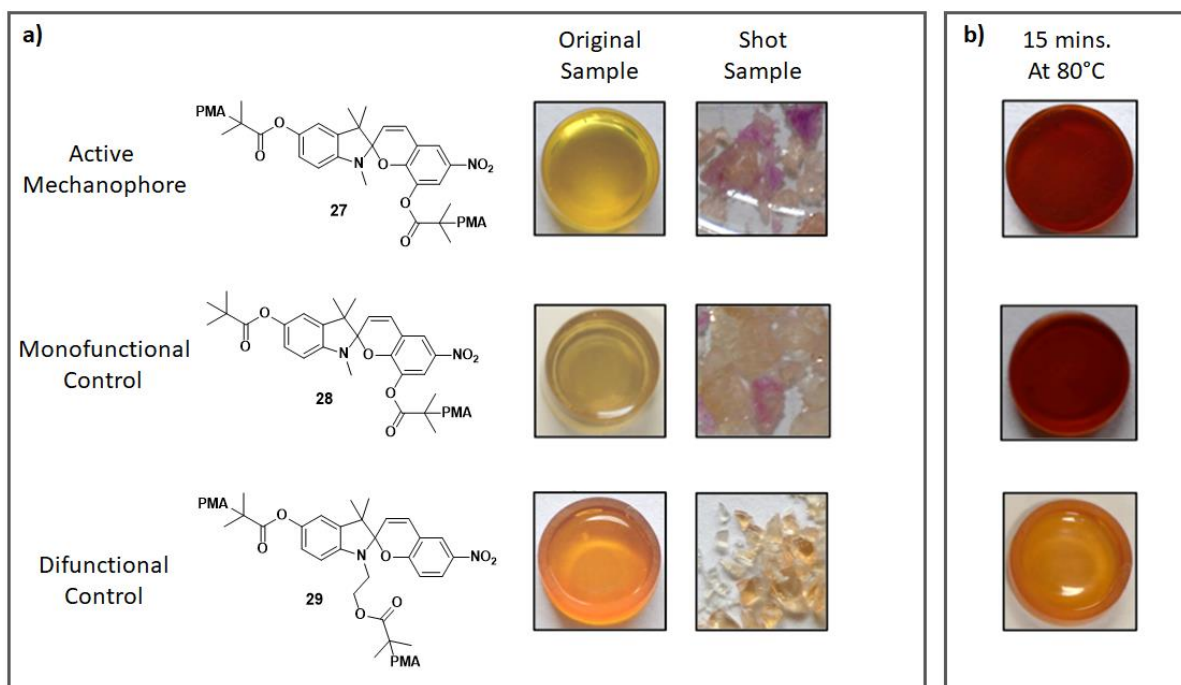


Figure 2.11: Results of impact testing on spiroyrpan mechanophores and controls embedded in PMMA. (a) Activation occurs in active mechanophore and monofunctional control. (b) Static testing shows that both the active mechanophore and monofunctional control are thermally active, while the difunctional control is not.

The results of the testing are shown in figure 2.11a. Both the difunctional spiroyrpan and the monofunctional control show activation. Interestingly, the difunctional control shows no activation. To understand the nature of thermal activation, each of these samples were heated in an oven as a comparison (Figure 2.11b). This showed that both the mechanophore and the monofunctional control could be activated by thermal heating. This indicates that most of the color seen is likely thermal, as impact events can reach the temperatures required to activate spiroyrpans.^{16,17} These tests show the importance of careful design of control molecules. The difunctional control is structurally different enough that it is not thermally

active. If this had been the only control used, it is possible that incorrect conclusions could have been drawn.

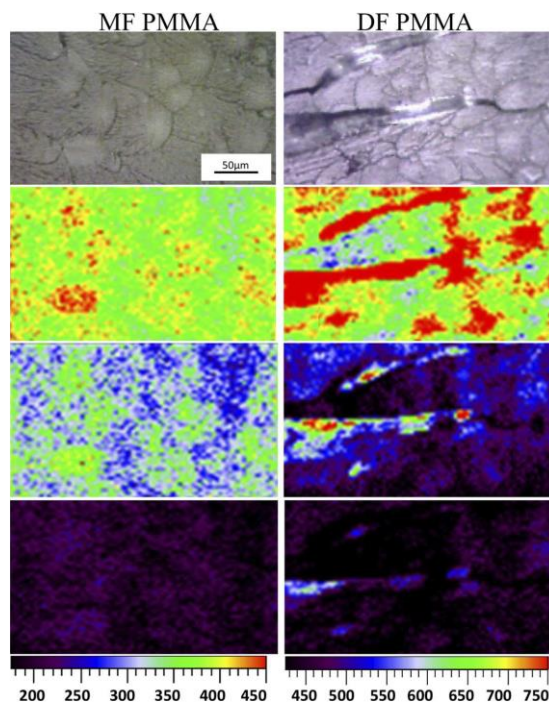


Figure 2.12: Fluorescence microscopy of the surface of a fragment of a monofunctional control sample (left) and an active mechanophore sample (right). The colors correspond to fluorescence intensity. Though widespread activation is seen both samples, the mechanophore sample seems to show enhanced activation in microcracks. Reprinted with permission from (14). Copyright (2014) Wiley.

Although we were discouraged by these initial results from a mechanochemistry perspective, we sought to investigate the results of the test further with fluorescence microscopy (Figure 2.12). Fragments of the active mechanophore samples as well as those from the monofunctional control were selected. They were irradiated with a 514 nm Ar laser and emission as monitored between 590 nm and 680 nm.¹⁸ Though widespread background activation occurs in both samples, the active mechanophore sample seems to show enhanced

fluorescence in the region of crack channels. This type of activation was not observed in the monofunctional control sample. Therefore it is possible that in these craze regions a mechanochemical effect is observed. However, at present it is difficult to decouple this from the thermal activation.

In the end we were able to successfully synthesize a difunctional spiropyran mechanophore and integrate it into acrylate polymers through controlled and free radical polymerization. We also were able to successfully synthesize control spiropyrans, and even synthesize and design a control molecule that more accurately represented the active mechanophore. We tested the polymer samples at high strain rate, and analyzed the fragments at the microstructure using fluorescence microscopy. Detailed study of the fluorescent imaging showed some evidence mechanical activation. While the results of using this particular mechanophore to sense strain at high strain rate are not clear, we were inspired to explore the use of small molecules as temperature sensors for high strain rate events.

2.4 Thermochromic compounds for high strain rate studies

Our work with spiropyran mechanophores led to us investigating the use of small molecule thermochromic compounds to sense heat at high strain rate. Since we had shown thermochromic activation in the model polymer of PMMA, we next set out to explore a polymer that would be commonly used in explosive formulation and rocket motors, where high strain rate heating studies would be important. We chose hydroxyl terminated polybutadiene (HTPB), as it is a binder in most military and civilian solid rocket motors, as well as a common binder in explosive compositions.

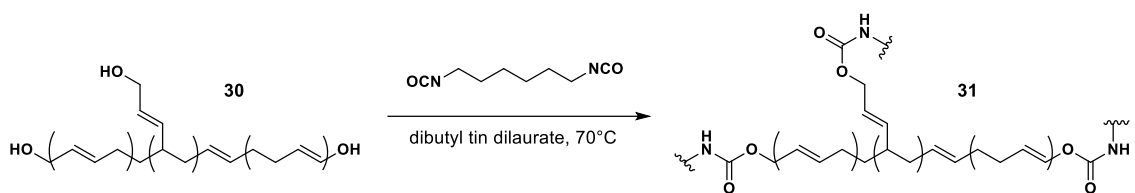


Figure 2.13: HTPB pre-polymer, left, is cured with a diisocyanate to form an elastomer.

HTPB begins as a oligomer that is combined with a diisocyanate to cure into a tough elastomer. Organotin is generally used as a catalyst. Initially, we attempted to incorporate small molecule spiropyrans into the HTPB pre-polymer. However, upon heating, we saw no thermal activation. This is likely due to the very non-polar nature of the HTPB, which likely sufficiently destabilizes the highly polar merocyanine form so that thermodynamically favored state is in the closed, colorless form. We sought to investigate other small molecules which could be used as thermal sensors.

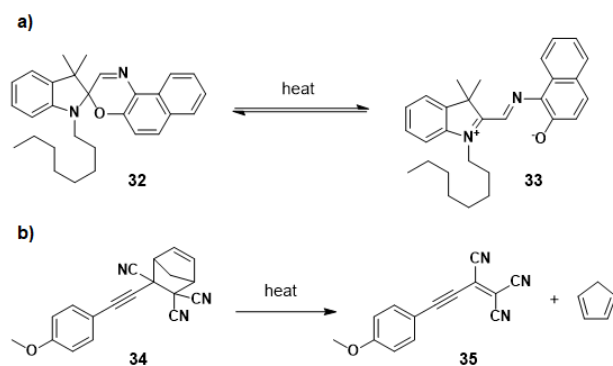


Figure 2.14: Attempts of using thermochromic molecules in HTPB. (a) spirooxazine, which quickly reverts to its closed form at room temperature. (b) A Diels-Alder adduct that was inactive at high strain rates.

We attempted to utilize several compounds known in the literature to be thermochromic. Spirooxazines, compounds similar to spiropyran, are known to be thermochromic (Figure 2.14a). We synthesized a standard spirooxazine, but with a long alkyl

chain added to enhance solubility and stability in the non-polar matrix. Though we saw thermochromic activation with this molecule, the thermal reversion rates were so high that it would prove to be an ineffective diagnostic tool. Next, we explored Diels–Alder adducts of conjugated dye molecules. We synthesized a donor acceptor dye (Figure 2.14b), and capped it with a cyclopentadienyl group. Upon heating at room temperature, the sample turned yellow. However, at high strain rates no activation was observed. This is likely to due to the relatively slow rate of reaction, while an impact occurs on a very short time scale. We then decided to investigate the use of the novel class of Donor Acceptor Stenhouse Adduct (DASA) photoswitches for use as thermochromic sensor.¹⁹

2.5 DASA-HTPB thermochromic polymer synthesis.

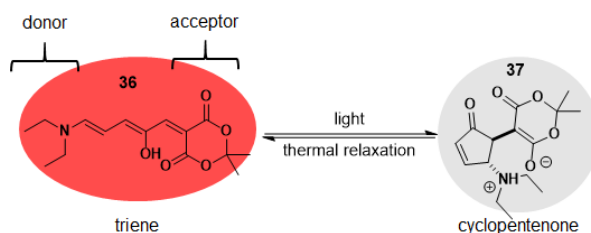


Figure 2.15: Basic structure of DASA. It is thermodynamically stable in the open colored form, and visible light can cause it to cyclized into a colorless form.

The basic structure of the DASA is shown in figure 2.15. It has brightly colored open triene form that can be cyclized into a colorless closed cyclopentenone form.^{20,21} Thermally it can relax back into the open form, and this can be accelerated with heat. More detailed information can be found in the introduction section of this document.

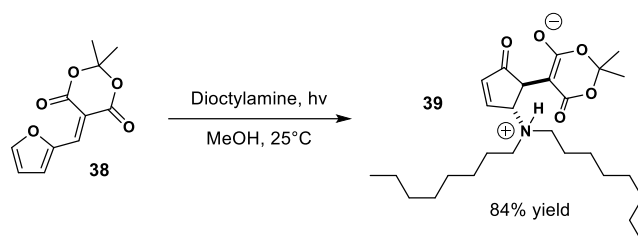


Figure 2.16: Synthesis of the closed form of diethylamine DASA.

Our initial studies show that if the cyclized form of the DASA was placed in HTPB, it would convert to the open form with heating and cause the sample to turn red. This red color was quite stable, and could be used to give a thermal history of the polymer sample. To investigate this compound at high strain rate, we synthesized a large quantity of cyclized DASA. The synthesis is shown in figure 2.16. Diethylamine is used as a donor amine to maximize compatibility with HTPB. This amine was added to Meldrum's acid furan adduct in methanol. The reaction was allowed to stir overnight under broadband visible light irradiation from a fluorescent lamp. The next day, large quantities of light pink solid were observed as precipitate. This was isolated to yield a grey solid with a pink hue. The pink hue disappears after standing at room temperature for several weeks, leaving a white solid.

To make the HTPB samples, a small amount of closed DASA was added to the HTPB pre-polymer, followed by a diisocyanate such as hexamethylene diisocyanate (HMDI) or isophorone diisocyanate (IPDI). This was thoroughly stirred to make homogenous mixture, then poured into a syringe with one end closed up. This was put under vacuum to remove small bubbles. To cure the polymer, a catalytic amount of dibutyl dilaurate (DBTDL) was added. The polymerization was carried out by placing the syringe in an oil bath at 70°C. After curing overnight, the syringe was removed and rinsed with hexanes to remove the oil. Then the syringe could be cut away to reveal an HTPB cylinder containing DASA.

2.6 Testing of DASA-HTPB thermochromic polymer

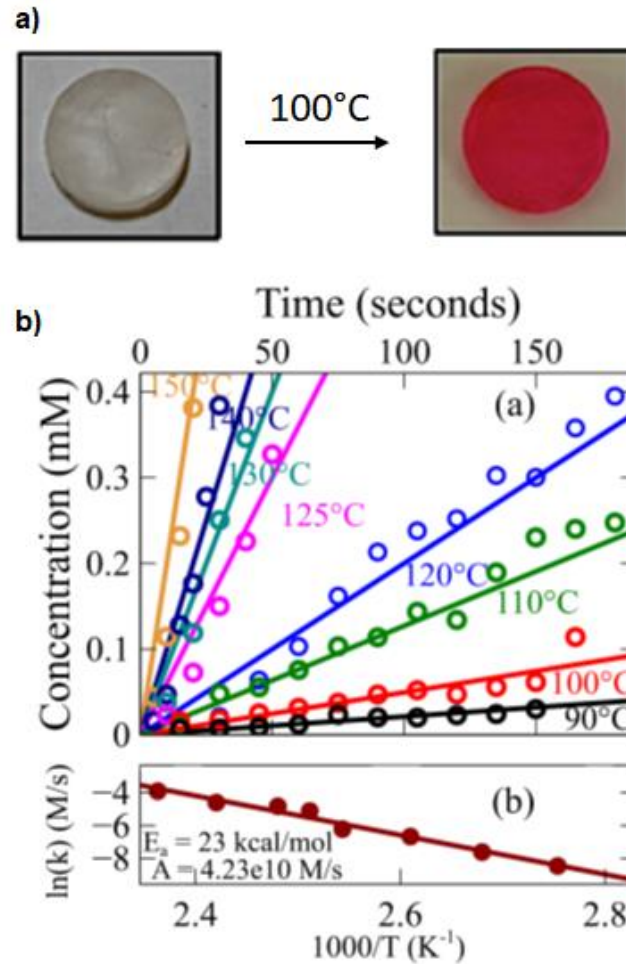


Figure 2.17: Static testing of HTPB DASA. (a) DASA activates when heated in an oven. (b) Kinetics of DASA activation in HTPPB. Reprinted with permission from (19). Copyright (2016) Applied Physics Letters.

Static heating of the HTPB-DASA shows clear activation. As the colorless HTPB sample is heated past 100 °C, the sample uniformly becomes bright red (Figure 2.17a). To control for possible mechanical effects, the sample was also loaded in a static press and compressed. No activation was observed, confirming the purely thermal nature of the coloration. To better understand the rate of activation with temperature, small samples were

heated at a range of temperatures for different time periods (Figure 2.17b). This gave good data showing linear rates of activation at different temperature. From this information we could make an Arrhenius plot and determined the energy of activation of the DASA in HTPB to be 23 kcal/mol.

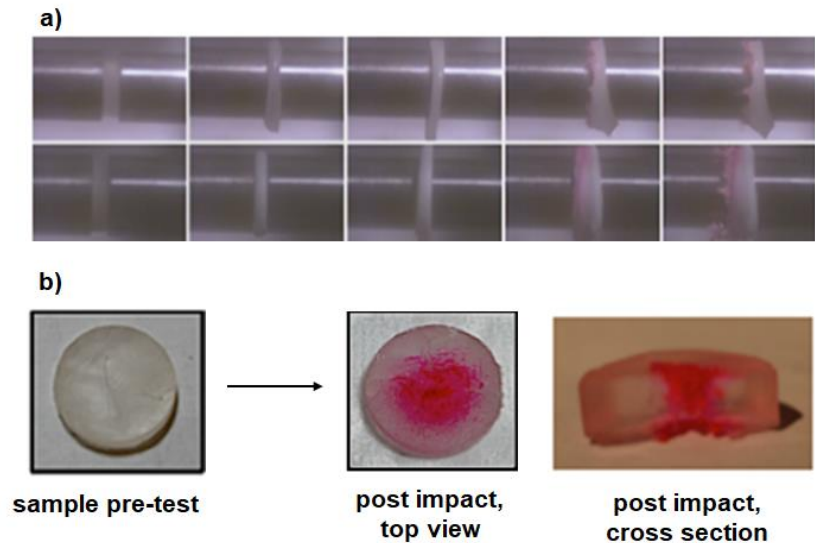


Figure 2.18: High strain rate testing of HTPB with embedded DASA. (a) Frames from a high speed camera, showing activation at the edges of the material forced out. (b) View of the sample before and after the test, showing localized activation.

Like the mechanophore studies, the thermochrome studies were initially carried out using a Hopkinson bar (Figure 2.18a). As HTPB has a low glass transition temperature, the fragmentation seen with PMMA was not observed. Rather, as the sample was compressed most of the material was forced outside of the compression zone. Only the sample nearest the center is fully compressed, and this experiences the high temperatures from the impact. This can be clearly seen in the post-mortem impact analysis (Figure 2.18b). Clearly, the thermochromic activation occurs most readily where the temperature is the highest.

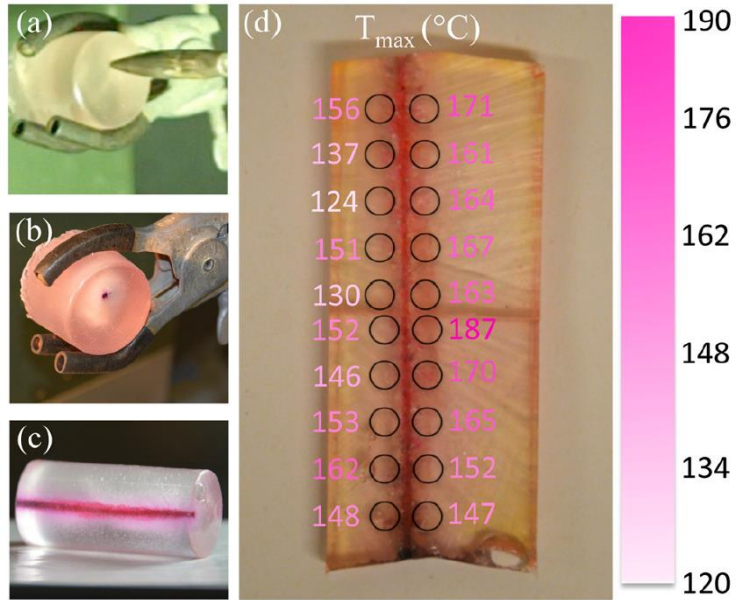


Figure 2.19: Bullet impact of DASA/HTPB. (a) Moment before bullet impact. (b) Sample post impact. (c) Larger sample post impact, showing bullet path. (d) Cross section of sample, showing approximate temperatures reached. Reprinted with permission from (19). Copyright (2016) Applied Physics Letters.

Further impact testing was carried out by shooting the HTPB sample with a .50 caliber bullet. The impact violently disturbs the polymer, and causes localized heating. This heating leaves a trail through the bullet's path as can be seen in figure 2.19. Further analysis was performed by taking a very thin slice of this sample across the penetration channel. Then absorption measurements were taken at various points, and this was modeled along with the energies of activation to give approximate maximum temperatures reached at various points in the sample. Temperatures on one side are higher, likely due to the precession of the bullet. Further testing with mock formulated HTPB samples will allow us to validate models used to predict temperature raises during impact.

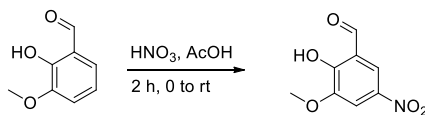
In conclusion, we have shown that we can successfully integrate spirpyran mechanophores and control molecules into acrylate polymers. We were able to test these at high strain rates, and analyze the results in great detail using fluorescence microscopy. Since we determined the activation to be largely thermal, we set out to integrate a thermally responsive small molecule into an important real world polymer, HTPB. This DASA HTPB mixture showed thermal activation from both compression and penetration impact events. In the future we would like to add additional thermochromic compounds with different activation energies and different wavelengths, so that even more detailed information can be extracted.

2.7 Experimental

Synthesis.

Syntheses were adapted from procedures outlined by Moore et al.¹

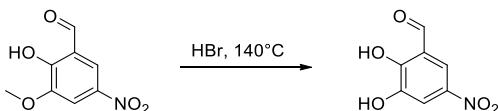
2-hydroxy-3-methoxy-5-nitrobenzaldehyde



O-vanillin (10.0 g, 65.6 mmol), acetic acid (59 mL), and water (2.3 mL) were combined in a round bottom flask. This was cooled with an ice bath. An addition funnel was added, and to this a solution of concentrated nitric acid (4.57 mL) in acetic acid (13 mL) was added. The nitric acid solution was allowed to slowly drip into the reaction flask. During this time a yellow precipitate is formed. After stirring for two hours, the reaction is quenched into 100 mL of water. This was then filtered, washed with water, and allowed to dry to yield a light

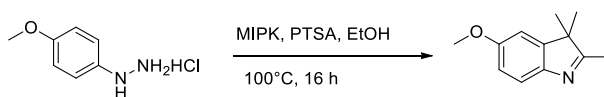
yellow solid (Yield 8.7 g, 72%). $^1\text{H NMR}$ (600 MHz, CDCl_3) δ 11.72 (s, 1H), 10.00 (s, 1H), 8.23 (d, $J = 2.5$ Hz, 1H), 7.94 (d, $J = 2.5$ Hz, 1H), 4.03 (s, 3H) ppm.

2,3-dihydroxy-5-nitrobenzaldehyde



2-hydroxy-3-methoxy-5-nitrobenzaldehyde (3.0 g) was placed in a round bottom flask along with concentrated (48%) aqueous hydrobromic acid. A reflux condenser was attached and the flask was heated in an oil bath to 140 °C for 4 hours. After this time the reaction was quenched into 60 mL of cold water. This was filtered and rinsed with water to yield a black solid. Purification was accomplished by dissolving the solid in 80 mL of hot ethyl acetate and adding decolorizing carbon. This was then filtered through a silica pad. The resulting liquid was cooled in a freezer, and the solid precipitate was filtered off. Further crops of product were obtained by removing solvent from the supernatant liquid through rotary evaporation. Product is in the form of yellow needles. (Yield 2.3 g, 83%). $^1\text{H NMR}$ (600 MHz, DMSO-d_6) δ 11.10 (br s, 2H), 10.31 (s, 1H), 7.99 (d, $J = 2.8$ Hz, 1H), 7.78 (d, $J = 2.9$ Hz, 1H).

5-methoxy-2,3,3-trimethyl-3H-indole

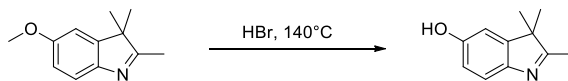


In a round bottom flask p-methoxyphenylhydrazine HCl (5g, 29 mmol), methyl isopropyl ketone (3.1 mL, 29 mmol), and para-toluyil sulfonic acid (540 mg, 2.8 mmol) were dissolved in absolute ethanol (250 mL). A reflux condenser was attached and the solution allowed to

reflux overnight. The reaction mixture was allowed to cool, and the solvent was then removed under reduced pressure. The residue was dissolved in 50 mL 1N HCl and placed in a separatory funnel. This was then washed twice with hexanes and once with ethyl acetate to remove organic impurities. The aqueous layer was then neutralized with sodium bicarbonate and extracted with dichloromethane. The organic layers were combined, dried over MgSO₄, and the solvent was removed under reduced pressure. Product is a brown solid (Yield 3.8 g, 76%). ¹H NMR (600 MHz, CDCl₃) δ 7.43 (d, J = 8.2 Hz, 1H), 6.84 (d, J = 2.4 Hz, 1H), 6.82 (dd, J = 8.3, 2.6 Hz, 1H), 3.83 (s, 3H), 2.24 (s, 3H), 1.29 (s, 7H) ppm.

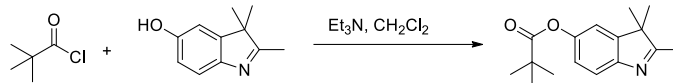
R_f = 0.12 in 3:1 Hexanes:Ethyl Acetate.

2,3,3-trimethyl-3H-indol-5-ol



5-methoxy-2,3,3-trimethyl-3H-indole (4.0 g, 21.13 mmol) was placed in a round bottom flask and then 66 mL concentrated (48%) aqueous hydrobromic acid was added. A reflux condenser was attached and the flask was heated in an oil bath to 140 °C for 2 hours. The reaction was allowed to cool, and then was quenched into water (275 mL). This was neutralized with sodium bicarbonate, then extracted with dichloromethane. The organic layers were combined, dried over MgSO₄, and the solvent was removed under reduced pressure. Product is a brown solid (Yield 3.6 g, 97%). ¹H NMR (400 MHz, CDCl₃) δ 7.34 (d, J = 8.3 Hz, 1H), 7.23 (s, 1H), 6.82 (d, J = 2.4 Hz, 1H), 6.76 (dd, J = 8.3, 2.5 Hz, 1H), 2.25 (s, 3H), 1.29 (s, 6H) ppm.

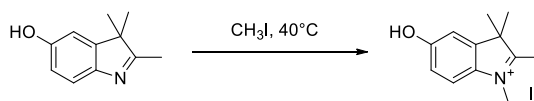
2,3,3-trimethyl-3H-indol-5-yl pivalate



2,3,3-trimethyl-3H-indol-5-ol (1.00 g, 5.71 mmol) was placed in a flask and a septa was attached. The flask was flushed with nitrogen, then placed under a positive nitrogen atmosphere. Then dry dichloromethane (20 mL) was added, followed by triethylamine (854 μ L, 6.85 mmol). Trimethyl acetyl chloride (843 μ L, 6.85 mmol) was added dropwise. The reaction was allowed to run overnight. The reaction was quenched with 1N HCl, then extracted with dichloromethane. The aqueous layer was then neutralized with sodium bicarbonate and extracted with dichloromethane. The organic layers were then combined, dried over MgSO₄, and the solvent removed under reduced pressure. Purified with flash column chromatography using a gradient of 10% to 40% ethyl acetate in hexanes (Yield 780 mg, 53%). ¹H NMR (600 MHz, CDCl₃) δ 7.50 (d, J = 8.2 Hz, 1H), 6.99 (d, J = 2.2 Hz, 1H), 6.97 (dd, J = 8.2, 2.3 Hz, 1H), 2.28 (s, 3H), 1.37 (s, 9H), 1.31 (s, 6H) ppm.

R_f = 0.14 in 20% ethyl acetate in hexanes.

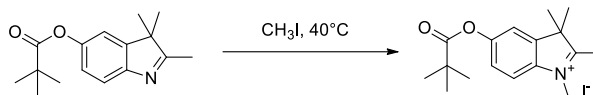
5-hydroxy-1,2,3,3-tetramethyl-3H-indol-1-ium iodide



2,3,3-trimethyl-3H-indol-5-ol (2.6 g, 14.8 mmol) and methyl iodide (15 mL) were combined and refluxed at 40 °C for 24 hours. The reaction was allowed to cool, then filtered and washed with benzene. The powder was collected and then recrystallized from minimal ethanol to yield light purple crystals. Further crops of crystals could be obtained from the mother liquor by reducing its volume through rotary evaporation (Yield 4.1 g, 87%). ¹H

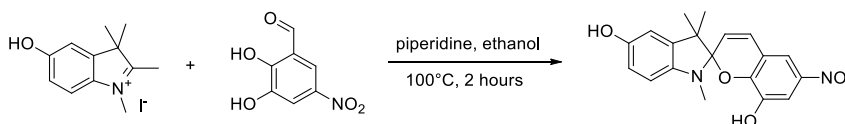
NMR (400 MHz, DMSO- d_6) δ 10.26 (d, $J = 1.3$ Hz, 1H), 7.68 (d, $J = 8.7$ Hz, 1H), 7.12 (d, $J = 2.4$ Hz, 1H), 6.94 (dd, $J = 8.7, 2.4$ Hz, 1H), 3.89 (s, 3H), 2.66 (d, $J = 1.2$ Hz, 3H), 1.46 (s, 6H) ppm.

1,2,3,3-tetramethyl-5-(pivaloyloxy)-3H-indol-1-ium iodide



2,3,3-trimethyl-3H-indol-5-yl pivalate (780 mg, 3.01 mmol) and methyl iodide (5.6 mL) were combined and refluxed overnight. The reaction was allowed to cool, then was filtered and washed with benzene. The powder was collected and recrystallized from ethanol. The crystals were rinsed with diethyl ether (Yield 1.11 g, 93%). ^1H NMR (600 MHz, DMSO- d_6) δ 7.95 (d, $J = 8.6$ Hz, 1H), 7.68 (d, $J = 2.3$ Hz, 1H), 7.39 (dd, $J = 8.6, 2.3$ Hz, 1H), 3.96 (d, $J = 1.2$ Hz, 3H), 2.74 (d, $J = 1.2$ Hz, 3H), 1.52 (s, 6H), 1.33 (s, 9H) ppm.

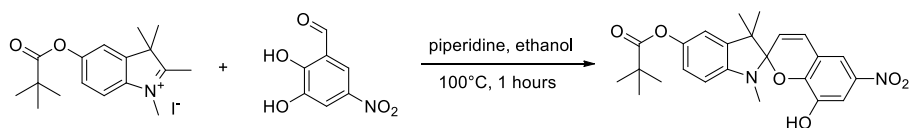
1',3',3'-trimethyl-6-nitrospiro[chromene-2,2'-indoline]-5',8-diol (dihydroxyl spiropyran)



Indolium iodide (1.73 g, 5.46 mmol) and dihydroxy nitrobenzaldehyde (1.00 g, 5.46 mmol) were combined in a round bottom flask and suspended in 50 mL of absolute ethanol. Piperidine (1.08 mL, 10.92 mmol) was added, and a reflux condenser affixed to the flask. The reaction was then refluxed at 100 °C for two hours. The reaction was then allowed to cool, filtered, and washed with ethanol to yield a black powder (Yield 1.854 g, 96%).

8-hydroxy-1',3',3'-trimethyl-6-nitrospiro[chromene-2,2'-indolin]-5'-yl pivalate

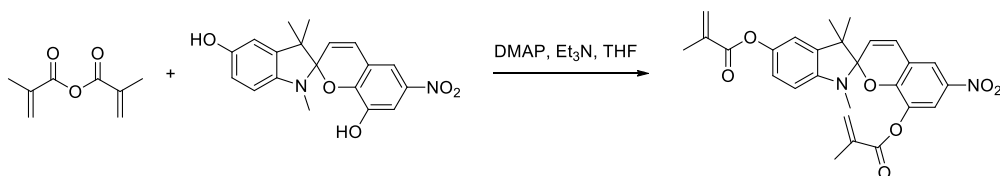
(monohydroxyl spiropyran)



Tert-butyl acyl indolium iodide (300 mg, 0.75 mmol) and dihydroxy nitrobenzaldehyde (138 mg, 0.75 mmol) were combined in a round bottom flask and absolute ethanol (10 mL) was added. Then piperidine (150 μ L, 1.50 mmol) was added and a reflux condenser was affixed to the flask. The reaction was then refluxed at 100 °C for an hour. The reaction was allowed to cool, then the solvent was removed under reduced pressure. Dichloromethane was added, and then this solution was washed with saturated aqueous ammonium chloride. The organic layer was dried with $MgSO_4$ and the solvent was removed under reduced pressure. This crude product was used in the subsequent reaction without further purification.

Not isolated.

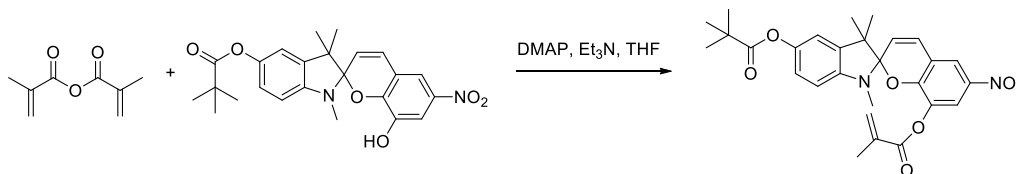
1',3',3'-trimethyl-6-nitrospiro[chromene-2,2'-indoline]-5',8-diyl bis(2-methylacrylate) (difunctional spiropyran)



Dihydroxyl spiropyran 8 (100 mg, 0.28 mmol) was dissolved in dry tetrahydrofuran with triethylamine (120 μ L, 0.86 mmol) and *N,N*-dimethylaminopyridine (8 mg, 0.06 mmol). The solution was sparged with nitrogen and cooled to 0 °C, and methacrylic anhydride (100 μ L, 0.67 mmol) was added dropwise. After 1 hour at 0 °C, the reaction was allowed to warm to room temperature and monitored by thin layer chromatography ($R_f=0.6$ with 20% ethyl acetate in hexanes on silica). The reaction did not go to completion after 16 hours, so the

product spot was isolated by flash chromatography, concentrated by rotary evaporation, and immediately recrystallized from dichloromethane in boiling hexanes to yield pale yellow crystals (Yield 34 mg, 23%). ¹H NMR (500 MHz, CDCl₃) δ 7.96 (d, J = 2.6 Hz, 1H), 7.92 (d, J = 2.6 Hz, 1H), 6.98 (d, J = 10.4 Hz, 1H), 6.86 (dd, J = 8.3, 2.4 Hz, 1H), 6.79 (d, J = 2.3 Hz, 1H), 6.45 (d, J = 8.3 Hz, 1H), 6.32 (p, J = 1.0 Hz, 1H), 5.93 – 5.90 (m, 2H), 5.73 (p, J = 1.6 Hz, 1H), 5.51 (p, J = 1.5 Hz, 1H), 2.65 (s, 3H), 2.07 (dd, J = 1.5, 0.9 Hz, 3H), 1.69 (dd, J = 1.6, 1.0 Hz, 3H), 1.24 (s, 3H), 1.21 (s, 3H) ppm.

1',3',3'-trimethyl-6-nitro-5'-(pivaloyloxy)spiro[chromene-2,2'-indolin]-8-yl methacrylate (monofunctional spiropyran).



Crude monohydroxyl spiropyran 9 (approx. 328 mg, 0.748 mmol) was transferred to a flask using dichloromethane, then the solvent was removed under reduced pressure. Then DMAP (9.1 mg, 0.075 mmol) was added and the flask was capped and flushed with nitrogen. Anhydrous THF (15 mL) was added, then triethylamine (250 μL, 1.794 mmol) and methacrylic anhydride (266 μL, 1.794 mmol) were added. The reaction was allowed to run overnight. The reaction was then diluted with diethyl ether, filtered, and the solvent removed under reduced pressure. The crude material was purified by flash column chromatography using a gradient 0% to 10% ethyl acetate in hexanes. The crude material was loaded onto the column using carbon tetrachloride. The pure fractions were then combined, and the solvent removed under reduced pressure. The residue was then dissolved in minimal dichloromethane and added dropwise to 10 mL of boiling hexanes. After leaving the hexanes

solution in the freezer overnight, the product precipitated out as yellow crystals (Yield 126 mg, 33%). ¹H NMR (500 MHz, CDCl₃) δ 7.95 (d, J = 2.6 Hz, 1H), 7.91 (d, J = 2.6 Hz, 1H), 6.98 (d, J = 10.4 Hz, 1H), 6.79 (dd, J = 8.3, 2.3 Hz, 1H), 6.71 (d, J = 2.3 Hz, 1H), 6.43 (d, J = 8.3 Hz, 1H), 5.95 – 5.88 (m, 2H), 5.49 (p, J = 1.6 Hz, 1H), 2.64 (s, 3H), 1.68 (s, 0.7 Hz, 3H), 1.36 (s, 9H), 1.24 (s, 3H), 1.21 (s, 3H) ppm.

R_f = 0.63 in 20% ethyl acetate in hexanes. When the fully developed TLC plate is heated without any stains, the spiropyran spots will change color.

Representative Synthesis of Mechanochromic PMMA-Spiropyran Disks

All acrylates are first passed through a plug of basic alumina immediately before use to remove inhibitor.

Benzoyl peroxide (15 mg), and difunctional spiropyran (4 mg) were added to a 2 dram vial, followed by methyl methacrylate (1 mL), and ethylene glycol dimethacrylate (18 μL). Finally, dimethyl aniline (6 μL) was added and the solution was mixed by swirling before sparging with nitrogen for 1 min. The vial was then capped, wrapped with electrical tape, and left overnight in a room temperature water bath to mitigate hot spot formation in the reaction. Removal of the polymer discs was accomplished by carefully breaking the glass vial around the sample.

HTPB DASA Synthesis

Synthesis The integration into HTPB proceeded in the following way. Dioctyl-DASA²¹ (3 mg) was dissolved in hydroxyl-terminated polybutadiene (HTPB, M_n = ~2800 g/mol, M_w = ~6200 g/mol) (6.0 g). This viscous solution was combined with hexamethylene

dissocyanate (HMDI) (0.5 mL) and dibutyltin dilaurate (5 microliters), then sealed in a 10 mL disposable polyethylene syringe for 18 hours. The resulting elastomeric polymer was carefully cut out of the syringe. Samples were sectioned after being cooled in a freezer to avoid activation from the cutting process. Uniform activation is observed under heating, and localized activation is observed following high-rate compression on a split Hopkinson bar system.

2.8 References

- (1) Urtiew, P. A.; Tarver, C. M. *Combust. Explos. Shock Waves* **2005**, *41* (6), 766.
- (2) Berghout, H. L.; Son, S. F.; Skidmore, C. B.; Idar, D. J.; Asay, B. W. *Thermochim. Acta* **2002**, *384* (1–2), 261.
- (3) Tarver, C. M.; Chidester, S. K.; Nichols, A. L. *J. Phys. Chem.* **1996**, *10* (100), 5794.
- (4) Caruso, M. M.; Davis, D. A.; Shen, Q.; Odom, S. A.; Sottos, N. R.; White, S. R.; Moore, J. S. **2009**, 5755.
- (5) Piermattei, A.; Karthikeyan, S.; Sijbesma, R. P. *Nat Chem* **2009**, *1* (2), 133.
- (6) Jakobs, R. T. M.; Sijbesma, R. P. *Organometallics* **2012**, *31* (6), 2476.
- (7) Hickenboth, C. R.; Moore, J. S.; White, S. R.; Sottos, N. R.; Baudry, J.; Wilson, S. R. *Nature* **2007**, *446* (7134), 423.
- (8) Berkowski, K. L.; Potisek, S. L.; Hickenboth, C. R.; Moore, J. S. *Macromolecules* **2005**, *38* (22), 8975.
- (9) Diesendruck, C. E.; Steinberg, B. D.; Sugai, N.; Silberstein, M. N.; Sottos, N. R.; White, S. R.; Braun, P. V.; Moore, J. S. *J. Am. Chem. Soc.* **2012**, *134* (30), 12446.
- (10) Davis, D. A.; Hamilton, A.; Yang, J.; Cremar, L. D.; Van Gough, D.; Potisek, S. L.;

- Ong, M. T.; Braun, P. V.; Martínez, T. J.; White, S. R.; Moore, J. S.; Sottos, N. R. *Nature* **2009**, *459* (7243), 68.
- (11) Beiermann, B. A.; Kramer, S. L. B.; Moore, J. S.; White, S. R.; Sottos, N. R. *ACS Macro Lett.* **2012**, *1* (1), 163.
- (12) Beiermann, B. A.; Davis, D. A.; Kramer, S. L. B.; Moore, J. S.; Sottos, N. R.; White, S. R. *J. Mater. Chem.* **2011**, *21* (23), 8443.
- (13) Degen, C. M.; May, P. A.; Moore, J. S.; White, S. R.; Sottos, N. R. *Macromolecules* **2013**, *46* (22), 8917.
- (14) Hemmer, J. R.; Smith, P. D.; Van Horn, M.; Alnemrat, S.; Mason, B. P.; De Alaniz, J. R.; Osswald, S.; Hooper, J. P. *J. Polym. Sci. Part B Polym. Phys.* **2014**, *52* (20), 1347.
- (15) Potisek, S. L.; Davis, D. A.; Sottos, N. R.; White, S. R.; Moore, J. S. *J. Am. Chem. Soc.* **2007**, *129* (45), 13808.
- (16) Estevez, R.; Basu, S.; Van Der Giessen, E. *Int. J. Fract.* **2005**, *132* (3), 249.
- (17) Bjerke, T. W.; Lambros, J. *J. Mech. Phys. Solids* **2003**, *51* (6), 1147.
- (18) Van Horn, M.; Smith, P.; Mason, B. P.; Hemmer, J. R.; Read De Alaniz, J.; Hooper, J. P.; Osswald, S. *J. Appl. Phys.* **2015**, *117* (4).
- (19) Mason, B. P.; Whittaker, M.; Hemmer, J.; Arora, S.; Harper, A.; Alnemrat, S.; Mceachen, A.; Helmy, S.; Read de Alaniz, J.; Hooper, J. P. *Appl. Phys. Lett.* **2016**, *108*, 41906.
- (20) Helmy, S.; Leibfarth, F. A.; Oh, S.; Poelma, J. E.; Hawker, C. J.; Read De Alaniz, J. *J. Am. Chem. Soc.* **2014**, *136* (23), 8169.
- (21) Helmy, S.; Oh, S.; Leibfarth, F. A.; Hawker, C. J.; Read De Alaniz, J. *J. Org. Chem.* **2014**, *79* (23), 11316.

Chapter 3: DASAs with aniline based donors

3.1 Introduction

Photochromism has long been of interest for the ability to change molecular properties using only light as a stimulus. Upon exposure to light, a photochromic material will transform from its thermodynamically stable form into a metastable form. The compound will return to its thermodynamically stable form with heat or in some cases by irradiation with a second wavelength of light. The two forms of photoswitch have differing absorption spectra, molecular size, and polarity. These property changes have been used in number of applications such as surface polarity¹, membrane permeability², and nanoparticle clustering.³

Most photochromic compounds are classified as positive photochromes, meaning that upon light irradiation they transform from a stable molecular configuration with a shorter absorption wavelength to one with a longer wavelength absorption.⁴ This shorter wavelength light is usually UV light, which has limited depth of penetration in materials such as polymers and biological tissue.⁵ Because of this limitation, there has been growing interest in compounds that can undergo photoswitching with longer wavelengths of light.⁶ Longer wavelengths allow the use of visible light, which is more readily available, less damaging, and is absorbed less by most materials than UV light.

Some visible light photochromic compounds include dihydropyrene,^{7,8} dihydroazulenes,^{9,10} and imidazole diradicals.^{11,12} In the past decade, advances with azobenzene based photoswitches demonstrated by Aprahamian,^{13,14} Hecht,¹⁵ Herges,¹⁶ and Woolley¹⁷ have allowed for photoswitching across a broad range of wavelengths from visible

to near IR. However, in many of these photochromic systems switching occurs between two colored states and often the absorption wavelength of the two forms is very similar. This characteristic limits their use in applications such as sensing, that benefit from a more notable color change.¹⁸ Further, since both isomers are photoswitches, the wavelength for photoswitching must be carefully controlled. To address these challenges, we sought to design a robust and highly tunable photoswitch platform using inexpensive reagents and simple syntheses to provide a *colored-to-colorless* transformation using *broadband visible* light.

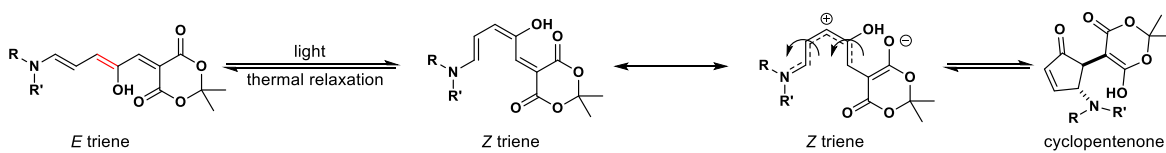


Figure 3.1: Upon light irradiation, the triene form of the DASA undergoes an *E/Z* isomerization. The *Z* triene can then undergo a 4π electrocyclization to yield the closed cyclopentenone form.

Donor-acceptor Stenhouse adducts (DASAs) are a class of novel photochromic materials that can be easily synthesized in two steps from readily available commercial materials was recently developed by our group.¹⁹ They are highly colored compounds that are able to undergo photoswitching to a closed colorless form upon visible light irradiation. This is the result of a photoisomerization of a double bond followed by a 4π electrocyclization to form a cyclopentenone (Figure 3.1).²⁰

DASAs are synthesized by combining an electron rich secondary amine with an furan containing an activating group.²¹ The furan adducts are the simply the Knoevenagel adduct of furfural and a strong carbon acid, most commonly Meldrum's acid or barbituric acid. While

this first generation of DASA exhibited desirable properties such as good fatigue resistance, polarity and color change with switching, and large molecular size change, several characteristics limited their adaptation into polymers and materials. Most importantly, reversible photoswitching could only be observed in very non-polar solvents such as toluene, benzenes, or hexanes. In addition, reversible switching could not be achieved in polymer matrices. Finally, the absorption wavelength was limited by the acceptor, thus photoswitching DASAs were limited to either 540 nm or 570 nm.

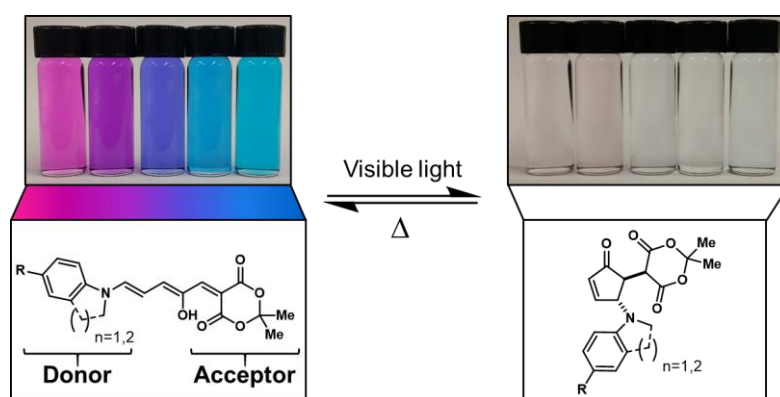


Figure 3.2: General structure of the second generation of DASAs. The open triene form is shown on the left, and the cyclized cyclopentenone form on the right. The various colors shown on the left are dependent on the donor aniline used. Reprinted with permission from (22). Copyright (2016) American Chemical Society.

To overcome the limitations described above, we set out to improve on the original DASA scaffold to enable enhanced properties. In this context, a second generation of DASAs utilizing anilines as donors was developed (Figure 3.2). This new system has allowed for high tunability of switching properties and absorption wavelengths. Moreover, it has opened the door to photoswitching in a variety of organic solvents, as well as photoswitching in polymer matrices. Additionally, absorption wavelength can be finely tuned over a range of

nearly 100 nm through modification of the donor amine. This wavelength tunability has allowed for orthogonal photoswitching of two different DASAs in both organic solvent and polymeric films. This second generation of DASA has greatly expanded the capabilities of the DASA photoswitch.²²

3.2 Synthesis

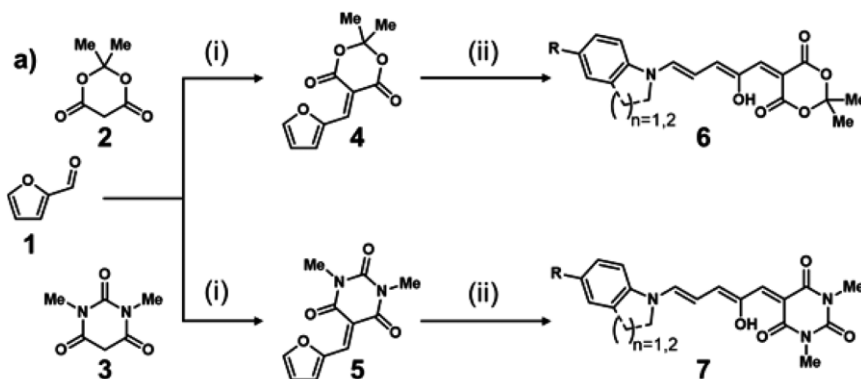


Figure 3.3: General synthesis scheme for aniline based DASAs with Meldrum's or barbituric acid acceptors. Reagents and conditions; (i) H₂O (ii) aniline derivative, neat, THF, DCM, or MeOH. Reprinted with permission from (22). Copyright (2016) American Chemical Society.

Similar to secondary amine DASAs, the synthesis of aniline based DASAs begins with either Meldrum's or barbituric furan acid adducts. These adducts are then combined with the desired secondary amine to synthesize the DASA. However, anilines have a much lower basicity than secondary amines. While secondary amines have pK_a's generally around 9, anilines generally lie in a range from 3 to 5 pK_a units. This negatively affects the synthesis and isolation of aniline DASAs. First, the reduced basicity lowers the rate of the reaction, as rate of reaction to form the DASA is directly related to the nucleophilicity of the amine and correlates to the pK_a. Because of this, while more electron rich anilines such as *para*-methoxy

N-methylaniline reacts quite quickly with a single equivalent of amine, *para*-chloro *N*-methylaniline requires multiple equivalents of aniline and longer reaction times. All of the aniline DASA reactions are noticeably slower and give lower yields than those using secondary amines.

The second complication with synthesis of aniline DASAs is that they are far more likely to exist in an equilibrium mixture of the closed and open form, which can complicate the isolation. The equilibrium between open and closed will be discussed in detail later, but in short less electron rich amines create DASAs that favor the closed form. The increased amount of closed form creates problems in synthesis, in that the closed form is vulnerable to nucleophilic attack from the amine used to create the DASA.²³ Though some amount of decomposition can be removed from the product during isolation, too much side-products makes the isolation of the pure product impossible. Therefore, much care must be taken when running reactions with aniline based DASAs that the reaction does not run for too long. TLC is an excellent analysis tool for monitoring this process.

The open/closed equilibrium also becomes an issue when using silica based column chromatography. With the first generation di-alkyl DASAs, some of the DASAs would cyclize into their closed form upon contact with silica. Still, enough remained in the open form in DCM/methanol that pure open form could be isolated after chromatography. With the aniline based DASAs, a much larger percentage of material goes into the closed form. Because of this, isolation of the open aniline DASAs has generally resulted in low yield and impure product. The most success in using chromatography to purify aniline DASAs has come from isolating the closed form. Here, the open DASA and all impurities are flushed off the column, and then the closed form is pushed off using methylene chloride with relatively

high (>10%) percentages of methanol. Overall, column chromatography has not proven very effective for purifying aniline based DASAs.

After much experimentation, trituration was found to be the most effective method of purification. After the reaction is deemed complete by TLC, a poor solvent such as hexanes or diethyl ether is added. This results in crystallization, and these crystals are isolated by filtration, followed by washing with more of a poor solvent. However, it should be noted that often this crude product is still not completely clean. The crude solid can be placed in a vial and a minimal amount of a more polar solvent such as diethyl ether, ethyl acetate, or tetrahydrofuran can be added. The DASA is more soluble in these more polar solvents, so care must be taken not to add too much. This slurry can then be sonicated and then filtered. Since the starting aniline causes decomposition of the product DASA, it is imperative that all of the aniline be removed. In some cases, especially those with dimethyl barbituric acid, the resulting DASA is more soluble than the starting furan adduct. In these cases, excess aniline can be added to drive the reaction further to completion. Still, losses must be taken in to fully remove the furan adduct. Unfortunately, the less electron rich anilines tend to result in more soluble DASAs. This is another factor contributing to the low yield of electron poor anilines.

The basicity of the amine used determines the solvent that can be used for the synthesizing the DASA. In the case of electron poor anilines such as *N*-methylaniline (NMA), multiple equivalents of amine must be used neat. In the case of more electron rich anilines such as indolines, a slight excess of amine may be used, along with solvents like THF or methanol. Highly conjugated DASAs are rarely soluble in methanol, making it a good choice for very planar compounds with lots of π -stacking.

Despite the challenges of synthesizing the aniline DASAs, yields remain in the double digits from a 2-3 step synthesis. Both starting materials are easy to obtain in large quantities

and are inexpensive. Further, once the conditions are figured out, trituration allows for fast, easy, and scalable synthesis. Finally, their enhanced properties over 1st generation DASAs make the effort worthwhile.

3.3 Properties

3.4 Wavelength tunability

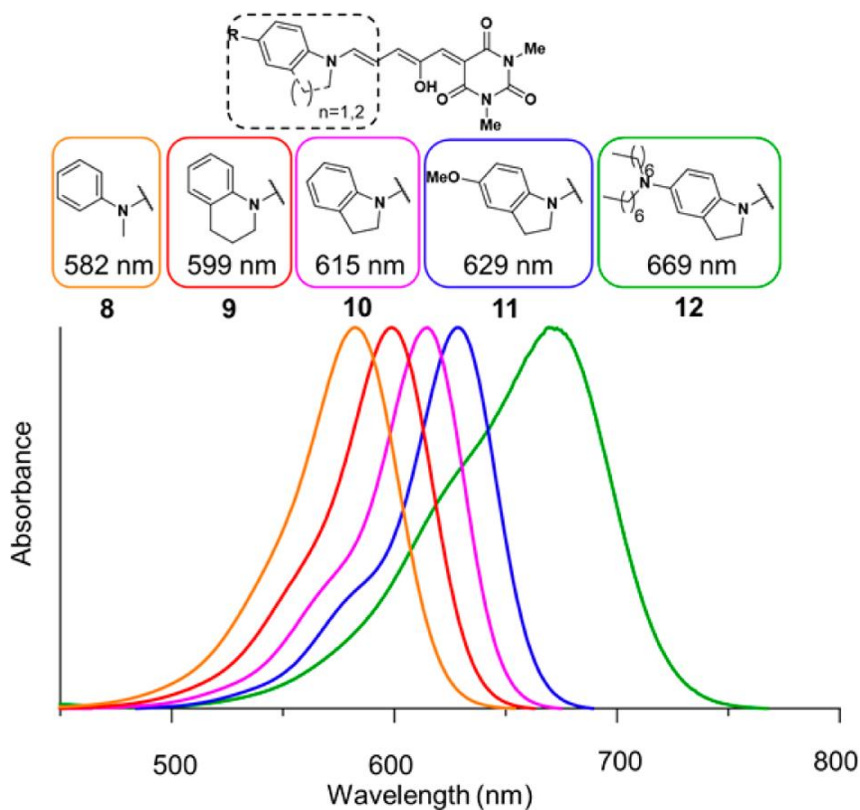


Figure 3.4: Normalized absorption profile for DASAs with barbituric acid acceptor and a range of aniline donors. Reprinted with permission from (22). Copyright (2016) American Chemical Society.

The nature of the aniline has a drastic effect on the wavelength of the DASA, as shown in figure 3.3. DASAs were synthesized with an array of donor anilines, using both Meldrum's acid and barbituric acid acceptors. Shown are wavelengths of barbituric acid DASAs.

Meldrums acid DASAs follow an identical trend, but their wavelengths are blue shifted by about 15 nm. Going from NMA to tetrahydroquinoline (THQ) to indoline barbituric acid DASAs, the wavelength increases from 582 nm to 599 nm to 615 nm. Addition of electron donating groups to the indolines causes a further increase in wavelength. The methoxy group adds 14 nm to the wavelength of the indoline, and the dialkyl amino derivative adds 54 nm. This results in DASAs with wavelengths 629 nm and 669 nm for the methoxy indolines and diheptyl amino indolines derivatives, respectively. In all, maximum absorptions can easily be tuned over a range of nearly 100 nm, a feature not often found in photoswitches.

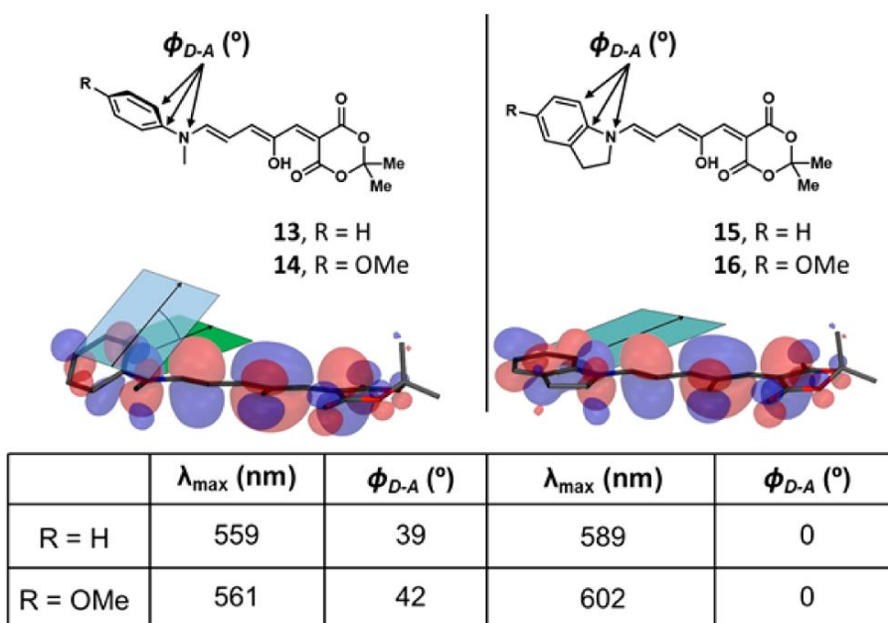


Figure 3.5: Comparing dihedral angles (from DFT calculations) of NMA to indoline donors. The relatively large dihedral angle present in DASAs with the NMA donor reduces the absorption wavelength and reduces the effect of electron donating groups have on the absorption. Reprinted with permission from (22). Copyright (2016) American Chemical Society.

Planarity of the DASA compound has two direct effects on the absorption wavelength of DASA. First, increasing planarity contributes to the red-shift in absorption from NMA to THQ to indolines. Second, the planarity of the DASA dictates how influential electron donating groups are at increasing the wavelength. This can be highlighted with the case of NMA and indolines donors. The equilibrium geometries for two NMA and two indolines derivatives were calculated, and the structures examined. NMA has an approximately 40° dihedral angle while indoline which has a 0° dihedral angle (Figure 3.4). In the case of NMA the addition of a methoxy group adds only 1 nm to the absorption maximum. This contrasts with indoline, which sees a 13 nm wavelength increase by adding a methoxy group. Clearly, planarity is critically important to increasing the wavelength through hyperconjugation.

3.5 DASA photoswitching properties

Like the secondary amine DASAs, aniline DASAs have very high molar absorptivity. This was measured for NMA, THQ, and indoline. In each case, the value was around $10^5 \text{M}^{-1} \text{cm}^{-1}$. This strong dye character is not common in photoswitches, and allows minute concentrations to be detected. This feature makes them ideal for highly sensitive sensing applications.

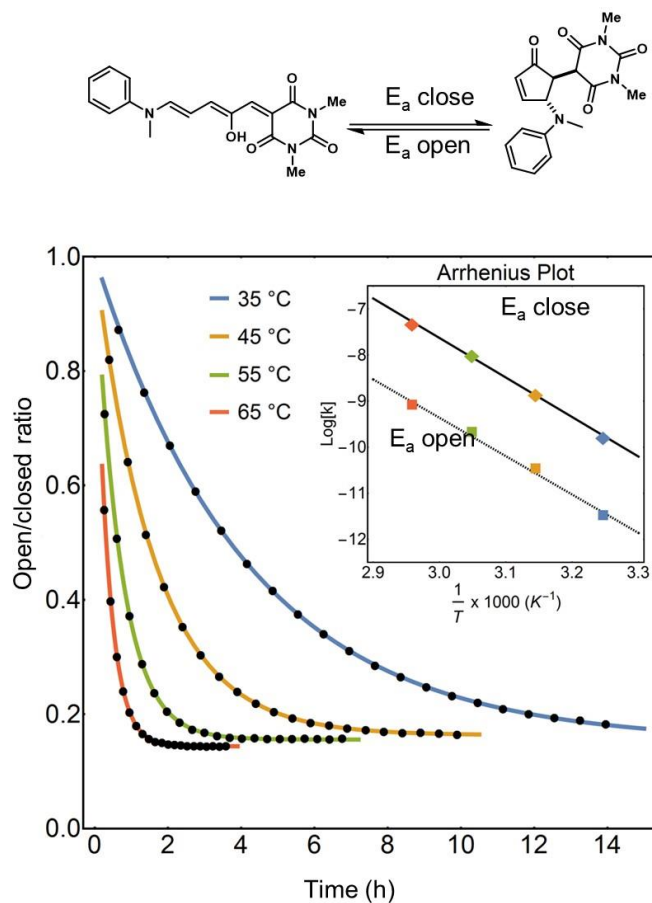


Figure 3.6: Closing kinetics of *N*-methylaniline donor barbituric acid acceptor DASA at 4 different temperatures. The Arrhenius plot is shown in the insert. Reprinted with permission from (22). Copyright (2016) American Chemical Society.

During our studies with the aniline-based DASAs, we observed that the kinetics of ring closing under light and well as the thermal relaxation back reaction were dependent on the aniline substituent use. We sought to investigate this more thoroughly using by using ^1H NMR studies to monitor the opening and closing rates of several DASAs. These experiments were performed by integration of protons unique to the open and closed forms. The data was fit to an isomer equilibrium model assuming first order rates. A sample experiment is shown in figure 3.6, and two subsequent experiments were performed with THQ and indolines

donor, barbituric acid acceptor DASAs. The results showed that the activation energies for opening and closing to be around 60-71 kJ/mol. The cyclization rates show an increasing order from THQ to NMA to indolines, with indolines being around 3.5 times faster than aniline.

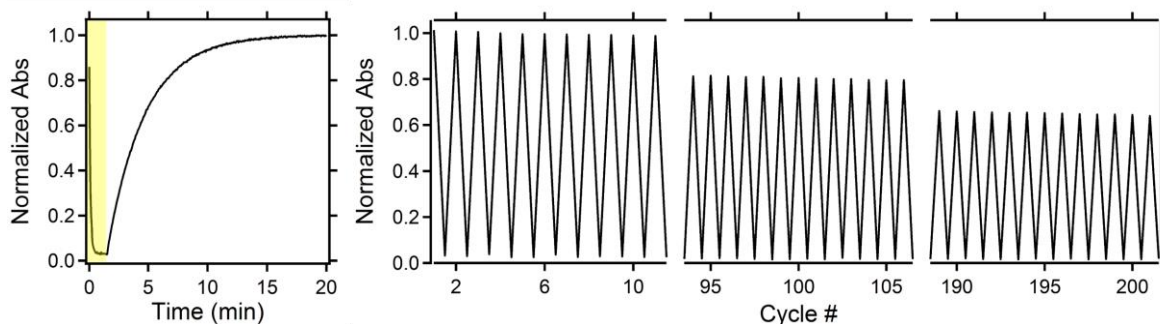


Figure 3.7: Left: sample of a single switching cycle. The light irradiation period is shaded yellow. Right: Cycling study show up to 200 cycles. Reprinted with permission from (22). Copyright (2016) American Chemical Society.

3.6 Solvent and polymer photoswitching

Reversibility and stability are further crucial performance parameters in photochromic systems, in particular for applications that rely on recyclability of the photoswitch (e.g., actuators, sensors, mechanophores, etc.) To test the robustness of these aniline-based DASA derivatives, we performed extensive cycling tests with the *p*-methoxy indoline barbituric acid derivative given its fast reversible kinetics (Figure 3.7). Pump-probe absorption spectroscopy with a broadband white light emitting diode (LED) for excitation and a heated stage for equilibration (50 °C in chlorobenzene, 67% open by ¹H NMR) were used for the cycling experiments under ambient atmospheric conditions. Figure 3.7 shows a detailed plot of absorption at λ_{max} (629 nm) during the first cycle, where a snap-shot (100 ms exposure time) of the absorption trace was taken every 5 seconds over the course of 20 minutes, with

irradiation for the first 30 seconds, then off for the remaining time. The following cycles were recorded by taking individual measurements immediately following photoswitching and thermal equilibration. Similar to the previously reported dialkyl DASAs, minimal degradation was observed after 10 cycles.¹⁹ Extending to 100 cycles then 200 cycles showed slow degradation with 80% and 60% absorbance recovery respectively with no observable change to the absorption profile. These in-depth cycling experiments highlight the stability of DASAs in the presence of oxygen and at elevated temperatures, making them excellent candidates for applications requiring a recyclable color-to-transparent photoswitch that operates under ambient conditions.

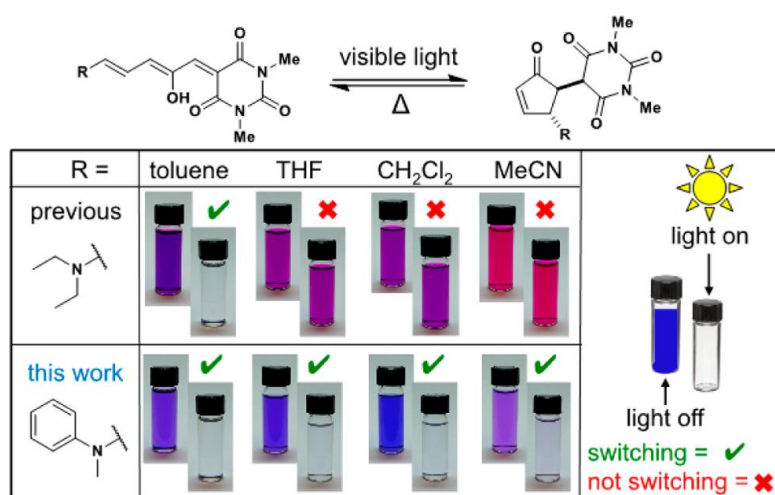


Figure 3.8: Comparison of photoswitching of dialkyl DASAs to aniline DASAs in a range of four solvents. Diethylamine DASA (top) only exhibits photoswitching only in toluene, while aniline DASA photoswitches in toluene, THF, methylene chloride, and acetonitrile. Reprinted with permission from (22). Copyright (2016) American Chemical Society.

A significant advantage of these second generation aniline-based DASAs is photoswitchability in a variety of solvents. While the previously reported dialkyl DASAs

were limited to photoswitching in non-polar solvents (e.g., toluene, xylenes, etc.), the aniline DASAs are capable of photoswitching in more polar solvents such as THF, DCM, ethyl acetate and acetonitrile. The photoswitching of *N*-methylaniline barbituric acid DASA is shown in figure 3.8. In each solvent cases, quantitative photoconversion, evident by the generation of colorless solutions and disappearances of the absorbance in UV/Vis was observed. The ability to photoswitch in a variety of solvents was dependent on the basicity of the aniline used. More basic anilines were limited to less polar solvents for easy photoswitching, while less basic anilines are able to undergo complete photocyclization in a wider range of solvents.

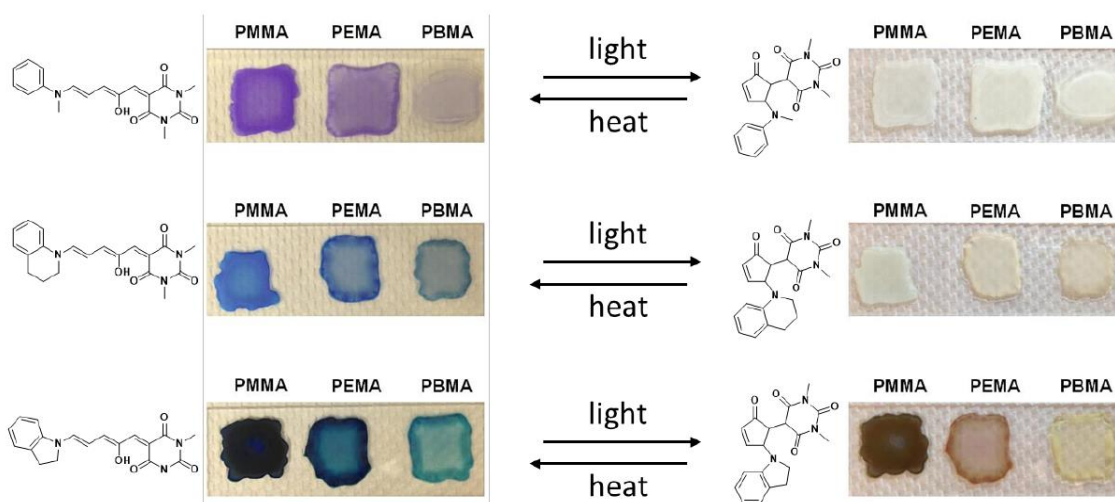


Figure 3.9: Photoswitching of three barbituric acid aniline DASAs drop cast each with three different acrylate polymers. Reprinted with permission from (22). Copyright (2016) American Chemical Society.

Photoswitching in polymer matrices is advantageous for a variety of applications. At this time, reversible photoswitching of the dialkyl DASAs in polymers has not been confirmed. Encouraged by the expanded ability of the second generation to photoswitch in a variety of solvents, we sought to test its ability to function in polymers. For our initial studies,

we simply co-dissolved NMA, THQ, and indoline barbituric acid DASAs with 3 acrylate polymers. DASA was added to solid polymer at 1% weight, then these were dissolved in methylene chloride. These solutions were then dripped onto glass slides and allowed to dry. Upon irradiation with white light, we were pleased to see that the DASAs underwent photocyclization to the closed form, and returned to the open form on heating. This preliminary study shows that aniline DASAs have the capability to photoisomerize in bulk solid polymers, which is critically important towards their use in materials applications.

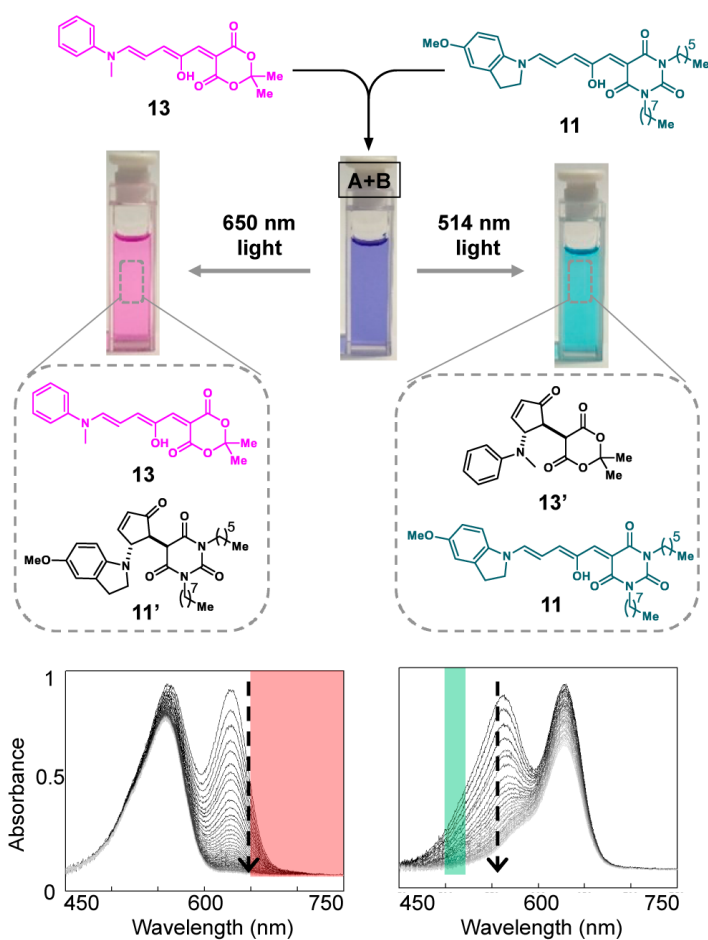


Figure 3.10: Selective photoswitching of two mixed DASAs, *N*-methylaniline Meldrum's acid 13 and indoline barbituric acid 11 using filtered broadband white LED. Compounds 11 and 13 were mixed in toluene followed by photoswitching through a 514 nm

bandpass filter to cyclize 13 or a 650 nm long-pass filter to cyclize 11. Reprinted with permission from (22). Copyright (2016) American Chemical Society.

An enabling aspect of the aniline-based DASAs is their addressability (the difference in absorption wavelengths between two different isomers or photoswitches), which relies on the inherent tunability of the absorption wavelength. This feature is critical for independently controlling two different photoswitches and holds great potential for various applications. Accordingly, we sought to demonstrate the selective switching of two different DASAs in solution (Figure 3.10). DASA with NMA donor and Meldrum's acid acceptor group (λ_{\max} , 560 nm in toluene) and DASA *p*-methoxy indoline donor and barbituric acid acceptor group (λ_{\max} , 623 nm in PhMe) were chosen based on their minimal absorption overlap. First, a longpass 650 nm filter (red light) was used to selectively switch the indoline/barbituric DASA at room temperature, converting the initially violet solution to pink. For the alternative case a 514 nm bandpass filter (green light) was used to selectively switch the NMA/Meldrum's DASA with minimal switching of the longer wavelength indoline DASA. As a result, the initial violet solution was converted to turquoise. Alternatively, by using a broad spectrum white LED light source, both DASAs switched to their colorless cyclized form at the same time.

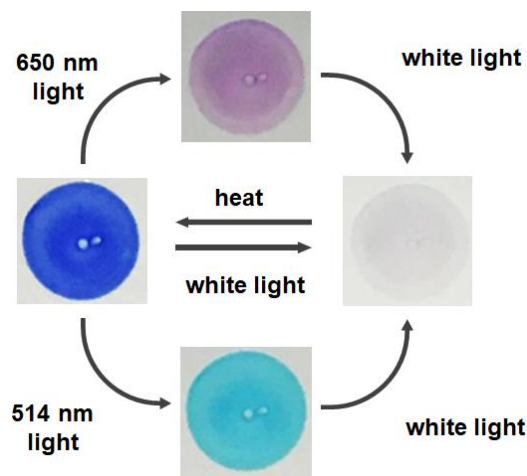


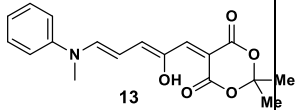
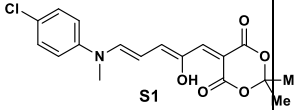
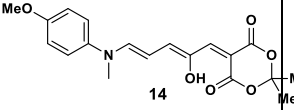
Figure 3.11: Selective switching of DASA in dropcast PMMA film. Reprinted with permission from (22). Copyright (2016) American Chemical Society.

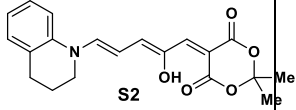
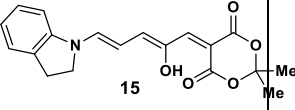
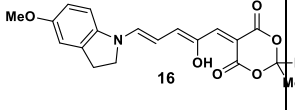
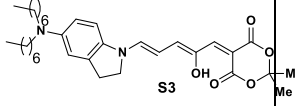
Encouraged by these results, the selective switching methodology was also investigated for the same pair-wise combination of DASA derivatives dispersed in a solid matrix of poly(methyl methacrylate) (PMMA) (Figure 3.11). The films were prepared by drop-casting a DCM solution containing 100 mg/mL PMMA and ~1 mg/mL of NMA/Meldrum's DASA and indoline/barbituric DASA onto a glass slide. Irradiation of the DASA blend in PMMA with a 650 nm LED again resulted in a distinct color change from purple to pink due to the selective photoswitching of NMA/Meldrum's. Alternatively, indoline/barbituric DASA could be selectively switched by irradiating with a 450 nm LED to give a turquoise film. Finally, broad-spectrum white light led to the cyclization of both derivatives, leaving a transparent film, while heating the sample at 50 °C for 2 min reverted the sample back to its original colored state. This clearly demonstrates for the first time the ability to selectively and reversibly switch mixtures of DASA derivatives in both solution and the solid state.

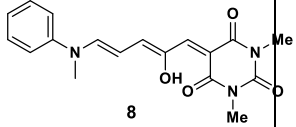
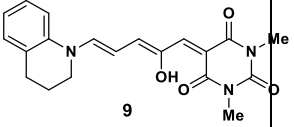
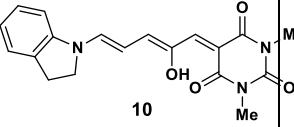
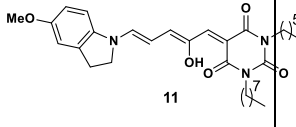
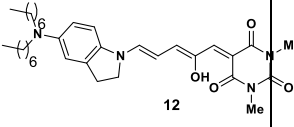
3.7 Conclusion

In conclusion, use of anilines as donors for DASAs greatly improves the properties of DASA. These photoswitches have highly tunable visible range absorptions with parts of the absorption spectra of some compounds extending to over 700 nm. The range of wavelengths is broad enough to allow two DASAs to be selectively switched in the presence of each other. Further, structure property relationships of DASA photoswitches are now far better understood. DASA can now switch in a variety of solvents, and the ease of closing can be easily tuned by careful selection of the basicity of the donor amine. Further, reversible switching in polymer matrix was demonstrated. In addition to vastly improved physical properties, the second generation DASA retains the key elements of a simple and scalable synthesis only two steps from commercially available starting materials. This second generation of DASA will significantly expand the possible applications of this novel photoswitch.

3.8 Tables of Aniline DASA properties:

DASA Compound	 13	 S1	 14
λ_{\max} CH ₂ Cl ₂ (nm)	558	558	561
% open (solvent)	2 (CD ₂ Cl ₂)	12 (CD ₂ Cl ₂)	41 (CD ₂ Cl ₂)
pKa of aniline	5.1	4.4	5.9
ϕ_{D-A} (°)	39	38	42

light induced cyclization rate (s^{-1}) *100 ^a	1.32	2.35	1.31
DASA Compound			
λ_{\max} CH ₂ Cl ₂ (nm)	575	590	603
% open (solvent)	20 (CD ₂ Cl ₂)	29 (CD ₂ Cl ₂)	70 (CD ₂ Cl ₂)
pKa of aniline	4.7	5.6	--
ϕ_{D-A} (°)	23	0	0
light induced cyclization rate (s^{-1}) *100 ^a	2.35	2.39	1.71
DASA Compound			
λ_{\max} CH ₂ Cl ₂ (nm)	648		
% open (solvent)	68 (CD ₂ Cl ₂)		
pKa of aniline	--		
ϕ_{D-A} (°)	1.2		
light induced cyclization rate (s^{-1}) *100 ^a	1.72 ^b		

DASA Compound			
λ_{\max} CH ₂ Cl ₂ (nm)	582	599	615
% open (solvent)	11 (CD ₂ Cl ₂) 16 (C ₆ D ₅ Cl) 13 ((CD ₃) ₂ SO)	19 (CD ₂ Cl ₂) 27 (C ₆ D ₅ Cl) 17 ((CD ₃) ₂ SO)	31 (CD ₂ Cl ₂) 45 (C ₆ D ₅ Cl) 38 ((CD ₃) ₂ SO)
pKa of aniline	5.1	4.7	5.6
ϕ_{D-A} (°)	38	24	0
E _{open} (kJ/mol)	69	60	63
E _{closed} (kJ/mol)	71	67	68
k _{open} (S ⁻¹), *10 ⁵	1.01 (35 °C), 2.80 (45 °C) 6.18 (55 °C), 11.16 (65 °C)	2.11 (35 °C), 3.97 (45 °C) 8.90 (55 °C), 16.05 (65 °C)	10.31 (35 °C), 22.42 (45 °C) 52.56 (55 °C), 88.08 (65 °C)
k _{close} (S ⁻¹), *10 ⁵	5.67 (35 °C), 14.34 (45 °C) 33.56 (55 °C), 66.37 (65 °C)	5.02 (35 °C), 10.27 (45 °C) 23.62 (55 °C), 50.53 (65 °C)	10.69 (35 °C), 24.94 (45 °C) 52.55 (55 °C), 108.52 (65 °C)
ϵ (M ⁻¹ cm ⁻¹)	115,000	89,000	107,000
light induced cyclization rate (s ⁻¹) *100 ^a	2.93	2.36	2.96
DASA Compound			

λ_{max} CH ₂ Cl ₂ (nm)	629	669	
% open (solvent)	58 (CD ₂ Cl ₂)	99 (CD ₂ Cl ₂)	
pK _a of aniline	--	--	
$\phi_{\text{D-A}}$ (°)	1	0	
light induced cyclization rate (s ⁻¹) *100 ^a	2.53	3.15 ^b	

3.9 Experimental

General Information

All commercially obtained reagents were used without purification, except furfural. Furfural was distilled before use and kept in a freezer. Room temperature reactions were carried out between 21–24 °C. Flash column chromatography was performed with Merck silica gel 60 (70-230 mesh). All chromatographic solvents were of ACS grade and used without further purification. Analytical thin-layer chromatography (TLC) was carried out with Merck silica gel 60 F₂₅₄ glass plates and visualized using combination of UV, bromocresol green, potassium permanganate, ceric ammonium molybdate, and iodine staining. ¹H and ¹³C NMR spectroscopy were recorded on a Varian VNMRs 600 (600 MHz for ¹H and 150 MHz for ¹³C) spectrometer or Varian Inova-500 (500 MHz for ¹H, and 125 MHz for ¹³C). Chemical shifts are reported relative to residual solvent peaks (δ 7.26 for CDCl₃ in ¹H NMR and δ 77.2 for CDCl₃ in ¹³C NMR). IR spectra were recorded on a Perkin Elmer Spectrum 2 FT/IR or a Perkin Elmer Spectrum 100 employing a Universal ATR

Sampling Accessory and are reported in terms of frequency of absorption (cm^{-1}). Mass spectral data were collected on a Micromass QTOF2 Quadrupole/Time-of Flight Tandem mass spectrometer (ESI-MS).

Time resolved optical measurements:

The photoinduced optical absorption kinetics were measured on a pump-probe setup. The pump beam was generated by a high power white light emitting diode (LED) source (Thorlabs MWWHF2) coupled into a multimode optical fiber terminated with an output collimator. The LED intensity was controlled either manually or through a digital-to-analog converter (National Instruments USB-6009) using LabVIEW. The probe beam was produced by an incandescent light bulb source (Ocean Optics LS1) coupled into a multimode fiber with an output collimator for the light delivery. The probe light was filtered by a Schott glass filter (KG3 or BG38) to suppress infrared light and attenuated by neutral density filters to mitigate DASA photoswitching by the probe light. The probe light was modulated by a shutter (Uniblitz CS25) which could be controlled manually or through a digital output port (National Instruments USB-6009) using LabVIEW. Pump and probe beams were overlapped using steering and focusing optics at a 90° angle inside a sample holder, which allowed for a 10×10 mm rectangular spectrophotometer cells that was connected to a circulating bath for temperature control. Additionally the solutions were stirred during the measurements by a miniature stirring plate inserted into the sample holder (Starna Cells SCS 1.11). The sample holder was placed into a metal enclosure to prevent exposure to ambient light. Both pump and probe beams were nearly collimated inside the cell with a diameter of about 2 mm. The pump beam was blocked after passing through the sample and the probe beam was directed by a system of lenses onto an input slit of a spectrometer (Princeton Instruments Acton SP 2150) equipped with a charge coupled device (CCD) detector (Andor Idus DV420AOE),

which acquired spectra of the probe light. The CCD camera was connected to a PC via USB port. The experiment was controlled by a National Instrument LabVIEW program which collected the probe light spectra, determined sample optical absorption spectra, controlled pump and probe light sources, and stored the data on the computer hard drive according to the experimental protocol. In addition to the 2 beam measurements, the photoinduced optical absorption kinetics were studied in a single beam degenerate configuration by attenuating the pump beam with neutral density filters, after passing through the sample, and directed into the spectrometer.

DFT Calculations:

Density functional theory (DFT) calculations at the B3LYP/6-31G(d) level were performed on aniline DASA variants to determine the character of the frontier orbitals, the dihedral angle between the donor and acceptor groups, and estimate the peak optical absorption. All calculations were performed with the Gaussian 09 software. Time-dependent DFT methods as well as larger basis sets and different hybrid functionals were also tested but gave an ordering of the HOMO-LUMO gaps in the DASA variants which was inconsistent with the absorption spectra results. Solvent effects were considered using a Polarizable Continuum Model, but were found to result in at most a 1% change in gap energies, very small compared to the variation in DFT methods. While a B3LYP/6-31G(d) calculation provides accurate ordering and separation of the absorption peaks, their absolute value is systematically overpredicted by 0.4 eV. All calculated values for the absorbance peaks were adjusted by this amount. While not truly predictive, this manner of empirical shift has been widely used in previous literature to obtain accurate HOMO-LUMO gaps and optical excitation energies.²⁴⁻²⁷

pKa Values:

The method for pKa determination was adopted from a previous report²⁸. Briefly, ~ 0.1 g of amine was combined with 50 g of deionized water. This solution was then titrated, while stirring, with 1 M HCl while monitoring the pH values. The amount of acid added was plotted vs. the pH, and the pH at the inflection point in this curve was taken as the amine's pKa. The pKa values agreed within +/- 0.2 for three trials. Literature pKa values for each amine were in agreement with ours within the error of our experiments.²⁹

NMR Procedures:

Although the DASA adducts are synthesized and isolated in the open triene form, the NMR characterization was often performed on the closed adducts. This was done in situations where the molecule cyclized so quickly that a clean spectrum of the open form could not be obtained. To get the spectrum of the closed form, the sample was dissolved in deuterated solvent then placed in the NMR tube. After dissolving, the sample was exposed to visible light irradiation until the sample was clear, then the spectrum was acquired.

Synthetic Procedures



5-((2Z,4E)-2-hydroxy-5-(methyl(phenyl)amino)penta-2,4-dien-1-ylidene)-2,2-dimethyl-1,3-dioxane-4,6-dione (13). To a 1 dram vial was added Meldrum's acid furan¹⁹ adduct **4** (106 mg, 0.48 mmol), followed by *N*-methylaniline (104 μ L, 0.96 mmol). The reaction was stirred vigorously for 1 h before filtering and washing the filtrate with hexanes. The resulting solid was taken up into tetrahydrofuran, sonicated, and diluted with diethyl ether before filtering to obtain a blue powder (62 mg yield, 39 %). NMR characterization is of the cyclized DASA. ¹H NMR (400 MHz, Chloroform-*d*) δ 7.64 (d, *J* = 5.9 Hz, 1H), 7.23

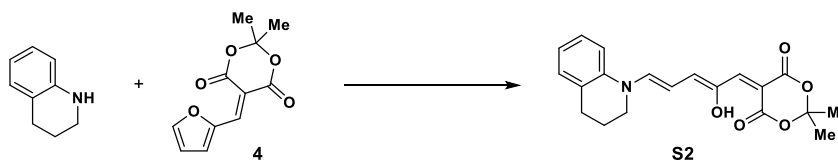
(t, $J = 7.9$ Hz, 1H), 6.83 (d, $J = 8.1$ Hz, 2H), 6.78 (t, $J = 7.4$ Hz, 1H) 6.44 (d, $J = 5.9$ Hz, 1H), 5.56 (s, 1H), 3.91 (s, 1H), 3.48 (s, 1H), 2.78 (s, 3H), 1.68 (d, $J = 3.5$ Hz, 6H). ^{13}C NMR (125 MHz, Chloroform-*d*) δ 202.2, 164.6, 164.4, 163.3, 149.2, 134.4, 129.7, 118.8, 113.8, 105.7, 63.1, 47.9, 47.83, 44.3, 44.3, 32.4, 32.4, 28.10, 27.03. IR (ATR) 3042, 2982, 2938, 1685, 1607, 1584, 1470, 1388, 1342, 1265, 1229 cm^{-1} . HRMS (ESI+) m/z 352.1168, calc. 352.1155 for $[\text{M} + \text{Na}]^+$



5-((2Z,4E)-5-((4-chlorophenyl)(methyl)amino)-2-hydroxypenta-2,4-dien-1-ylidene)-2,2-dimethyl-1,3-dioxane-4,6-dione : To a 1 dram vial was added Meldrum's acid furan adduct **4** (315 mg, 1.41 mmol), followed by 4-chloro-*N*-methylaniline (340 μL , 2.84 mmol). The reaction was stirred until complete (24 h). To the crude mixture, 1mL of DCM was added and this was sonicated for 1 minute. The mixture was added to vigorously stirring hexanes. The pure product was filtered, washed with hexanes, redissolved in DCM, and run through a plug of silica using DCM:MeOH (100:0 to 90:10) to afford a purple solid (191 mg, 37%). NMR characterization is of the cyclized DASA. ^1H NMR (500 MHz, Chloroform-*d*) δ 7.65 (dd, $J = 5.9, 2.0$ Hz, 1H), 7.27 (s, 1H), 7.24 – 7.15 (d, $J = 9.1$ Hz 2H), 6.79 – 6.72 (d, $J = 9.1$ Hz, 2H), 6.48 (dd, $J = 5.9, 2.2$ Hz, 1H), 5.47 (dt, $J = 4.3, 2.3$ Hz, 1H), 4.02 (s, 1H), 3.48 (dd, $J = 4.2, 2.0$ Hz, 1H), 2.78 (s, 3H), 1.72 (d, $J = 13.5$ Hz, 6H). ^{13}C NMR (125 MHz, Chloroform-*d*) δ 201.7, 164.5, 164.1, 162.8, 147.8, 134.3, 129.3, 123.5, 115.0, 105.7, 105.0, 63.2, 47.7, 44.2, 32.4, 28.0, 27.0. IR (ATR) 2884, 1781, 1742, 1713, 1596, 1497, 1470, 1325, 1275, 1201, 1107, 928, 811 cm^{-1} . HRMS (ESI+) m/z 386.0785, calc. 386.0766 for $[\text{M} + \text{Na}]^+$



5-((2Z,4E)-2-hydroxy-5-((4-methoxyphenyl)(methyl)amino)penta-2,4-dien-1-ylidene)-2,2-dimethyl-1,3-dioxane-4,6-dione (14): To a 1 dram vial was added Meldrum's acid furan adduct **4** (222 mg, 1.0 mmol), followed by *p*-methoxy-*N*-methylaniline (274 mg, 2.0 mmol). The reaction became completely solid after 15 minutes. 1 mL of THF was added to dissolve the residue. This was then dripped into 10 mL rapidly stirring Et₂O. The resulting blue crystals were then filtered to yield 130 mg of product (36% yield). ¹H NMR (400 MHz, Chloroform-*d*) δ 11.24 (s, 1H), 7.51 (d, *J* = 12.5 Hz, 1H), 7.25 – 7.12 (m, 3H), 6.96 (d, *J* = 8.6 Hz, 2H), 6.76 (d, *J* = 12.2 Hz, 1H), 3.82 (s, 3H), 3.50 (s, 3H), 1.69 (s, 6H). ¹³C NMR (201 MHz, Chloroform-*d*) δ 202.3, 166.8, 164.6, 164.3, 163.4, 153.3, 152.8, 148.0, 146.3, 143.4, 139.1, 134.1, 122.5, 116.8, 115.0, 114.9, 103.9, 103.8, 77.3, 65.2, 55.7, 55.6, 46.9, 44.2, 38.6, 33.1, 28.0, 26.9, 26.9. IR (ATR) 2990, 2937, 2838, 1705, 1613, 1484, 1455, 1340, 1229, 1199, 1146, 1103, 1037, 1006 cm⁻¹. HRMS (ESI+) *m/z* 382.1307, calc. 382.1261 for [M + Na]⁺



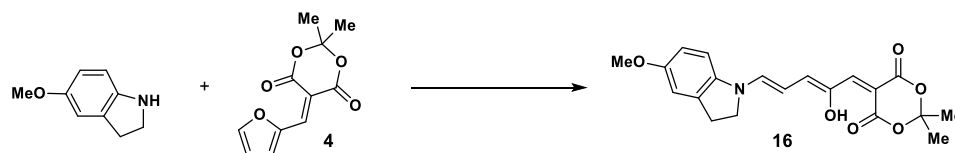
5-((2Z,4E)-5-(3,4-dihydroquinolin-1(2H)-yl)-2-hydroxypenta-2,4-dien-1-ylidene)-2,2-dimethyl-1,3-dioxane-4,6-dione (S2): To a 1 dram vial was added Meldrum's acid furan adduct **4** (222 mg, 1.0 mmol) and tetrahydroquinoline (250 μL, 2 mmol). This was allowed to react neat for 4 hours, monitoring by TLC. Then 1 mL THF was added, the mixture

sonicated, filtered, and rinsed with minimal THF then Et₂O to yield a blue solid, (183 mg, 51%). NMR characterization is of the cyclized DASA. ¹H NMR (400 MHz, Chloroform-*d*) δ 7.64 (dd, *J* = 5.9, 2.0 Hz, 1H), 7.00 (m, 2H), 6.71 (d, *J* = 8.7 Hz, 1H), 6.64 (t, *J* = 7.3 Hz, 1H), 6.45 (dd, *J* = 5.9, 2.2 Hz, 1H), 5.65 (m, 1H), 4.08 (s, 1H), 3.62 (dd, *J* = 4.3, 1.9 Hz, 1H), 3.23 (m, 1H), 3.12 (m, 1H), 2.83 – 2.72 (m, 2H), 1.97 (m, 2H), 1.76 (d, *J* = 6.7 Hz, 6H). ¹³C NMR (100 MHz, Chloroform-*d*) δ 202.4, 164.8, 164.5, 163.7, 144.8, 134.3, 130.5, 127.3, 123.9, 117.6, 110.5, 105.8, 60.1, 47.8, 44.5, 43.4, 28.3, 27.1, 22.1. IR (ATR) 2947, 1687, 1624, 1480, 1461, 1388, 1332, 1256, 1195, 1125, 1109, 1002, 926 cm⁻¹. HRMS (ESI+) *m/z* 378.1329, calc. 378.1312 for [M + Na]⁺

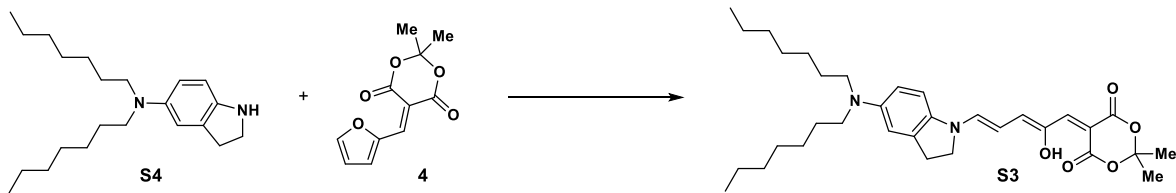


5-((2Z,4E)-2-hydroxy-5-(indolin-1-yl)penta-2,4-dien-1-ylidene)-2,2-dimethyl-1,3-dioxane-4,6-dione (15): To a 1-dram vial was added a solution of Meldrum's acid furan adduct **4** (111.1 mg, 0.50 mmol) in 0.5 mL of dichloromethane. Upon completion of reaction (2 h, monitored by TLC), 1 mL of THF was added and sonicated for 1 min. An additional 1 mL of Et₂O was added and sonicated for 1 min. The heterogeneous mixture was then added to vigorously stirring hexane (50 mL) dropwise. The product was filtered and washed with hexane to afford blue crystals (110 mg, 65 % yield). NMR characterization is of the cyclized DASA. ¹H NMR (500 MHz, Methylene Chloride-*d*₂) δ 7.64 (dt, *J* = 6.0, 1.8 Hz, 1H), 7.13 – 7.06 (m, 1H), 7.01 (t, *J* = 7.6 Hz, 1H), 6.67 (t, *J* = 7.5 Hz, 1H), 6.50 (d, *J* = 7.8 Hz, 1H), 6.41 (dt, *J* = 6.0, 1.8 Hz, 1H), 5.20 (dq, *J* = 3.9, 2.0 Hz, 1H), 4.14 (s, 1H), 3.64 (tq, *J* = 4.8, 2.9, 2.5 Hz, 1H), 3.53 (qd, *J* = 8.3, 1.6 Hz, 1H), 3.27 (qd, *J* = 8.4, 1.6 Hz, 1H), 3.00 (t, *J* = 8.4 Hz,

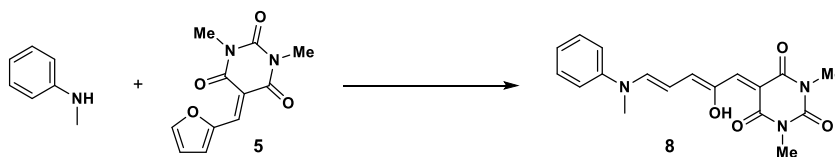
2H), 1.77 (s, 6H). ^{13}C NMR (125 MHz, Methylene Chloride- d_2) δ 202.2, 164.3, 162.2, 134.6, 130.3, 127.3, 125.0, 118.7, 106.7, 105.7, 60.3, 47.7, 46.6, 44.6, 28.1, 28.0, 26.7, 26.6. IR (ATR) 3063, 2980, 1696, 1608, 1485, 1459, 1344, 1276, 1197, 1148, 981 cm^{-1} . HRMS (ESI+) m/z 364.1156, calc. 364.1155 for $[\text{M} + \text{Na}]^+$



5-((2Z,4E)-2-hydroxy-5-(5-methoxyindolin-1-yl)penta-2,4-dien-1-ylidene)-2,2-dimethyl-1,3-dioxane-4,6-dione (16): 5-methoxyindoline³⁰ (100 mg, 0.670 mmol) was added to Meldrum's acid furan adduct **4** (149 mg, 0.670 mg) stirring in 10 mL methanol. Upon completion of reaction (monitored by TLC), the product was filtered and rinsed with additional methanol to yield 225 mg (90%) of product as blue crystals. ^1H NMR (400 MHz, Chloroform- d) δ 11.41 (s, 1H), 7.64 (d, $J = 12.4$ Hz, 1H), 7.22 (s, 1H), 7.05 (d, $J = 8.6$ Hz, 1H), 6.88 – 6.65 (m, 4H), 6.14 (t, $J = 12.3$ Hz, 1H), 4.13 (t, $J = 7.9$ Hz, 2H), 3.82 (s, 3H), 3.30 (t, $J = 8.0$ Hz, 2H), 1.72 (s, 6H). Due to low solubility, a ^{13}C NMR spectrum for compound **16** was unable to be obtained. DATA. IR (ATR) 3068, 2997, 2934, 2834, 1689, 1610, 1486, 1458, 1338, 1261, 1187, 1126, 984 cm^{-1} . HRMS (ESI+) m/z 394.1274, calc. 394.1261 for $[\text{M} + \text{Na}]^+$



5-((2Z,4E)-5-(5-(diheptylamino)indolin-1-yl)-2-hydroxypenta-2,4-dien-1-ylidene)-2,2-dimethyl-1,3-dioxane-4,6-dione (S3): *N,N*-diheptylindolin-5-amine (100 mg, 0.30 mmol) was added to a stirring flask containing Meldrum's acid furan adduct **4** (67.2 mg, 0.30 mmol) in 15 mL of methanol. After monitoring the reaction by TLC, the product was filtered and rinsed with methanol to give 125 mg of (75% yield) crystals. ¹H NMR (500 MHz, Chloroform-*d*) δ 11.50 (s, 1H), 7.69 (d, *J* = 12.1 Hz, 1H), 7.07 (d, *J* = 9.0 Hz, 1H), 6.96 (s, 1H), 6.76 (d, *J* = 12.6, 1H), 6.54 (dd, *J* = 9.0, 2.5 Hz, 1H), 6.49 (d, *J* = 2.4 Hz, 1H), 6.18 (t, *J* = 12.3 Hz, 1H), 4.12 (t, *J* = 7.7 Hz, 2H), 3.26 (t, *J* = 7.7 Hz, 6H), 1.72 (s, 6H), 1.55 (q, *J* = 7.2 Hz, 4H), 1.30 (m, 16H), 0.89 (t, *J* = 6.8 Hz, 6H). ¹³C NMR (125 MHz, Chloroform-*d*) δ 167.2, 165.4, 148.2, 147.9, 145.7, 142.9, 136.7, 135.2, 130.4, 112.1, 111.9, 108.1, 105.3, 103.3, 90.1, 51.6, 50.0, 32.0, 29.3, 27.9, 27.3, 27.2, 26.7, 22.7, 14.2. IR (ATR) 2922, 2852, 1601, 1490, 1462, 1345, 1275, 1189, 1139, 1099, 987, 919, 794, 766 cm⁻¹. HRMS (ESI+) *m/z* 575.3436, calc. 575.3461 for [M + Na]⁺



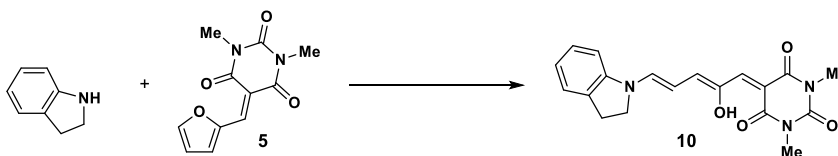
5-((2Z,4E)-2-hydroxy-5-(methyl(phenyl)amino)penta-2,4-dien-1-ylidene)-1,3-dimethylpyrimidine-2,4,6(1H,3H,5H)-trione (8): To a 1 dram vial was added barbituric acid furan adduct **5** (140 mg, 0.59 mmol), followed by *N*-methylaniline (520 μL, 4.78

mmol). Stirred vigorously for 3h, filtered and washed with ether to obtain a blue powder (130 mg, 65%). NMR characterization is of the cyclized DASA. ¹H NMR (500 MHz, Chloroform-*d*) δ 7.69 (dd, *J* = 5.9, 2.0 Hz, 1H), 7.21 (t, *J* = 7.92 Hz 2H), 6.85 – 6.76 (m, 3H), 6.46 (dd, *J* = 5.9, 2.3, 1H), 5.55 (s, 1H), 3.99 (s, 1H), 3.57 (dd, *J* = 4.2, 1.9 Hz, 1H), 3.30 (s, 3H), 3.00 (s, 3H), 2.77 (s, 3H). ¹³C NMR (125 MHz, Chloroform-*d*) δ 202.6, 167.0, 166.7, 163.2, 150.8, 134.4, 129.4, 114.0, 63.8, 48.9, 46.6, 32.2, 28.7, 28.6. IR (ATR) 2943, 2527, 1701, 1669, 1631, 1578, 1482, 1463, 1416, 1351, 1310, 1234, 1207, 1153, 1118, 1025, 951, 772, 751 cm⁻¹. HRMS (ESI+) *m/z* 364.1282, calc. 364.1268 for [M + Na]⁺



5-((2Z,4E)-5-(3,4-dihydroquinolin-1(2H)-yl)-2-hydroxypenta-2,4-dien-1-ylidene)-1,3-dimethylpyrimidine-2,4,6(1H,3H,5H)-trione (9): To a 1-dram vial, barbituric acid furan adduct¹⁹ **5** (158 mg, 0.67 mmol) and 0.17 mL of 1,2,3,4-tetrahydroquinoline (0.17 mL, 1.347 mmol) were added and stirred at room temperature overnight (18 h). After confirming the completion of reaction by TLC, 1 mL of dichloromethane was added and sonicated for 1 min. The mixture was then added to vigorously stirring hexane (50 mL) dropwise. The product was filtered and washed with hexane and subject to a short plug of silica with dichloromethane as the eluent. The solvent was removed in vacuo and blue crystals (75 mg, 30% yield) were obtained. NMR characterization is of the cyclized DASA. ¹H NMR (500 MHz, Chloroform-*d*) δ 7.66 (dd, *J* = 6.0, 2.1 Hz, 1H), 6.97 (d, *J* = 7.60 Hz, 1H), 6.92 (t, *J* = 7.75 Hz, 1H), 6.68 (d, *J* = 8.3 Hz, 1H), 6.62 (td, *J* = 7.4, 1.0 Hz, 1H), 6.43 (dd, *J* = 5.9, 2.3 Hz, 1H), 5.68 (s, 1H), 4.03 (d, *J* = 2.0 Hz, 1H), 3.70 (dd, *J* = 4.1, 2.0 Hz, 1H), 3.34 (s, 3H),

3.23 – 3.09 (m, 2H), 3.05 (s, 3H), 2.85 – 2.69 (m, 2H), 2.04 – 1.89 (m, 2H). ¹³C NMR (125 MHz, Chloroform-*d*) δ 203.0, 167.1, 166.8, 163.8, 144.7, 134.1, 130.3, 126.9, 124.1, 117.5, 110.6, 61.4, 49.0, 46.8, 43.3, 28.8, 28.6, 28.1, 21.8. IR (ATR) 2937, 1674, 1640, 1598, 1541, 1495, 1455, 1417, 1368, 1311, 1259, 1218, 1201, 1005, 953, 877, 746 cm⁻¹. HRMS (ESI+) *m/z* 390.1436, calc. 390.1424 for [M + Na]⁺



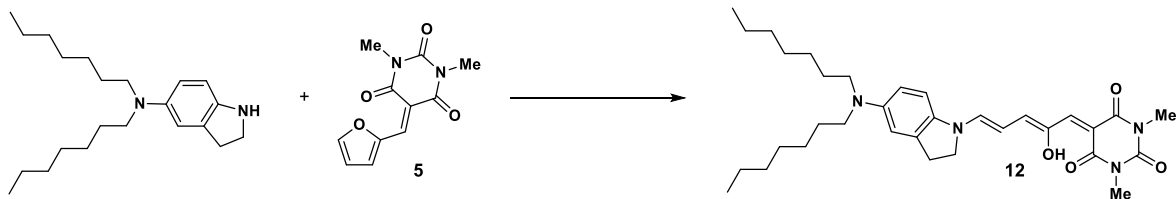
5-((2Z,4E)-2-hydroxy-5-(indolin-1-yl)penta-2,4-dien-1-ylidene)-1,3-

dimethylpyrimidine-2,4,6(1H,3H,5H)-trione (10): To a 1-dram vial, a solution of barbatunic acid furan adduct⁷ **5** (117 mg, 0.50 mmol) in 0.5 mL of dichloromethane was added, followed by indoline (59 μL, 0.53 mmol). The mixture was stirred at room temperature until the reaction was completed (monitored by TLC). The crude mixture was added with 1 mL of dichloromethane and sonicated for 1 min. The mixture was then added to vigorously stirring hexane (50 mL) dropwise. The product was filtered and washed with hexane to afford blue crystals (96.2 mg, 54% yield). NMR characterization is of the cyclized DASA. ¹H NMR (500 MHz, Methylene Chloride-*d*₂) δ 7.71 (d, *J* = 5.9, 1H), 7.11 (d, *J* = 7.3 Hz, 1H), 6.98 (t, *J* = 7.6 Hz, 1H), 6.68 (t, *J* = 7.2 Hz, 1H), 6.47 – 6.39 (m, 2H), 5.39 – 5.27 (m, 2H), 4.09 (s, 1H), 3.74 (dt, *J* = 3.9, 1.7 Hz, 1H), 3.49 (q, *J* = 8.4 Hz, 1H), 3.39 – 3.27 (m, 4H), 3.10 (d, *J* = 1.7 Hz, 3H), 3.02 (dq, *J* = 15.8, 8.7, 8.2 Hz, 2H). ¹³C NMR (125 MHz, Methylene Chloride-*d*₂) δ 203.0, 167.0, 162.7, 134.4, 130.3, 127.1, 125.0, 118.5, 106.3, 60.4, 47.4, 47.3, 47.2, 28.6, 28.4, 28.2. IR (ATR) 2931, 1682, 1602, 1546, 1500, 1457, 1417, 1365,

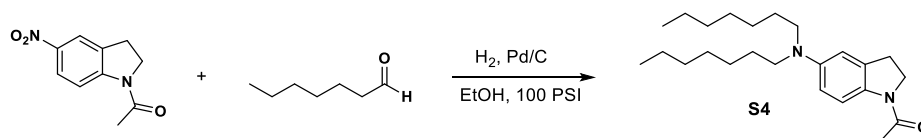
1277, 1221, 1152, 1082, 749 cm^{-1} . HRMS (ESI+) m/z 376.1265, calc. 376.1268 for $[\text{M} + \text{Na}]^+$



(E)-1-hexyl-5-((2Z,4E)-2-hydroxy-5-(5-methoxyindolin-1-yl)penta-2,4-dien-1-ylidene)-3-octylpyrimidine-2,4,6(1H,3H,5H)-trione (11): 5-methoxyindoline³⁰ (100 mg, 0.67 mmol) was added to barbituric acid furan adduct⁷ **5** (270 mg, 0.67 mmol) stirring in 2 mL THF. Upon completion of reaction (monitored by TLC), 1 mL DCM added, then the reaction product was dripped into 10 mL MeOH, filtered and rinsed with additional methanol to yield 109 mg (29%) of product as blue crystals. ¹H NMR (400 MHz, Chloroform-*d*) δ 12.59 (s, 1H), 7.59 (d, $J = 12.5$ Hz, 1H), 7.27 (s, 1H), 7.00 (d, $J = 8.4$ Hz, 1H), 6.80 (m, 2H), 6.69 (d, $J = 12.3$ Hz, 1H), 6.13 (t, $J = 12.4$ Hz, 1H), 4.12 (t, $J = 8.0$ Hz, 2H), 3.90 (t, $J = 7.7$ Hz, 4H), 3.80 (s, 3H), 3.28 (t, $J = 8.0$ Hz, 2H), 1.37 – 1.19 (m, 20H), 0.87 (m, 6H). ¹³C NMR (100 MHz, Chloroform-*d*) δ 167.01, 166.6, 164.7, 162.7, 158.1, 151.0, 150.6, 147.6, 134.2, 113.8, 111.3, 100.8, 55.8, 55.7, 31.8, 31.5, 29.3, 29.2, 28.1, 28.8, 27.8, 27.7, 27.6, 27.0, 26.6, 22.6, 14.0. IR (ATR) 3383, 3222, 2956, 2922, 2853, 2414, 1694, 1611, 1587, 1543, 1451, 1416, 1357, 1332, 1277, 1223, 1206, 1189, 1122, 1087, 1036, 952, 896, 778 cm^{-1} . HRMS (ESI+) m/z 574.3242, calc. 574.3251 for $[\text{M} + \text{Na}]^+$

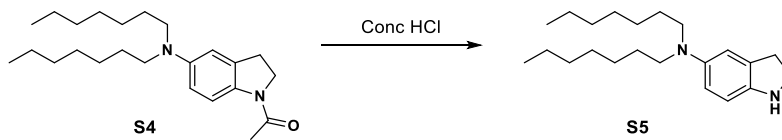


5-((2Z,4E)-5-(5-(diheptylamino)indolin-1-yl)-2-hydroxypenta-2,4-dien-1-ylidene)-1,3-dimethylpyrimidine-2,4,6(1H,3H,5H)-trione (12): *N,N*-diheptylindolin-5-amine (100 mg, 0.30 mmol) was added to a stirring flask containing barbituric acid furan adduct⁷ **5** (70mg, 0.30 mmol) in 15 mL of methanol. After monitoring the reaction by TLC, the product was filtered and rinsed with methanol to give 90 mg of (53% yield) crystals. ¹H NMR (500 MHz, Chloroform-*d*) δ 12.61 (s, 1H), 7.60 (d, *J* = 12.0 Hz, 1H), 6.93 (d, *J* = 8.8 Hz, 1H), 6.87 (s, 1H), 6.72 (d, *J* = 12.6 Hz, 1H), 6.47 – 6.37 (m, 2H), 6.17 (t, *J* = 12.3 Hz, 1H), 4.13 (t, *J* = 7.5 Hz, 2H), 3.31 – 3.13 (m, 12H), 1.85 (s, 2H), 1.58 (s, 4H), 1.56 (s, 4H), 1.46 – 1.17 (m, 18H), 0.89 (t, *J* = 6.7 Hz, 6H). ¹³C NMR (125 MHz, Chloroform-*d*) δ 164.7, 163.2, 151.7, 148.5, 148.0, 147.0, 142.9, 135.5, 134.6, 130.2, 112.1, 111.4, 107.6, 106.5, 97.3, 51.6, 50.1, 32.0, 32.0, 29.3, 28.4, 28.2, 27.9, 27.4, 27.2, 22.7, 14.2. IR (ATR) 3376, 295, 2854, 1691, 1611, 1580, 1424, 1348, 1274, 1233, 1196, 1145, 1099, 833, 773, 752 cm⁻¹. HRMS (ESI+) *m/z* 587.3563, calc. 587.3568 for [M + Na]⁺



1-(5-(diheptylamino)indolin-1-yl)ethan-1-one (S4): 1-acetyl-5-nitroindoline (720 mg, 3.49 mmol) and heptanal (1.5 mL, 10.47 mmol), 80 mg 10% Pd/C, were combined in a flask with 30 mL EtOH. This was then hydrogenated in a bomb at ~100PSI. After running

overnight, the reaction was filtered through celite and the solvent was removed under reduced pressure. The crude product was purified with flash column chromatography using 20-35% ethyl acetate in hexanes as eluent. (1.09g, 84% yield). ^1H NMR (500 MHz, Chloroform-*d*) δ 8.04 (d, $J = 8.7$ Hz, 1H), 6.53 – 6.40 (m, 2H), 3.98 (t, $J = 8.3$ Hz, 2H), 3.21 (q, $J = 7.7$ Hz, 4H), 3.13 (t, $J = 8.3$ Hz, 2H), 2.17 (s, 3H), 1.55 (m, 4H), 1.31 (m, 16H), 0.89 (t, $J = 7.0$ Hz, 6H). ^{13}C NMR (125 MHz, Chloroform-*d*) δ 167.3, 145.6, 133.0, 132.5, 117.9, 111.1, 108.7, 51.7, 51.6, 48.9, 48.1, 32.0, 29.3, 28.7, 27.7, 27.4, 27.3, 24.3, 23.9, 22.7, 14.2. IR (ATR) 2923, 2854, 1651, 1619, 1583, 1696, 1466, 1404, 1369, 1119, 1026, 802, 724 cm^{-1} . HRMS (ESI+) m/z 372.3136, calc. 372.3141 for $[\text{M} + \text{Na}]^+$



N,N-diheptylindolin-5-amine (S5): 100 mg of **S4** was placed in a flask with 1 mL of concentrated HCl. This was then heated to reflux for one hour. After being allowed to cool, the reaction was carefully basified with saturated K_2CO_3 , then extracted with dichloromethane. This was then dried over Na_2SO_4 , and the solvent removed under reduced pressure. Product darkens rapidly upon exposure to air. The crude material was used without further purification.

3.10 References

- (1) Rosario, R.; Gust, D.; Hayes, M.; Jahnke, F.; Springer, J.; Garcia, A. A. *Langmuir* **2002**, *18* (21), 8062.
- (2) Schöller, K.; Küpfer, S.; Baumann, L.; Hoyer, P. M.; De Courten, D.; Rossi, R. M.; Vetushka, A.; Wolf, M.; Bruns, N.; Scherer, L. J. *Adv. Funct. Mater.* **2014**, *24* (33), 5194.
- (3) Kundu, P. K.; Samanta, D.; Leizrowice, R.; Margulis, B.; Zhao, H.; Börner, M.; Udayabhaskararao, T.; Manna, D.; Klajn, R. *Nat. Chem.* **2015**, *7* (8), 646.
- (4) BOUAS-LAURENT, H.; DÜRR, H. *IUPAC Tech. Rep.* **2001**, *73* (4), 639.
- (5) Avci, P.; Gupta, A.; Sadasivam, M.; Vecchio, D.; Pam, Z.; Pam, N.; Hamblin, M. R. *Semin. Cutan. Med. Surg.* **2013**, *32* (1), 41.
- (6) Bléger, D.; Hecht, S. In *Photon-Working Switches*; Yokoyama, Y., Nakatani, K., Eds.; Springer Japan: Tokyo, 2017; pp 93–114.
- (7) Ayub, K.; Mitchell, R. H. *J. Org. Chem.* **2014**, *79* (2), 664.
- (8) Mitchell, R. H.; Ward, T. R.; Chen, Y.; Wang, Y.; Weerawarna, S. A.; Dibble, P. W.; Marsella, M. J.; Almutairi, A.; Wang, Z. **2003**, No. 6, 5885.
- (9) Broman, S. L.; Petersen, M. Å.; Tortzen, C. G.; Kadziola, A.; Kilså, K.; Nielsen, M. B. *J. Am. Chem. Soc.* **2010**, *132* (26), 9165.
- (10) Daub, J.; Knöchel, T.; Mannschreck, A. *Angew. Chemie (Int. ed.)* **1984**, *23* (12), 960.
- (11) Hatano, S.; Horino, T.; Tokita, A.; Oshima, T.; Abe, J. *J. Am. Chem. Soc.* **2013**, *135* (8), 3164.
- (12) Yamaguchi, T.; Kobayashi, Y.; Abe, J. *J. Am. Chem. Soc.* **2015**, *138*, 906.
- (13) Yang, Y.; Hughes, R. P.; Aprahamian, I. *J. Am. Chem. Soc.* **2014**, *136* (38), 13190.

- (14) Yang, Y.; Hughes, R. P.; Aprahamian, I. *J. Am. Chem. Soc.* **2012**, *134* (37), 15221.
- (15) Bléger, D.; Schwarz, J.; Brouwer, A. M.; Hecht, S. *J. Am. Chem. Soc.* **2012**, *134* (51), 20597.
- (16) Siewertsen, R.; Neumann, H.; Buchheim-Stehn, B.; Herges, R.; Näther, C.; Renth, F.; Temps, F. *J. Am. Chem. Soc.* **2009**, *131* (43), 15594.
- (17) Dong, M.; Babalhavaeji, A.; Samanta, S.; Beharry, A. A.; Woolley, G. A. *Acc. Chem. Res.* **2015**, *48* (10), 2662.
- (18) Mason, B. P.; Whittaker, M.; Hemmer, J.; Arora, S.; Harper, A.; Alnemrat, S.; Mceachen, A.; Helmy, S.; Read de Alaniz, J.; Hooper, J. P. *Appl. Phys. Lett.* **2016**, *108*, 41906.
- (19) Helmy, S.; Leibfarth, F. A.; Oh, S.; Poelma, J. E.; Hawker, C. J.; Read De Alaniz, J. *J. Am. Chem. Soc.* **2014**, *136* (23), 8169.
- (20) Lerch, M. M.; Wezenberg, S. J.; Szymanski, W.; Feringa, B. L. *J. Am. Chem. Soc.* **2016**, *138*, 6344.
- (21) Helmy, S.; Oh, S.; Leibfarth, F. A.; Hawker, C. J.; Read De Alaniz, J. *J. Org. Chem.* **2014**, *79* (23), 11316.
- (22) Hemmer, J. R.; Poelma, S. O.; Treat, N.; Page, Z. A.; Dolinski, N. D.; Diaz, Y. J.; Tomlinson, W.; Clark, K. D.; Hooper, J. P.; Hawker, C.; Read De Alaniz, J. *J. Am. Chem. Soc.* **2016**, *138* (42), 13960.
- (23) ŠAFÁŘ, P.; POVAŽANEC, F.; PRÓNAYOVÁ, N.; BARAN, P.; KICKELBICK, G.; KOŽÍŠEK, J.; BREZA, M. *Collect. Czech. Chem. Commun.* **2000**, *65*, 1911.
- (24) Meguellati, K.; Ladame, S.; Spichy, M. *Dye. Pigment.* **2011**, *90* (2), 114.
- (25) Hutchison, G. R.; Ratner, M. A.; Marks, T. J. *J. Phys. Chem. A* **2002**, *106*, 10596.
- (26) Online, V. A. *Phys. Chem. Chem. Phys.* **2014**, *16*, 24853.

- (27) Finnerty, J. J.; Koch, R. *J. Phys. Chem. A* **2010**, *114*, 474.
- (28) Yang, D.; Zuccarello, G.; Mattes, B. R. *Macromolecules* **2002**, *35* (13), 5304.
- (29) Abrams, W. R.; Kallen, R. G. *J. Am. Chem. Soc.* **1976**, *98*, 7777.
- (30) Gangjee, A.; Vasudevan, A.; Queener, S. F. *J. Med. Chem.* **1997**, *40* (4), 479.

Chapter 4: DASAs covalently bound to polymers

4.1 Introduction

Photoswitches have long been of interest for their ability to alter their molecular structure and properties using only light as a stimulus. However, applications for photoswitching in an organic solvent are rather limited. In order to increase the utility of photoswitches, integration into materials such as polymers is critical, and polymer bound photoswitches have been the subject of extensive study. A number of applications of polymer bound photoswitches have been developed, including reversible gel formation¹, drug delivery²⁻⁵, and mechanochemistry⁶⁻⁸.

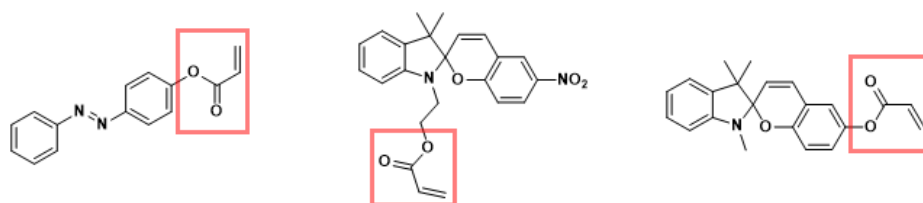


Figure 4.1: Acrylate functionalization of azobenzene and spiropyran photoswitches. The acrylate group is highlighted with a red box.

Most commonly, photoswitches are incorporated into polymers through co-polymerization. Photoswitches are functionalized with a monomer-like functional group which is then mixed with unmodified monomer and polymerized. Acrylate groups are widely used to functionalize photoswitches for use in co-polymerizations. Several examples of acrylate functionalized photoswitches are shown in figure 4.1. Generally, a hydroxyl functionalized photoswitch is acylated with (meth)acryloyl chloride in the presence of trimethylamine as a base. This technique has proven successful with both azobenzene⁹ and spiropyran.^{10,11} Acylation provides a versatile and reliable way of incorporating

photoswitches into polymers. Photoswitches have also been incorporated into polymers through ring opening metathesis,^{12,13} ring opening polymerization,¹⁴ cross coupling polymerization,¹⁵ and polyurethanes.¹⁶

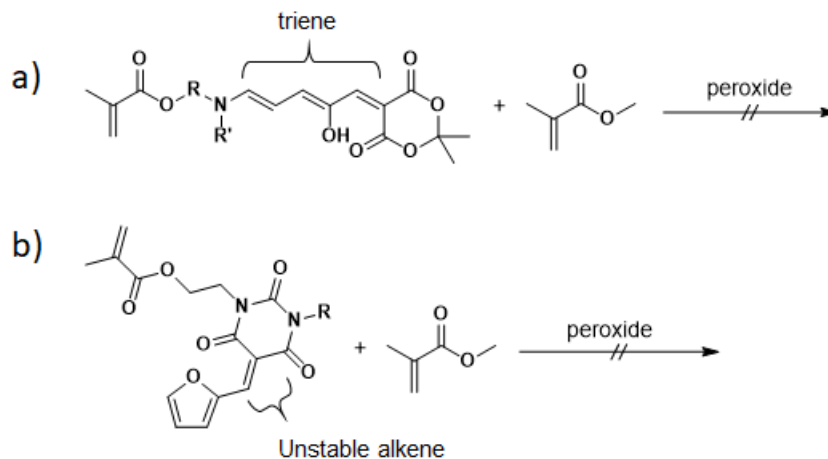


Figure 4.2: Attempts to co-polymerize DASA with acrylates. (a) Unstable triene degrades in radical conditions. (b) Unstable alkene degrades in polymerization conditions.

In effort to expand the utility of DASA in materials, we sought to incorporate DASA into acrylate polymers. We first attempted to polymerize acrylate functionalized DASA as a co-monomer with methyl methacrylate using benzoyl peroxide and *N,N*-dimethylaniline (Figure 4.2). Unfortunately, the highly conjugated triene backbone was rapidly destroyed by the polymerization conditions. If enough DASA was added, some color could be retained. However, upon photoswitching, the polymer would show brown from the decomposition rather than clear. Some success was had using the ATRP conditions shown in chapter 2, likely because the copper causes the DASA to cyclize into the closed form. However, we had difficulty synthesizing and purifying the aniline DASA with the isobutyl bromide group.

We attempted to incorporate the furan adduct into the polymer, which could subsequently be reacted with an amine to form a DASA. This reaction also failed, as the furan adduct methylene is highly reactive to radical conditions (Figure 4.2b).

Clearly, it would be ideal to avoid exposing the DASA to radical polymerization conditions. Fortunately, a variety of post-functionalization techniques exist to conjugate molecules onto existing polymers. Conjugation reactions generally involve the use of mild and highly orthogonal reaction conditions. Many of these have even been used with photoswitches, such as epoxide ring opening,¹² DCC coupling reactions,¹⁷ and pentafluorophenyl esters.^{18,19} In particular, the use of pentafluoro ester post-functionalization attracted our attention.

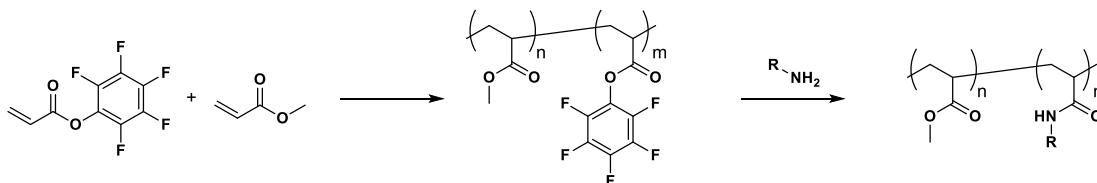


Figure 4.3: Pentafluorophenyl ester conjugation chemistry. The reaction is highly selective to primary amines.

Pentafluorophenyl acrylate (PFA) or pentafluorophenyl methacrylate (PFPMA) monomers can be co-polymerized with standard acrylate monomers to make a co-polymer. The pentafluorophenyl esters can then be reacted with primary amines to displace pentafluorophenol and create an amide. This reaction occurs with high selectivity, even over secondary and other amines.²⁰ We hoped that pentafluorophenyl ester chemistry would allow us to take advantage of the versatile nature of DASAs through a modular synthetic approach.²¹

4.2 DASA polymer synthetic approach

Our general strategy is shown in figure 4.4. First, monomers of acrylate and PFPA are co-polymerized at the desired ratio to give us polymer with pentafluorophenol ester functionality. Next, a molecule containing a primary amine and a secondary aniline are reacted with the polymer. The high degree of selectivity of pentafluorophenyl esters for primary amines would give us a polymer with free anilines. This was a key step, as it allows us to functionalize one large batch of PFP polymer with a variety of different anilines. Finally, this polymer would be dissolved in a solution containing furan adduct to yield our desired DASA polymer. This final step further increases the modularity of this approach as different furan adducts can be combined with one batch of amine polymer.

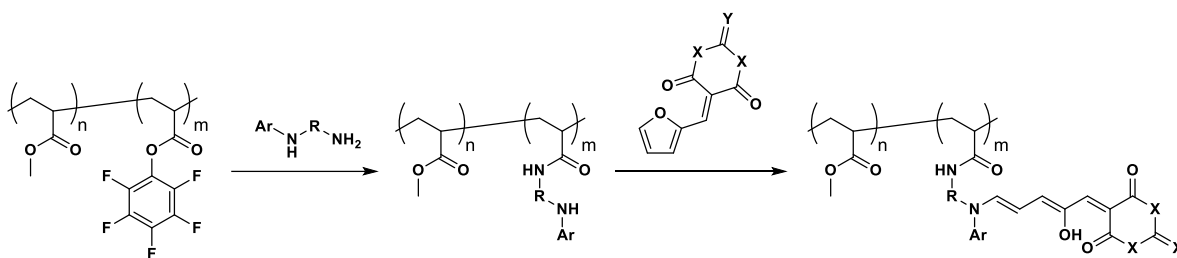


Figure 4.4: General scheme of polymer bound DASA synthesis. First, primary amine functionalized aniline is reacted with the polymer. The aniline functionalized polymer then reacts with a furan adduct to yield DASA.

We began by synthesizing PFP polymers. Pentafluorophenyl acrylate was synthesized from pentafluorophenyl and acryloyl chloride using trimethylamine as a base.²² The synthesis easily provides gram scales of monomer in high yield with simple purification. Pentafluorophenyl methacrylate was purchased from commercial sources, but it could be made in a way analogous to PFP acrylate. Then we performed simple free radical polymerizations to synthesize pentafluorophenyl ester polymers. Typically, we aimed for

around 4 mol % of pentafluorophenol incorporation. The actual amount of PFP incorporation could be verified by using ^{19}F NMR with pentafluorophenol as an internal standard. Due to the highly hydrophobic nature of the polymer, the polymerizations could be easily purified by precipitating into methanol.

4.3 Small molecule synthesis

Next we synthesized two primary amine-aniline molecules for conjugation with the polymer. We sought to use two amines that would give us different wavelength DASAs, but still give us good reaction rates. We chose to pursue a *p*-methoxy-*N*-methylaniline derivative and an indoline derivative, as they were both relatively reactive anilines and give good wavelength separation.²³ We chose to use *N*-(4-methoxyphenyl)-1,3-diaminopropane (MPDP) for the *p*-methoxy-*N*-methylaniline analogue. This was synthesized in one step through a Buchwald coupling of 1,3-diaminopropane and 4-iodoanisole (Figure 4.5a).²⁴ The reaction was performed rapidly at gram scale in good yield.

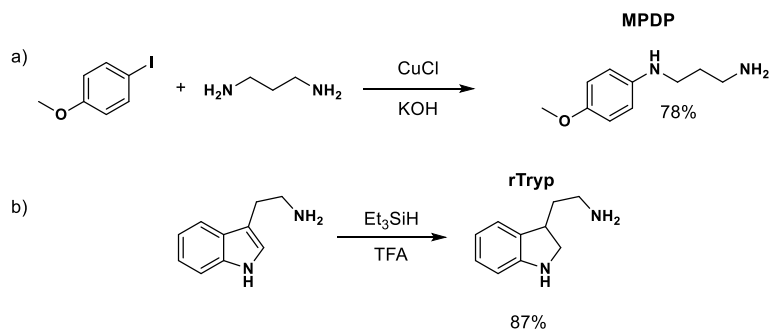


Figure 4.5: Synthesis of primary amine functionalized anilines: a) solvent free Buchwald coupling to give MPDP b) triethylsilane reduction of tryptamine

To give an additional wavelength, we sought the simplest indoline we could that had a primary amine functionality. We noticed that through a reduction of the indole in the alkaloid tryptamine, we could yield an indoline with a primary amine (rTryp). This reduction

proved more challenging than we initially had expected. Conditions using THF led to polymerization of the solvent and loss of all product. The polarity of the final product made chromatography very difficult, so the reaction needed to proceed cleanly with complete consumption of the starting material. Finally we settled on the conditions outlined by Somei using TFA and triethyl silane.²⁵ This gave us the desired indolines rTryp in good yield (Figure 4.5b). rTryp is a sensitive compound and can decompose quite easily, so care must be taken to store it in the freezer.

4.4 Polymer functionalization

With pentafluorophenyl ester functionalized polymer and primary amine functionalized anilines in hand, we set out to make the aniline functionalization conditions. To minimize the chance of an aniline reacting with an ester, we used an excess of the amine so that plenty of primary amine would always be in solution. We also added trimethylamine to soak up the pentafluorophenyl that was generated.

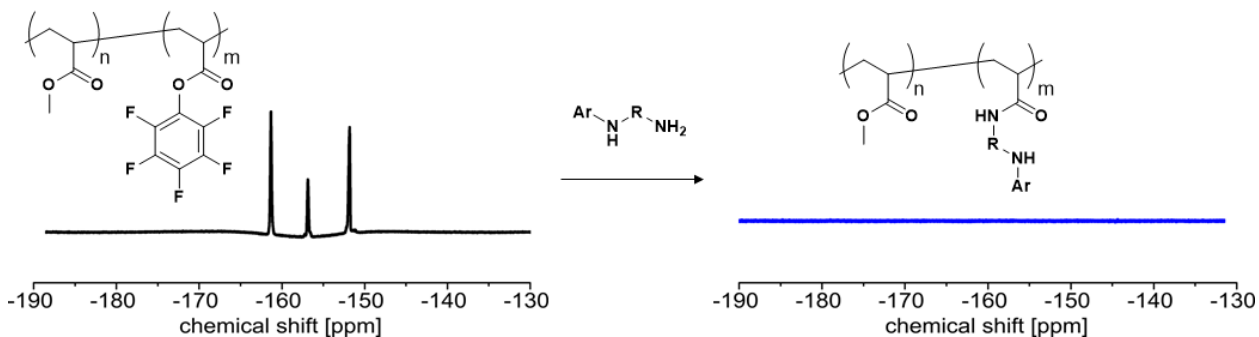


Figure 4.6: Monitoring the displacement of pentafluorophenol by ¹⁹F NMR. Adapted with permission from (21). Copyright (2017) American Chemical Society.

This reaction could be easily and accurately monitored through ¹⁹F NMR (Figure 4.6). The ¹⁹F NMR spectra showed distinct signals for free pentafluorophenol and pentafluorophenyl ester. Interestingly, the reaction rates of PFPA and PFPMA esters are very

different. While the PFPA reaction is finished in under an hour at room temperature, the PFPMA reaction can take over a day at 40°C. This is due to the increased steric hindrance of the additional methyl group. Upon completion, the reaction mixture was twice precipitated into a cold solution of 5:1 methanol:water with a few drops of ammonia added. Due to the added polarity of the amines, the addition of water was essential to maintain acceptable yields.

It should be noted that while the reaction of the MPDP with the pentafluorophenyl copolymer proceeded smoothly, the reaction with rTryp proved to be much more difficult. If slight excess of amine was used as in the MPDP case, the final polymer would crosslink after purification. Therefore, a very large excess of rTryp was used to minimize this problem. Still, the rTryp polymer should be kept in the freezer at all times.

To synthesize the DASA on the polymer, the amine functionalized polymer was simply dissolved in THF and furan adduct was added. Reaction progress could be monitored with UV/Vis spectroscopy by taking out a small aliquot and diluting it into a solution with a measureable absorbance. Unfortunately, the reduced reactivity of the aniline DASAs mean that the reactions could be extremely slow. We quickly discovered that by using minimal solvent and a large amount of furan adduct, the reactions could be completed in a few days. The diethyl barbituric acid furan adduct used in previous DASA studies was hampered by its low solubility. In order to increase the speed of the reaction, the barbituric acid furan adduct would have to be made more soluble. This was achieved by using dibutyl barbituric acid. The dibutyl barbituric acid furan adduct gave good solubility in organic solvents and allowed us to load large amounts into the solvent, giving acceptable reaction times.

For unknown reasons, the reaction of the rTryp donor functionalized polymer with the barbituric acid acceptor was problematic. The reaction was the slowest of the four DASA

reactions, so it had to be left for several days. Unfortunately, the final product seemed very unstable. In many cases, the entire polymer reaction became an insoluble gel. It was impossible to extract any product from this cross-linked gel. Even when the product was isolated, it decomposed over the course of a day if left at room temperatures. The problem of the gelation was solved by using even more excess furan adduct and running the reaction 5 times more dilute. This prevented gelation during the reaction, and the product seemed more stable. Still, this polymer should be kept in the freezer to limit decomposition.

Purification of the DASA polymer was initially attempted by silica gel column chromatography. The DASA polymer had a tendency to streak heavily and there was difficulty flushing it off the column even with eluting with methylene chloride and methanol. This led to poor yields and poor separation from the furan adduct starting material. Fortunately, the solution came in the form of using size exclusion beads. The only difficulty was that the THF used as an eluent had to be distilled before use to remove the BHT inhibitor. Once clean THF was acquired, the purification was very simple. The entire reaction mixture was loaded on the column, and eluted with THF. However, it was important to only use a drip column, and not compressed air. The ease of this chromatography was enhanced by the bright yellow color of the furan adduct and the bright purple to blue color of the DASA polymer. In this way, pure polymer was obtained with near quantitative yield.

4.5 DASA polymer photoswitching properties

We first sought to illustrate the versatility of this synthesis by making a large single batch of poly(methyl acrylate) (PMA) functionalized with pentafluorophenyl acrylate. This was divided into two small batches, one of which was reacted with MPDP and the other with rTryp. Each of these polymers were further split into two groups; one to be reacted with

Meldrum's acid furan adduct, the other to be reacted with barbituric acid furan adduct. In the end, this gave us 4 different polymer with 4 separate wavelengths from a single starting polymer.

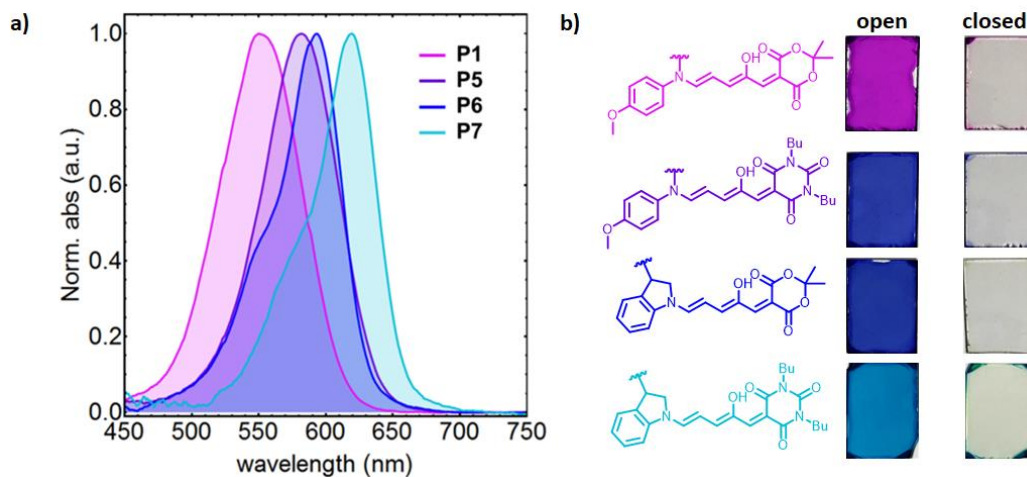


Figure 4.7: Poly methylacrylate functionalized with four different DASAs. a) UV/Vis absorption spectrum. b) Samples spun coat onto glass slides, showing both open and closed states. Adapted with permission from (21). Copyright (2017) American Chemical Society.

The wavelengths of the 4 DASA polymers is shown in figure 4.7a. The absorption wavelengths of the DASA polymers spanned from 554 nm with the MPDP/Meldrums DASA to 620 nm with the rTryp/barbituric acid DASA. To test the photoswitching of the DASA polymers we began by dissolving them in chlorobenzene. Upon light irradiation, we observed that they all cyclized into their colorless form. Next, we investigated switching in the solid polymer by spin coating each of the four polymers onto glass slides. These were then irradiated with broadband white light to achieve photoswitching and heated to return the color (Figure 4.7b).

During our photoswitching studies we observed that photocyclization of the DASA polymers was slower in the solid than in solution. In order to understand why this occurred,

we began to investigate the influence of the glass transition temperature of the polymer on photoswitching. We synthesized 3 polymers of varying T_g 's and functionalized each with MPDP donor and Meldrum's acceptor. The polymers were chosen by the T_g of their homopolymer to give a range of glass transition temperatures around room temperature. The polymers used were: poly(ethyl methacrylate) ($T_g = 65^\circ\text{C}$), poly(propyl methacrylate) ($T_g = 35^\circ\text{C}$), and poly(butyl methacrylate) ($T_g = 20^\circ\text{C}$).²⁶

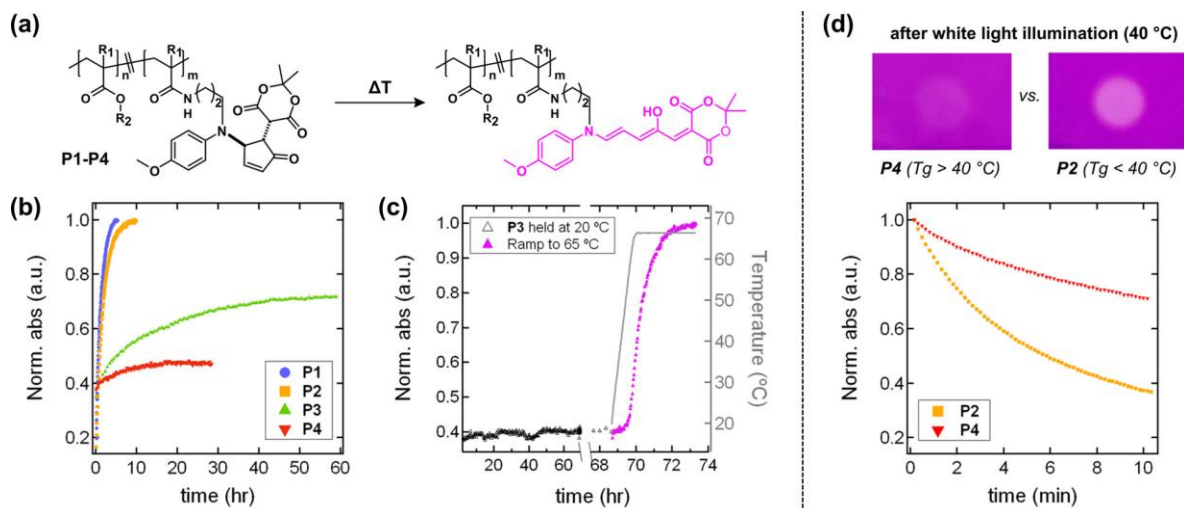


Figure 4.8: Matrix T_g effects on DASA switching. (a) Structures of the open and closed DASA functionalized polymers. (b) Thermal equilibrium at 40°C , showing faster equilibration for DASAs with polymer T_g below 40°C . (c) DASA/poly(ethyl methacrylate) (parent $T_g=65^\circ\text{C}$) being heated to 60°C , showing a rapid absorption increase on heating. (d) Effect of T_g on photocyclization. DASA polymers at temperatures below their parent T_g are slower to photocyclize. Adapted with permission from (21). Copyright (2017) American Chemical Society.

To study the effect of matrix T_g , each of the polymers were spun coat onto a glass slide. Then each polymer was brought above its parent polymer T_g and irradiated with white light to push the DASA into the colorless form. Then each sample was cooled to 40°C , and

the thermal isomerization back to the colored state was monitored by UV/Vis absorption spectroscopy (Figure 4.8b). The DASA polymers with parent polymer T_g 's below 40°C returned to equilibrium after a couple of hours. DASA polymers with parent polymer T_g 's above 40°C did not reach equilibrium even after 24 hours. The effect of T_g was further shown by photoisomerizing the poly(propyl methacrylate) ($T_g = 35^\circ\text{C}$) to the cyclized form, and leaving it at room temperature for a time, and then heating it to 65°C (Figure 4.8c). Almost no change in absorbance was seen while the polymer was kept at room temperature, while rapid isomerization was observed during heating. The matrix effect also holds for photocyclization (Figure 4.8d). Two DASA polymers with different T_g 's were heated to 40°C and irradiated with white light. The polymer with the lower T_g photoisomerized much more rapidly than the one with the higher T_g . These results give strong evidence that isomerization rates of DASAs covalently bound to polymers are heavily dependent on the T_g 's of those polymers.

Varying DASA absorption provides an alternative tunable handle that allows for selective switching. As demonstrated earlier, modifying the donor and acceptor components provided MPDP/Meldrums polymer and rTryp/barbituric acid polymer, which have little absorption overlap at ~620 nm. Blending the two copolymers and casting a uniform thin film leads to a linear combination of absorption profiles, as shown in figure 4.9a. Significantly, irradiating the film with orange light ($\lambda_{\text{max}} = 617 \text{ nm}$) gives rise to a rapid decrease in absorption for the low energy peak that corresponds to rTryp/barbituric acid polymer, leaving behind MPDP/Meldrums DASA in its colored state (Figure 4.8a). This has potential applications in rewriteable data storage that extends beyond binary coding given the system's reversible switchability and selectivity. As a demonstration, the blended polymer film was irradiated through a photomask with white light, switching both DASA components to their

colorless state (Figure 4.8b). Subsequent irradiation with orange light through an alternate photomask selectively switches rTryp/barbituric acid polymer, providing a ternary pattern containing three states: both colored, purple; both bleached, colorless; and MPDP/Meldrums colored/ rTryp/barbituric colorless, pink. The pattern can then be completely erased through heating the sample above T_g , returning the film to the full colored state. This efficient pattern transfer is made possible by covalently binding the DASAs to polymers, since it eliminated phase separation and allows for the facile fabrication of uniform films.

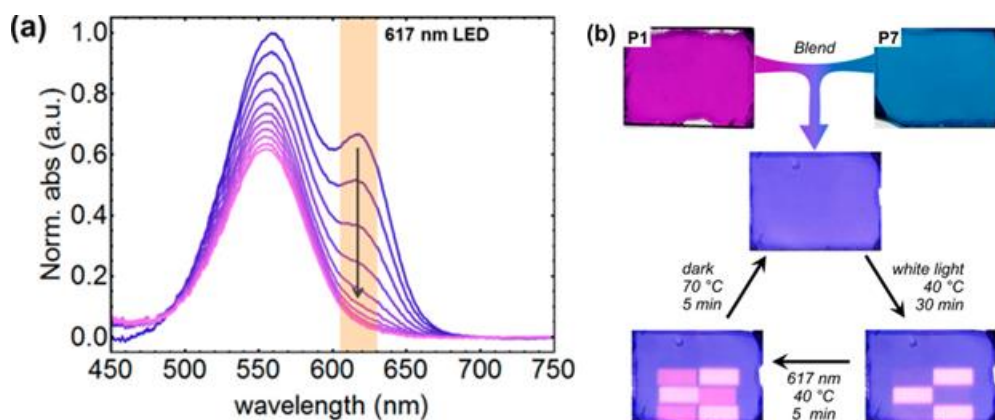


Figure 4.9: (a) Selective cyclization of rTryp/barbituric acid polymer with 617 nm light. (b) Selective switching of rTryp/barbituric, then both rTryp/barbituric and MPDP/Meldrum's polymer with spatial control using a photomask. Adapted with permission from (21). Copyright (2017) American Chemical Society.

In conclusion, we have successfully synthesized polymers covalently bound to DASA in a modular approach by taking advantage of pentafluorophenyl ester post-functionalization chemistry. This modular approach has allowed us to easily create multiple different DASA polymers from a single batch of polymer containing pentafluorophenyl esters. We have shown the ability of a variety of DASA polymer to undergo photoswitching in solution as well as in the solid state. Additionally, we were able to synthesize DASA polymers of

varying T_g 's to investigate the effect of the glass transition temperature on the photoswitching process. This work will greatly expand the capabilities and potential applications of DASA photoswitches.

4.6 Experimental

General methods:

All chemicals were obtained from *Sigma Aldrich*, *TCI Europe* or *Fisher Scientific* and used without purification unless stated otherwise. Commercially obtained monomers were passed through a short plug of basic alumina before use. Anhydrous solvents were either obtained from *Sigma Aldrich* or from a solvent purification system. Size exclusion beads (Bio-Beads S-X1 Support) were obtained from *Bio-Rad Laboratories*.

The ^1H NMR spectra were recorded on a Bruker Avance III 400 NMR spectrometer, an Agilent Technologies 400 MHz, a Varian Unity Inova 500 MHz, or an Varian Unity Inova AS600 600MHz spectrometer. The ^{19}F NMR spectra were recorded on a Bruker Avance III 400 NMR spectrometer or an Agilent Technologies 400 MHz spectrometer. The ^1H NMR chemical shifts were calibrated to the resonances of chloroform at $\delta = 7.26$, the ^{19}F NMR chemical shifts were calibrated externally to the signal of CFCl_3 at 0.0 ppm. For diffusion edited ^1H NMR, a 40 % gradient was used to remove residual solvent signals. FTIR spectra were recorded either on a Perkin Elmer Spectrum 100 FT-IR Spectrometer or a Varian 640-IR FT-IR spectrometer. Dynamic scanning calorimetry (DSC) measurements were conducted on a NETZSCH DSC 214 Polyma and analyzed using NETZSCH Proteus-Thermal Analysis software. Samples were equilibrated above the T_g for several minutes, cooled down rapidly and measured at 10 K/min. Glass temperatures were determined as the middle point of the

observed transition. Details for UV-vis absorption and photoswitching measurements are presented in the respective section.

The aromatic amine precursors **MPDP** was synthesized according to a procedure described by Yin et al. The reduction of tryptamine followed a procedure by Somei et al.²⁵ The meldrum's acid based and the barbituric acid based furan adducts, **Meld** and **Barb**, were synthesized according to procedures described by Helmy et al.²⁷ For **Barb**, n-butyl isocyanate was used instead of n-octyl isocyanate. The pentafluorophenyl acrylate, **PFPA**, was synthesized according to a procedure described by Choi et al.²²

General procedure: Aromatic amine precursor conjugation

In a typical procedure for the aminolysis of copolymers of PFPMA, the polymer (1.0 g) was dissolved in 11 mL of anhydrous DMF in a round bottom flask equipped with rubber septum and magnetic stir bar. The aromatic amine precursor (1.32 mmol) and TEA (200 μ L, 2.3 mmol) were dissolved in 2 mL anhydrous DMF and added to the polymer solution. The reaction mixture was stirred at 50 °C under nitrogen atmosphere for 2-3 days until completion. For copolymers of PFPMA, typically, the polymer (1.5 g) was dissolved in 8 mL of THF in a round bottom flask equipped with rubber septum and magnetic stir bar. The DASA amine precursor (1.32 mmol) and TEA (200 μ L, 2.3 mmol) were dissolved in 2 mL THF and added to the polymer solution. The reaction mixture was stirred at 40 °C under nitrogen atmosphere for 1-2 days until completion. After the reaction was completed, the polymer was precipitated into ice cold methanol/water (5:1) with a few drops of concentrated ammonia and centrifuged. The polymer pellet was dissolved in THF and re-precipitated at least one time. Finally, the polymer was dried under vacuum. Full conversion of the PFP active ester was confirmed via ¹⁹F-NMR from the complete disappearance of the fluorine signals. Contents of aromatic amine precursor were determined by ¹H-NMR.

P(EMA-MPDP)

Aromatic amine precursor conjugation according to the general procedure, but using 1.13 g of P(EMA-PFPMA). Yield: 1.02 g of a colorless solid.. Content of aromatic amine precursor: 4.3 mol%. ¹H-NMR (400 MHz, CDCl₃) δ/ppm: 6.73 (H_{Ar,1}), 6.62 (H_{Ar,2}), 6.47-6.28 (N-H_{Amide}), 4.01 (O-CH₂-), 3.72 (O-Me_{Ar}), 3.56 (N-H_{Amine}), 3.28 (CH_{2, Amine}), 3.14 (CH_{2, Amine}), 2.21-0.63 (polymer backbone). FT-IR (ATR mode) wavenumber/cm⁻¹: 3421 (N_{Ar}-H), 1715 (C=O, ester), 1660 (C=O, amide), 1509 (N-H, amide). GPC: M_n = 31.3 kDa, PDI = 1.6.

P(PMA-MPDP)

Aromatic amine precursor conjugation according to the general procedure. Yield: 0.540 g of a colorless solid. Content of aromatic amine precursor: 8.0 mol%. ¹H-NMR (400 MHz, CDCl₃) δ/ppm: 6.76 (H_{Ar,1}), 6.62 (H_{Ar,2}), 6.47-6.28 (N-H_{Amide}), 4.01 (O-CH₂-), 3.72 (O-Me_{Ar}), 3.56 (N-H_{Amine}), 3.28 (CH_{2, Amine}), 3.14 (CH_{2, Amine}), 2.18-0.62 (polymer backbone). FT-IR (ATR mode) wavenumber/cm⁻¹: 3406 (N_{Ar}-H), 1717 (C=O, ester), 1660 (C=O, amide), 1509 (N-H, amide). GPC: M_n = 24.0 kDa, PDI = 1.9.

P(BMA-MPDP)

Aromatic amine precursor conjugation according to the general procedure. Yield: 0.980 g of a colorless solid. Content of aromatic amine precursor: 3.9 mol%. ¹H-NMR (400 MHz, CDCl₃) δ/ppm: 6.77 (H_{Ar,1}), 6.62 (H_{Ar,2}), 6.43-6.20 (N-H_{Amide}), 3.92 (O-CH₂-), 3.73 (O-Me_{Ar}), 3.56 (N-H_{Amine}), 3.29 (CH_{2, Amine}), 3.15 (CH_{2, Amine}), 2.21-0.60 (polymer backbone). FT-IR (ATR mode) wavenumber/cm⁻¹: 3422 (N_{Ar}-H), 1717 (C=O, ester), 1656 (C=O, amide), 1510 (N-H, amide). GPC: M_n = 22.3 kDa, PDI = 2.3.

P(MA-MPDP)

Aromatic amine precursor conjugation according to the general procedure. Yield: 1.01 g of colorless rubbery solid. Content of aromatic amine precursor: 3.9 mol%. ¹H-NMR (400 MHz, CDCl₃) δ/ppm: 6.75 (H_{Ar,1}), 6.59 (H_{Ar,2}), 6.19 (N-H_{Amide}), 3.72 (O-Me_{Ar}), 3.64 (O-Me), 3.13 (CH_{2, Amine}), 2.50-1.25 (polymer backbone). FT-IR (ATR mode) wavenumber/cm⁻¹: 3387

(N-H), 1726 (C=O, methyl ester), 1671 (C=O, amide), 1513 (N-H, amide). GPC: $M_n = 38.6$ kDa, PDI = 2.7.

P(MA-rTryp)

Aromatic amine precursor conjugation according to the general procedure, but with 1.4 g of P(MA-**PFPA**). Yields 1.10 grams of colorless rubbery solid. Content of aromatic amine precursor: 3.1 mol%. $^1\text{H-NMR}$ (400 MHz, CDCl_3) δ/ppm : 7.10 ($\text{H}_{\text{Ar},1}$), 7.01 ($\text{H}_{\text{Ar},2}$), 6.70 ($\text{H}_{\text{Ar},3}$), 6.63 ($\text{H}_{\text{Ar},4}$), 6.09 ($\text{N-H}_{\text{Amide}}$), 3.66 (O-Me), 3.65-3.21 (2 x $\text{CH}_2_{\text{Amine}}$), 2.63-1.22 (polymer backbone). GPC: $M_n = 36.0$ kDa, PDI = 3.3.

Quantification of amine content:

The content of monomer units modified with the aromatic amine precursor was calculated from $^1\text{H-NMR}$ by comparing integrals for peaks in the aromatic region with the methoxy group of the acrylate co-monomer or the O-methylene for methacrylate copolymers, here shown for **PMA** copolymers.

$$\text{mol}\%_{\text{DP}} = \frac{\text{Int}_{\text{DP}}}{\text{Int}_{\text{OMe}} + \text{Int}_{\text{DP}}}$$

Here, $\text{mol}\%_{\text{DP}}$ stands for the mol% of aromatic amine precursor in the polymer, with Int_{DP} and Int_{OMe} as the values from integration of the $^1\text{H-NMR}$ spectrum. All values are divided by the number of protons per peak.

Copolymers conjugated to aromatic amine precursors.

Sample	Aromatic amine precursor	mol% Aromatic amine precursor^a	M_n (kDa)^b	PDI^b
P(MA- MPDP)	MPDP	3.9	38.6	2.7
P(MA- rTryp)	rTryp	3.1	36.0	3.3
P(EMA- MPDP)	MPDP	4.3	31.3	1.6
P(PMA- MPDP)	MPDP	8.0	24.0	1.9

P(BMA- MPDP)	MPDP	3.9	22.3	2.3
-----------------	-------------	-----	------	-----

^a determined by ¹H-NMR, ^b determined by chloroform GPC relative to linear PS standards.

DASA-polymer conjugates

General procedure: DASA functionalization of polymers

In a typical procedure, the amine functionalized polymer was dissolved in THF with the DASA acceptor precursor (200mg/mL) in a screw cap vial. The reaction proceeded at room temperature for several days without stirring and was monitored by UV-Vis spectroscopy: samples were taken, diluted in dioxane or THF and the UV-Vis absorbance was measured. The reaction was deemed complete when the value of absorbance for the DASA peak leveled off. Small increases in absorption could still occur due to THF evaporation over time. For this reason, completion of the reaction was confirmed by ¹H-NMR from the complete disappearance of aromatic amine precursor peaks in the aromatic range. The polymer was subsequently purified by size exclusion chromatography over Bio-Beads S-X1 Support with distilled THF as the eluent. The excess of activated furans could be recovered and reused after their purity had been confirmed by ¹H-NMR.

DASA-polymer conjugate P1: P(MA-MPDP-Meld)

Conversion of amine precursor to DASA according to the general procedure: P(MA-MPDP) (250 mg), Meld (500 mg, 2.25 mmol), THF (2.5 mL). Yield: 253 mg of deep purple solid.

DASA-polymer conjugate P2: P(BMA-MPDP-Meld)

Conversion of amine precursor to DASA according to the general procedure: P(BMA-MPDP) (300 mg), Meld (900 mg, 4.05 mmol), THF (3 mL). Yield: 229 mg of purple solid.

DASA-polymer conjugate P3: P(PMA-MPDP/MA)

Conversion of amine precursor to DASA according to the general procedure: P(PMA-MPDP) (300 mg), Meld (900 mg, 4.05 mmol), THF (3 mL). Yield: 245 mg of purple solid.

DASA-polymer conjugate P4: P(EMA-MPDP-Meld)

Conversion of amine precursor to DASA according to the general procedure: P(EMA-MPDP) (300 mg), **Meld** (900 mg, 4.05 mmol), THF (3 mL). Yield: 241 mg of purple solid.

DASA-polymer conjugate P5: P(MA-MPDP-Meld)

Conversion of amine precursor to DASA according to the general procedure: P(MA-MPDP) (250 mg), **Barb** (500 mg, 1.57 mmol), THF (2.5 mL). Yield: 222 g of deep blue solid.

DASA-polymer conjugate P6: P(MA-rTryp-Meld)

Conversion of amine precursor to DASA according to the general procedure: P(MA-rTryp) (300 mg), **Meld** (900 mg, 4.05 mmol), THF (3 mL). Yield: 251 mg of blue solid.

DASA-polymer conjugate P7: P(MA-rTryp-Barb)

Conversion of amine precursor to DASA according to the general procedure: P(MA-rTryp) (300 mg), **Meld** (900 mg, 4.05 mmol), THF (3 mL). Yield: 245 mg of deep blue solid.

T_g of DASA-PMA copolymers determined from DSC measurements

DASA-PMA conjugate	Glass temperature^a
MPDP-Meld	27 °C
MPDP-Barb	19 °C
rTryp-Meld	22 °C
rTryp-Barb	24 °C

^a The T_g was determined as the middle point of the observed transition

4.7 References

- (1) Wezenberg, S. J.; Croisetu, C. M.; Stuart, M. C. A.; Feringa, B. L. *Chem. Sci.* **2016**, 7 (7), 4341.
- (2) Broichhagen, J.; Frank, J. A.; Trauner, D. *Acc. Chem. Res.* **2015**, 48 (7), 1947.
- (3) Son, S.; Shin, E.; Kim, B. *Biomacromolecules* **2014**, 15, 628.
- (4) Petriashvili, G.; Devadze, L.; Zurabishvili, T.; Sepashvili, N.; Chubinidze, K. *Biomed. Opt. Express* **2016**, 7 (2), 442.
- (5) Lee, H. Il; Wu, W.; Oh, J. K.; Mueller, L.; Sherwood, G.; Peteanu, L.; Kowalewski, T.; Matyjaszewski, K. *Angew. Chemie - Int. Ed.* **2007**, 46 (14), 2453.
- (6) Hickenboth, C. R.; Moore, J. S.; White, S. R.; Sottos, N. R.; Baudry, J.; Wilson, S. R. *Nature* **2007**, 446 (7134), 423.
- (7) Davis, D. A.; Hamilton, A.; Yang, J.; Cremar, L. D.; Van Gough, D.; Potisek, S. L.; Ong, M. T.; Braun, P. V.; Martínez, T. J.; White, S. R.; Moore, J. S.; Sottos, N. R. *Nature* **2009**, 459 (7243), 68.
- (8) O'Bryan, G.; Wong, B. M.; McElhanon, J. R. *ACS Appl. Mater. Interfaces* **2010**, 2 (6), 1594.
- (9) Abrakhi, S.; Peralta, S.; Fichet, O.; Teyssié, D.; Cantin, S. *Langmuir* **2013**, 29 (30), 9499.
- (10) Abdollahi, A.; Mahdavian, A. R.; Salehi-Mobarakeh, H. *Langmuir* **2015**, 31 (39), 10672.
- (11) Suzuki, T.; Kato, T.; Shinozaki, H. *Chem Comm* **2004**, 2 (C), 2036.
- (12) Samanta, S.; Locklin, J. *Langmuir* **2008**, 24 (16), 9558.
- (13) Haque, H. A.; Kakehi, S.; Hara, M.; Nagano, S.; Seki, T. *Langmuir* **2013**, 29 (25),

7571.

- (14) Zhu, M. Q.; Zhang, G. F.; Hu, Z.; Aldred, M. P.; Li, C.; Gong, W. L.; Chen, T.; Huang, Z. L.; Liu, S. *Macromolecules* **2014**, *47* (5), 1543.
- (15) Sommer, M.; Komber, H. 57.
- (16) Lee, C. K.; Beiermann, B. A.; Silberstein, M. N.; Wang, J.; Moore, J. S.; Sottos, N. R.; Braun, P. V. *Macromolecules* **2013**, *46* (10), 3746.
- (17) Schöller, K.; Küpfer, S.; Baumann, L.; Hoyer, P. M.; De Courten, D.; Rossi, R. M.; Vetushka, A.; Wolf, M.; Bruns, N.; Scherer, L. J. *Adv. Funct. Mater.* **2014**, *24* (33), 5194.
- (18) Jo, H.; Haberkorn, N.; Pan, J. A.; Vakili, M.; Nielsch, K.; Theato, P. *Langmuir* **2016**, *32* (25), 6437.
- (19) Kessler, D.; Jochum, F. D.; Choi, J.; Char, K.; Theato, P. *ACS Appl. Mater. Interfaces* **2011**, *3* (2), 124.
- (20) Eberhardt, M.; Mruk, R.; Zentel, R.; Théato, P. *Eur. Polym. J.* **2005**, *41* (7), 1569.
- (21) Ulrich, S.; Hemmer, J. R.; Page, Z. A.; Dolinski, N. D.; Rifaie-Graham, O.; Bruns, N.; Hawker, C. J.; Boesel, L. F.; Read De Alaniz, J. *ACS Macro Lett.* **2017**, *6* (7), 738.
- (22) Choi, J.; Schattling, P.; Jochum, F. D.; Pyun, J.; Char, K.; Theato, P. *J. Polym. Sci. Part A Polym. Chem.* **2012**, *50* (19), 4010.
- (23) Hemmer, J. R.; Poelma, S. O.; Treat, N.; Page, Z. A.; Dolinski, N. D.; Diaz, Y. J.; Tomlinson, W.; Clark, K. D.; Hooper, J. P.; Hawker, C.; Read De Alaniz, J. *J. Am. Chem. Soc.* **2016**, *138* (42), 13960.
- (24) Yin, H.; Jin, M.; Chen, W.; Chen, C.; Zheng, L.; Wei, P.; Han, S. *Tetrahedron Lett.* **2012**, *53* (10), 1265.
- (25) Somei, M.; Yamada, F.; Shinmyo, D.; Nakajou, M. *Heterocycles* **2012**, *86* (1), 435.

- (26) Wood, L. A. *J. Polym. Sci.* **1958**, 28 (117), 319.
- (27) Helmy, S.; Oh, S.; Leibfarth, F. A.; Hawker, C. J.; Read De Alaniz, J. *J. Org. Chem.* **2014**, 79 (23), 11316.

Chapter 5: Novel acceptors for DASAs

5.1 Introduction

In Chapter 1 and 3 of this document, we have shown the motivation for studying the visible light photoswitches was driven by the desire to have avoid the use of UV light, which can be damaging and has little penetration through polymers or biological tissue. We have introduced donor acceptor Stenhouse adducts (DASAs) as a privileged class of negative photoswitch. The DASA consists of a donor amine, a conjugated backbone, and an electron withdrawing acceptor group (Figure 5.1). They are synthesized by combining the Knoevenagel adduct of furfural and a carbon acid with a secondary amine (Chapter 1, 2, 3). DASAs go from a colored form to a colorless form with visible light, and return to a thermodynamically stable equilibrium ratio of the two forms.^{1,2}

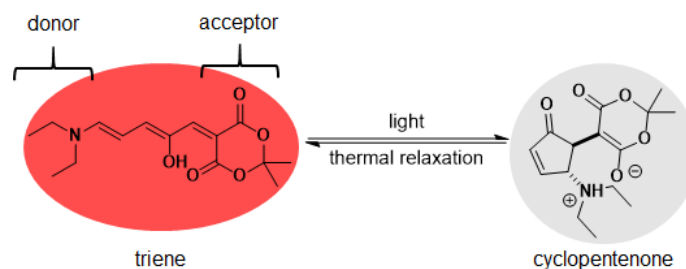


Figure 5.1: Basic structure and properties of the Donor Acceptor Stenhouse Adduct (DASA). Visible light causes the DASA to isomerize, which is followed by a cyclization to the closed form.

The first generation of DASAs used secondary alkyl amines for the donor group. However, solvent switching, absorption wavelength, and switching in a polymer were limited. In Chapter 3, we have shown that altering the structure of the donor group by using a secondary aromatic amine instead of a secondary alkyl amine provides enhanced properties.³

This second generation of DASA greatly increases the versatility and functionality of the DASA photoswitch and overcomes many of the shortcomings of the first generation DASA compounds. However, we believe that the full potential of the DASA photoswitch has not yet been realized. We aim to further improve the DASA architecture by making modification to the acceptor group.

One aspect of the aniline DASAs that is highly appealing is the ability to tune wavelength over a broad range.³ While the wavelength maxima of the DASAs can now extend up to 670 nm with a shoulder absorbing over 700 nm, reaching these long wavelengths requires the use of a very electron rich indoline donor. In Chapter 3 we discuss relationship between the basicity of the donor amine and the equilibrium open/closed ratio. The more electron rich the donor, the further in the open form the equilibrium resides, and the more difficult it is to cyclize the DASA. DASAs with equilibriums far in the open form require very non-polar solvents to photoswitch. The aniline required to achieve the 669 nm wavelength is so electron rich that photoswitching is only possible in a very non-polar mixture of toluene and hexanes. Therefore in practice, the wavelength maximum of photoswitching DASAs with good switching properties is limited to around 620 nm, using the methoxy indoline donor. This DASA absorbs a full 50 nm more in the blue than the diheptylamino indoline.

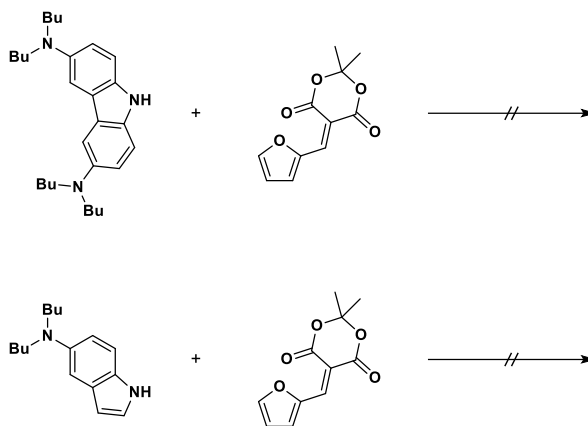


Figure 5.2. Carbazole and indole donors are unable to ring open the furan adduct.

To date, very few photoswitches are able to function with >700 nm light,⁴ so having a functional photoswitch absorbing this far in the red is still of interest. As such, we set out to further red-shift the DASA compound by modifying the structure of the donor. This effort focused on using more conjugated amines, as conjugation is known to cause a red-shift. Unfortunately, attempts to increase the wavelength while retaining good photoswitching properties by altering the donor group were met with limited success. For example, both carbazole and functionalized indole, commonly used aromatic amines, failed because they were not nucleophilic enough to ring open the activated furan and generate a DASA adduct (Figure 5.2). Due to difficulties in further increasing the wavelength through the donor group, and we began to explore modifying the acceptor group. Ideally, we could increase the wavelength of absorption through increased acceptor conjugation. Alternatively, we hypothesized that tuning the acceptor could allow the diheptylamino indoline to photoswitch efficiently in a wider range of solvents by offsetting the affects observed when using a basic amine donor.

In addition to the difficulty with photoswitching at long wavelengths, another limitation of the second generation DASA was their open closed equilibrium ratio. Most

photoswitches, such as azobenzene, discuss this in terms of the photostationary state. The photostationary state is the percentage of a photoswitch that can be converted from form **A** to form **B** with a wavelength of light, as well as the percentage that can be converted back. Typically, a good azobenzene photoswitch can achieve 70-95% conversion into the *cis* form, and a similar ratio back to the *trans* form.⁴⁻⁶ Applications of photoswitches generally rely on the change in shape, polarity, or absorption between the two forms. Therefore, the more of one form that can be converted into the other, the greater the desired effect is in the system.

DASAs are in special case, as they start as a mixture of two forms that are in equilibrium, and with light go completely into one form. In the ideal case, the DASA would start in 100% open form, and go to 100% closed form. However, this in practice is very difficult, especially with systems that have operate at higher wavelengths. To increase the percentage of open form, the basicity of the amine needs to be increased. However, this in turn makes cyclization more difficult and restricts the range of solvents that can be used for reversible switching. The reverse is true for closing, with more electron deficient donors showing more facile cyclization. While there is a certainly a balance between, the two, it would be ideal to have the best of both worlds: a long wave photoswitch that readily switches in a range of solvents completely from the open form (100% open) to the closed form (100% closed) with light. The change in equilibrium can easily be observed going from NMA, THQ, to indolines donors with barbituric acid acceptor. In these cases, the percentage in the open form are 11%, 17%, and 31% in methylene chloride, respectively (values are similar with both Meldrums and barbituric acid). This means in the NMA case, in DCM, the photoswitch goes form 11% in the open with light to ~0% in the open, or from 89% in the closed to >99% in the closed. This is a relatively small difference. For applications seeking a change in properties by increasing the amount of closed form with light, there is already a large

population of the cyclized form at equilibrium. We hope that through modification of the acceptor group, this open closed equilibrium can be increased while still retaining good solvent switching properties and wavelength tunability.

5.2 Carbon acid acceptor design

With these goals in mind, we began exploring new possible acceptors. The basic synthesis of a Meldrum's acid DASA is shown in figure 5.3a. A carbon acid is condensed with furfural, this furan ring is opened with an amine. Our first attempts centered on other relatively acidic carbon acids: malononitrile, dimedone, and diethylmalonate (Figure 5.3b). Each of these carbon acids was condensed with furfural and a yellow furan adduct was synthesized. However, when these were added to a secondary amine, no color formation resulted. Clearly, these furan adducts are not reactive enough to form DASAs.

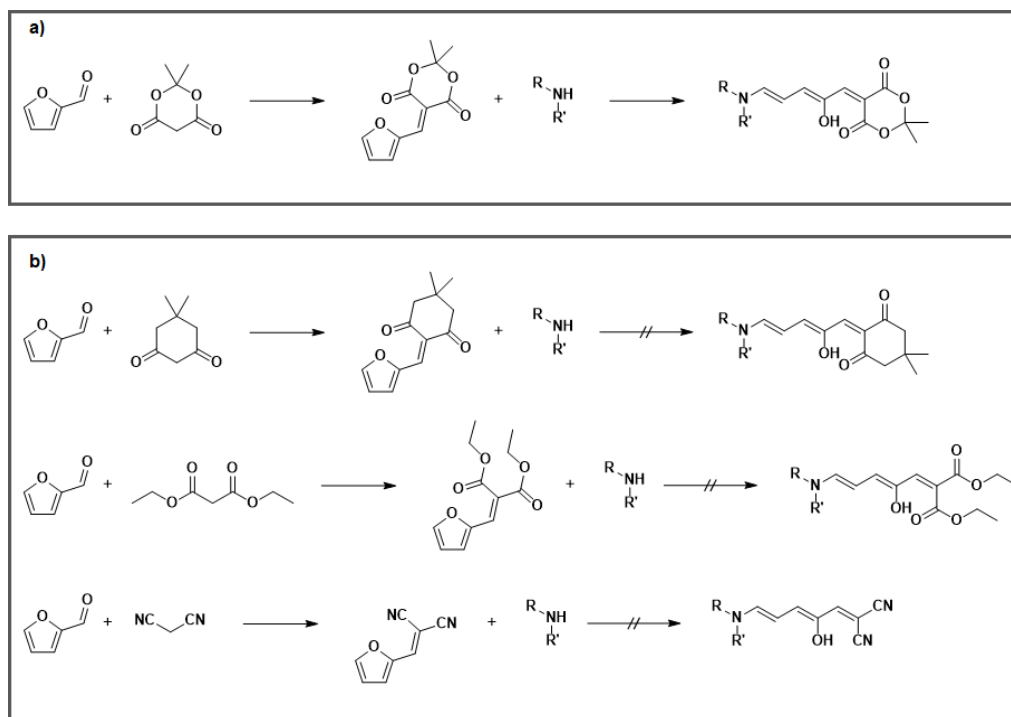


Figure 5.3: (a) A carbon acid (Meldrum's acid) is condensed with furfural to create a furan adduct. This is reacted with an amine to yield a DASA. (b) Early failed attempts at using other carbon acids.

After this setback, we sought to examine some properties of the two carbon acids that could be used to form a DASA: Meldrum's acid and barbituric acid. The most obvious common property they share is that they are very strong carbon acids (Figure 5.4). Meldrum's acid has a pKa of around 5.2⁷ in water and 7.3 in DMSO⁸, while diethyl malonate has a pKa of 4.7 in water.⁹ The DMSO acidities for dimedone, diethyl malonate, and malononitrile are 11.2, 16, and 11 respectively.¹⁰ For our next targeted acceptors, we searched the literature for compounds with pKas lower than Meldrum's or barbituric acid. We found benzoynitromethane (pKa 7.7 in DMSO¹¹), 1,3-cyclopentadione (pKa 4.5 in water¹²), and ethyl nitroacetate (pKa 5.8 in water, 9.1 in DMSO)¹³ (Figure 5.4). These compounds were synthesized into their furan adducts, and then reacted with amines.

Unfortunately, none of these derivatives gave color. This disappointing result indicated that acidity was not the only factor to consider.

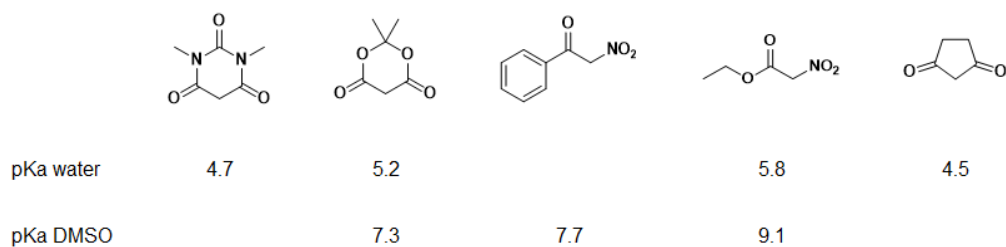


Figure 5.4: Left, Meldrum's and barbituric acid. Right, acidic acceptors that fail to produce DASAs.

While synthesizing furan adducts from new carbon acids, we found that the synthesis is not always as straightforward as stirring the carbon acids with furfural in water. This often gave incomplete reactions or no reaction at all. The reaction was further complicated by the fact that it was very common for the R_f value of the furan adduct to be the same as furfural. This makes isolation of the product of an incomplete reaction very difficult. A number of other methods of Knoevenagel condensations exist, including using $TiCl_4$,¹⁴ heating in ethanol with proline,¹⁵ and heating in acetic acid with piperidine.¹⁶ One technique that was found to be effective was to combine the furan adduct with furfural neat, then add a catalytic amount of proline. If no yellow color appeared, the reaction can be mildly heated. This nearly always brings about the condensation of a carbon acid with furfural.

5.3 Functional carbon acids

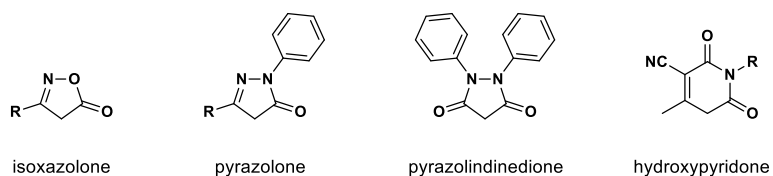


Figure 5.5: Carbon acids that can be used as acceptors to make DASAs.

After re-examining the results of the second carbon acid screen, we re-examined Meldrum's and barbituric acid. We saw that in addition to being highly acidic, the both compounds were small heterocycles, containing heteroatoms adjacent the carbonyl groups. This additional design constraint led us to several new carbon acid acceptors such as isoxazolone, pyrazolidinedione, pyrazolone, and hydroxypyridone (Figure 5.5). We combined these with furfural, and reacted them with secondary amines. Gratifyingly, these carbon acid furan adducts yielded brightly colored DASAs!

In effort to better understand how the acceptor group affected the properties of the DASA, six different carbon acids were used to synthesize their respective furan adducts (Figure 5.6). To compare the effects of the acceptor, each furan adduct was then reacted with 2-methylindoline (amine donor) to give six representative DASAs. 2-Methylindoline was used instead of indoline, as the indoline derivatives for many of these DASAs were completely insoluble. The additional methyl group reduces aggregation and increases the solubility of these DASAs.

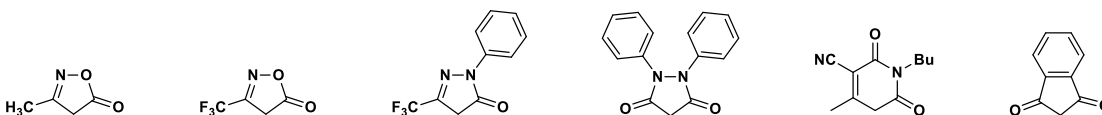


Figure 5.6: Carbon acids chosen for the acceptor study. From left to right, methyl isoxazolone, CF₃ isoxazolone, CF₃ pyrazolone, pyrazolidinedione, hydroxypyridone, and indanedione.

With carbon acid that had modifiable R groups, careful consideration was taken as to which derivatives would be synthesized. Methyl isoxazolone was chosen because it could be directly compared to the more acidic trifluoromethyl isoxazolone. In this way, the effect on altering the acidity of the furan adduct could be demonstrated. While diphenylpyrazolone

could be used to make a DASA, it showed very sluggish reactivity and difficult purification. We used trifluoromethyl phenylpyrazolone as it reacted much more readily with amines. The butyl chain on the hydroxypyridone acceptor was chosen to increase the solubility. Finally, indanedione was selected because the properties of this acceptor have not been thoroughly examined.

5.3 Characterization

We first examined the absorptions wavelengths of the new acceptors using indolines as donors. Pyrazolidinedione (614 nm) and methyl isoxazolone (616 nm) gave wavelengths very similar to barbituric acid (615 nm). Interestingly, trifluoromethyl isoxazolone (618 nm) red-shifts the wavelength only an additional 2 nm when compared to methyl isoxazolone. Clearly, the addition of additional electron withdrawing group has minimal effect on wavelength. Indandione (642 nm) gave a significant red shift in absorption compared to barbituric acid. This is consistent with what is observed with the dialkyl DASAs.² Trifluoromethyl pyrazolone gives a marked red shift compared with barbituric acid at 644 nm, with the end of the absorbance extending to 700 nm. Finally, the hydroxypyridone acceptor gives a wavelength of 675 nm. This is 60 nm red shifted compared to barbituric acid, and shows that modifying the acceptor can have a drastic effect on wavelength. This compound is even 6 nm more red-shifted than the longest wavelength second generation DASA, which used a very strong diheptylamino indole donor! Clearly, modification of the acceptor group allow for broad control of the absorption wavelength, from the Meldrum's acid absorbing at 589 nm to the hydroxypyridone at 675 nm.

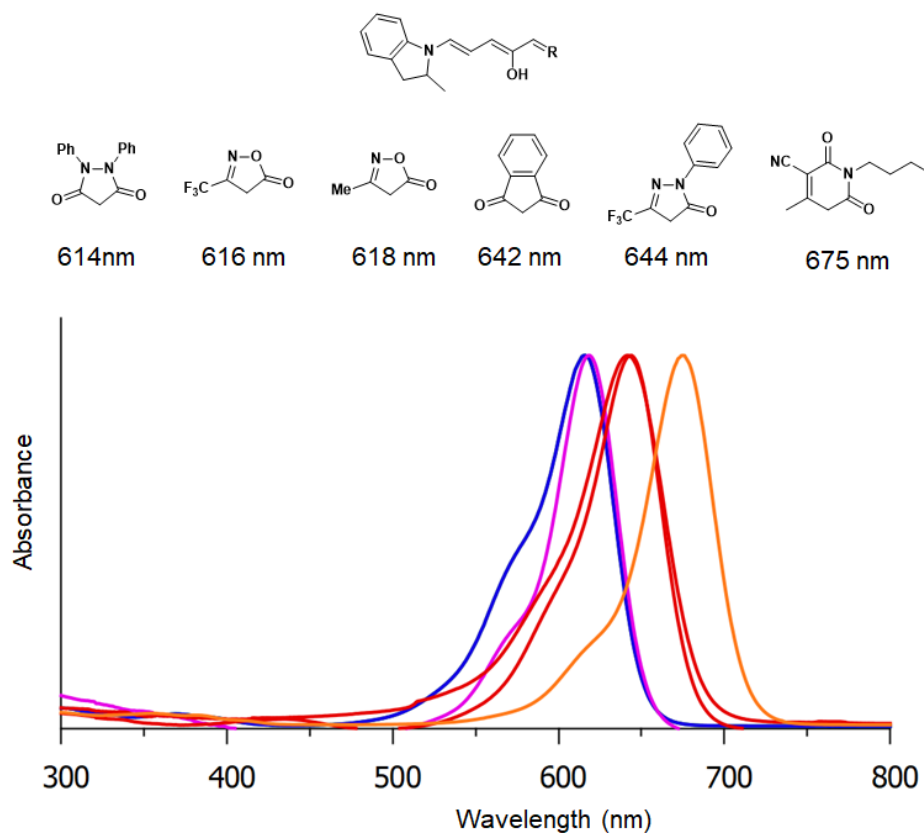


Figure 5.7: Absorption spectra of various acceptors with 2-methylindoline donor.

To examine equilibrium open closed ratios, the DASAs were placed in NMR tubes and allowed to stand in the dark. NMR spectra were periodically taken until significant changes were no longer observed. The ratio was determined using an internal standard. Figure 5.8 shows the equilibrium open percentages. Most notable is the comparison between trifluoromethyl isoxazolone and methyl isoxazolone. While trifluoromethyl isoxazolone has 100% in the open form, methyl has only 80% in the open. Both of these compounds are identical except for the added electron withdrawing nature of the fluorine atoms, compared to the protons. This shows that increasing electron withdrawing strength of the acceptor shifts the equilibrium more to the open form, which is consistent to what was observed with the

electron donating ability of the donors. This means that modification of the acceptor can be directly used as a tool to modify equilibrium open closed ratios.

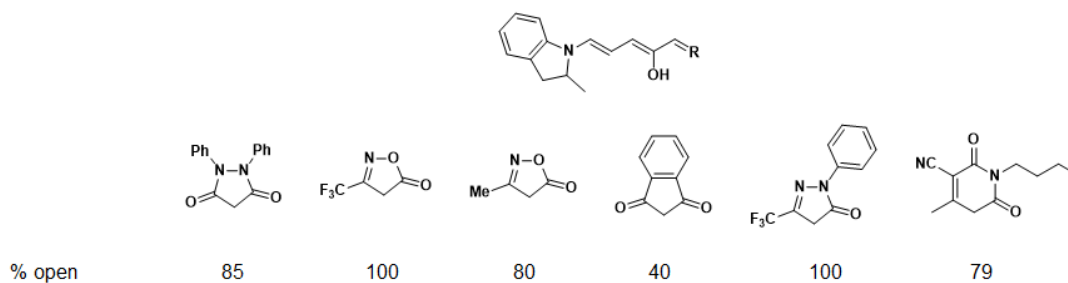


Figure 5.8: Percent open DASAs of various acceptors with 2-methylindoline donors.

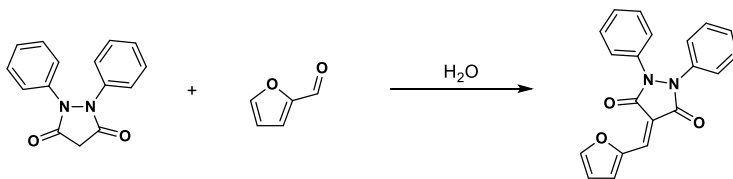
Indandione has an open ratio of 40%, indicating that significant amounts of this compound does go into the closed form. This is unexpected, as we have not yet been able to find conditions that will cause photoswitching for this compound. The hydroxypyridone acceptor gives an open ratio of 79%. Interestingly, if this compound is left in methylene chloride, the DASA crashes out in the cyclized form. Trifluoromethyl pyrazolone gives a ratio of 100% in the open form, showing that trifluoromethyl group is powerful electron withdrawing group. Pyrazolidinedione shows as open percentage of 85%.

Pyrazolidinedione (85%) and methyl isoxazolone (80%) are of particular interest when compared to barbituric acid (31%). This is significantly high open form than barbituric acid, despite the fact that the two share a similar absorption wavelength. More importantly, the methyl isoxazolone and pyrazolidinedione are able to photocyclize in solvents such as DCM, ethyl acetate, and acetone. This demonstrates that it is possible to increase the equilibrium open percentage while retaining good photoswitching properties.

In summary, we have shown that carbon acid acceptors other than Meldrum's or barbituric acid can be used to make DASA compounds. What exactly allow for the formation of DASA is not clear, but clearly high acidity and a cyclic, heteroaromatic structure are

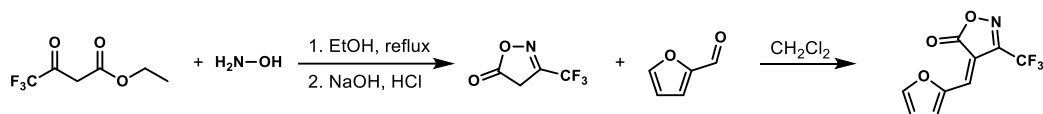
common traits of successful carbon acids. We have shown that altering the structure of the acceptor can change the absorption wavelength of the DASA over a range of 86 nm from Meldrum's to the hydroxypyridone acceptor. Finally, the equilibrium open closed ratio can be controlled through the acceptors. This allows for use DASAs that start out in the majority of the open form to go to the fully closed form. The gained understanding of these structure property relationships will help to increase the utility and practicality of DASA photoswitches.

5.4 Experimental



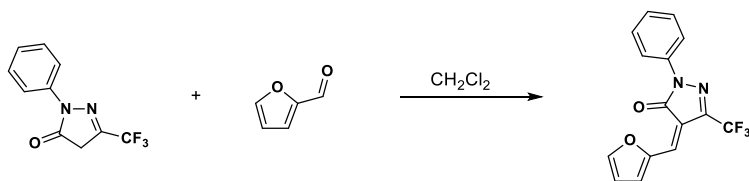
4-(furan-2-ylmethylene)-1,2-diphenylpyrazolidine-3,5-dione. Furfural (656 μ L, 7.92 mmol) and 1,2-diphenylpyrazolidine-3,5-dione (2.00 g, 7.92 mmol) were added to a flask containing 10 mL of water. The reaction was stirred rapidly, and monitored by TLC. Once the starting material was consumed, the reaction filtered, and rinsed with water. The crude product was then dissolved in ethyl acetate, washed with saturated sodium bicarbonate solution and then brine. The organic layer was then separated and dried over magnesium sulfate and filtered through a silica plug, eluting with ethyl acetate. The solvent was then removed under reduced pressure. The resulting oil was dissolved in ethyl acetate, and hexanes were added until a precipitate persisted. This was then filtered to yield an orange powder (1.0g, 38%). ¹H NMR (400 MHz, Chloroform-*d*) δ 8.67 (d, *J* = 3.8 Hz, 1H), 8.00 (s, 1H), 7.83 (d, *J* = 1.6 Hz, 1H), 7.42 (d, *J* = 8.0 Hz, 4H), 7.34 (q, *J* = 7.4 Hz, 4H), 7.18 (q, *J* =

7.3 Hz, 2H), 6.74 (dd, $J = 3.8, 1.6$ Hz, 1H). ^{13}C NMR (100 MHz, Chloroform- d) δ 163.94, 162.65, 150.89, 150.26, 136.91, 136.72, 135.60, 129.02, 129.00, 127.49, 126.62, 126.38, 122.63, 122.25, 115.29, 112.11, 77.48, 77.16, 76.84.



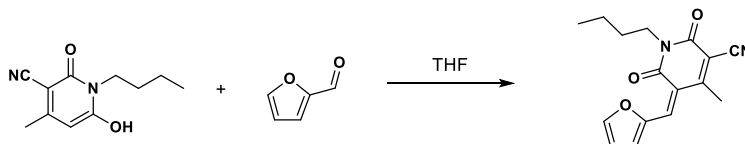
(Z)-4-(furan-2-ylmethylene)-3-(trifluoromethyl)isoxazol-5(4H)-one.

Ethyltrifluoromethylacetoacetate (2.4 g, 12 mmol) and hydroxylamine hydrochloride (1.9 g, 27 mmol) were refluxed in ethanol for 3 hours. The reaction was allowed to cool, and the solvent removed under reduced pressure. To this was added 10 mL of 4N NaOH, and that was allowed to stir for 10 minutes. This was then acidified with 1N HCl, and then the organic phase was extracted with methylene chloride. To the organic phase was then added furfural (1.76g, 18 mmol) and this was allowed to stir for about 1 hour until slightly brownish. Then water equaling 4x the amount of methylene chloride was added, and the mixture was placed under rotary evaporation to remove the DCM. The product crashed out and was filtered to give a brown solid (830 mg, 30%). ^1H NMR (500 MHz, Chloroform- d) δ 8.75 (d, $J = 4.0$ Hz, 2H), 7.95 (s, 2H), 7.73 (s, 2H).

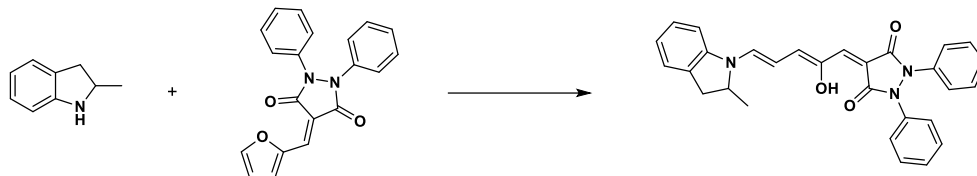


4-(furan-2-ylmethylene)-2-phenyl-5-(trifluoromethyl)-2,4-dihydro-3H-pyrazol-3-one. 2-phenyl-5-(trifluoromethyl)-2,4-dihydro-3H-pyrazol-3-one (2.00g, 8.70 mmol) and furfural (1.78g, 18.53 mmol) were combined in 20 mL methylene chloride and stirred for 2 hours. Then 60 mL of water was added, and the entire mixture was subjected to reduced pressure to remove the methylene chloride, leaving behind a solid (2.4g 89%). ^1H NMR (400

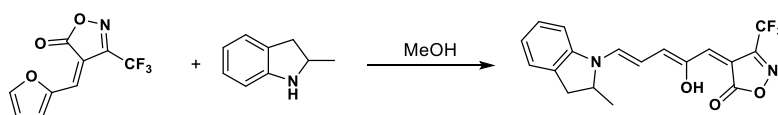
MHz, Chloroform-d) δ 8.92 (d, J = 3.9 Hz, 1H), 7.92 (d, J = 8.4 Hz, 2H), 7.88 (d, J = 1.7 Hz, 1H), 7.70 (s, 1H), 7.52 – 7.42 (t, J = 7.8 Hz, 2H), 7.29 – 7.26 (m, 1H), 6.81 (d, J = 3.6 Hz, 1H). ^{13}C NMR (125 MHz, Chloroform-d) δ 161.34, 150.76, 150.67, 139.78, 137.61, 131.57, 128.98, 127.95, 126.15, 122.17, 120.97, 119.86, 115.74, 115.62.



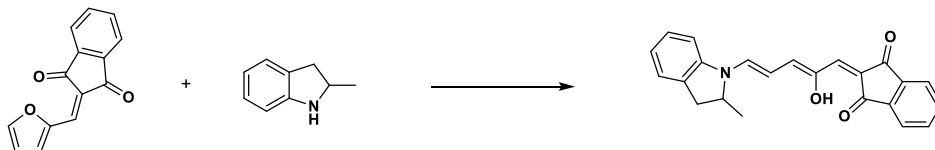
1-butyl-5-(furan-2-ylmethylene)-4-methyl-2,6-dioxo-1,2,5,6-tetrahydropyridine-3-carbonitrile. 500mg of the carbon acid was placed in a 20 mL scintillation vial and 5 mL of THF is added. The carbon acid does not completely dissolve. Then 1 mL of furfural is added and the reaction is allowed to stir. The reaction is monitored visually over the next 15-30 minutes. As the reaction progresses, the strength of the yellow color increases. Additionally, the carbon acid goes into solution. Shortly after the carbon acid goes into solution, the product begins to crash out. Once it seems most of the product has crashed out, the reaction is allowed to stand for an additional 10 minutes. After this, 10 mL of a solution of 25% water in methanol is added and the vial is shaken. This mixture is then filtered, and rinsed twice with the same methanol/water mixture to yield a yellow solid (412 mg, 60%). ^1H NMR (500 MHz, Chloroform-d) δ 8.67 (d, J = 3.9 Hz, 1H), 7.85 (d, J = 1.6 Hz, 1H), 7.67 (s, 1H), 6.77 (m, 1H), 4.01 – 3.94 (m, 2H), 2.61 (s, 3H), 1.65 – 1.54 (m, 2H), 1.38 (sext, J = 7.4 Hz, 2H), 0.95 (t, J = 7.4 Hz, 3H). ^{13}C NMR (125 MHz, Chloroform-d) δ 161.81, 160.48, 158.30, 151.51, 150.47, 136.72, 128.49, 118.83, 115.85, 114.68, 105.50, 77.41, 77.16, 76.91, 40.44, 30.00, 20.40, 19.17, 13.91.



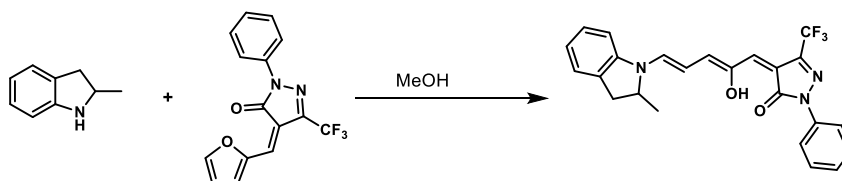
4-((2Z,4E)-2-hydroxy-5-(2-methylindolin-1-yl)penta-2,4-dien-1-ylidene)-1,2-diphenylpyrazolidine-3,5-dione. Furan adduct (200 mg, 0.61 mmol) and 2-methylindoline (80 mg, 0.61 mmol) were combined in minimal methanol. After the reaction is complete, the product is filtered to yield a blue solid (180 mg, 65%). ¹H NMR (500 MHz, Methylene Chloride-*d*₂) δ 13.17 (s, 1H), 7.98 – 7.91 (m, 2H), 7.80 (d, *J* = 12.5 Hz, 1H), 7.48 – 7.40 (m, 2H), 7.34 (t, *J* = 7.4 Hz, 2H), 7.30 – 7.16 (m, 3H), 6.85 (d, *J* = 12.3 Hz, 1H), 6.60 – 6.56 (m, 1H), 6.48 (t, *J* = 12.4 Hz, 1H), 4.81 – 4.75 (m, 1H), 3.56 (dd, *J* = 16.2, 8.7 Hz, 1H), 2.92 – 2.84 (m, 1H), 1.47 (d, *J* = 6.5 Hz, 3H). ¹³C NMR (126 MHz, Methylene Chloride-*d*₂) δ 167.46, 166.12, 144.11, 141.38, 138.28, 137.67, 137.53, 131.59, 128.59, 128.52, 128.23, 126.31, 125.89, 125.48, 125.27, 122.67, 122.31, 110.29, 103.85, 57.42, 53.85, 53.63, 53.41, 53.20, 52.98, 36.20, 19.29.



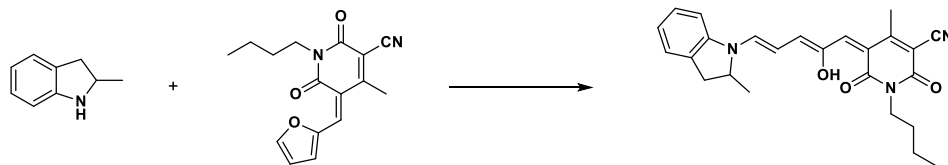
(Z)-4-((2Z,4E)-2-hydroxy-5-(2-methylindolin-1-yl)penta-2,4-dien-1-ylidene)-3-(trifluoromethyl)isoxazol-5(4H)-one. Furan adduct (200 mg, 0.86 mmol) dissolved in minimal methanol, then 2-methylindoline (114 mg, 0.86 mmol) added. The reaction was stirred for 30 minutes, then filtered to yield the product (250 mg, 80%). ¹H NMR (500 MHz, Methylene Chloride-*d*₂) δ 11.60 (s, 1H), 7.93 (d, *J* = 12.3 Hz, 1H), 7.42 – 7.34 (m, 2H), 7.33 – 7.23 (m, 2H), 6.92 (d, *J* = 12.6 Hz, 1H), 6.52 (t, *J* = 12.5 Hz, 1H), 6.34 (s, 1H), 4.82 (p, *J* = 7.1 Hz, 1H), 3.57 (dd, *J* = 16.4, 8.6 Hz, 1H), 2.95 – 2.87 (m, 1H), 1.47 (d, *J* = 6.6 Hz, 3H).



2-((2Z,4E)-2-hydroxy-5-(2-methylindolin-1-yl)penta-2,4-dien-1-ylidene)-1H-indene-1,3(2H)-dione. The indandione furan adduct (200 mg, 0.89 mmol) was dissolved in minimal methanol and 2-methyl indolines (200 mg, 0.89 mmol) was added. The reaction was allowed to stir for 3 hours and was then filtered to yield the product (44 mg, 14%). ¹H NMR (500 MHz, Methylene Chloride-*d*₂) δ 11.29 (s, 1H), 7.77 – 7.68 (m, 2H), 7.71 – 7.60 (m, 2H), 7.57 (s, 1H), 7.30 – 7.23 (m, 2H), 7.07 (t, *J* = 7.6 Hz, 2H), 6.89 (s, 1H), 6.63 (d, *J* = 11.9 Hz, 1H), 6.25 (s, 1H), 4.65 (s, 1H), 3.49 (dd, *J* = 16.1, 9.0 Hz, 1H), 2.84 – 2.76 (d, *J* = 16 Hz, 1H), 1.40 (d, *J* = 6.5 Hz, 3H).



(Z)-4-((2Z,4E)-2-hydroxy-5-(2-methylindolin-1-yl)penta-2,4-dien-1-ylidene)-2-phenyl-5-(trifluoromethyl)-2,4-dihydro-3H-pyrazol-3-one. The furan adduct (50 mg, 0.16 mmol) was stirred in methanol, then 2-methylindoline (21 mg, 0.16 mmol) was added. The product crashed out to yield (34 mg, 48%) green crystals. ¹H NMR (500 MHz, Methylene Chloride-*d*₂) δ 13.17 (s, 1H), 7.98 – 7.91 (m, 2H), 7.80 (d, *J* = 12.5 Hz, 1H), 7.48 – 7.40 (m, 2H), 7.34 (t, *J* = 7.4 Hz, 2H), 7.30 – 7.16 (m, 3H), 6.85 (d, *J* = 12.3 Hz, 1H), 6.58 (s, 1H), 6.48 (t, *J* = 12.4 Hz, 1H), 4.81 – 4.75 (m, 1H), 3.56 (dd, *J* = 16.2, 8.7 Hz, 1H), 2.88 (d, *J* = 16.3 Hz, 1H), 1.47 (d, *J* = 6.5 Hz, 3H). ¹³C NMR (126 MHz, Methylene Chloride-*d*₂) δ 150.46, 147.57, 144.56, 140.71, 138.65, 131.97, 128.64, 128.40, 126.55, 126.47, 125.50, 120.14, 106.15, 36.18, 19.48.



(Z)-1-butyl-5-((2Z,4E)-2-hydroxy-5-(2-methylindolin-1-yl)penta-2,4-dien-1-ylidene)-4-methyl-2,6-dioxo-1,2,5,6-tetrahydropyridine-3-carbonitrile. Furan adduct (100 mg, 0.352 mmol) was added to 2 mL THF, then 2-methylindoline (55 μ L, 0.422 mmol) was added. The reaction was allowed to stir until completion of starting material by TLC. The reaction was then filtered, and rinsed with diethyl ether to yield the product (76 mg, 52%). ^1H NMR (400 MHz, Chloroform-*d*) δ 13.19 (s, 1H), 7.80 (d, $J = 12.5$ Hz, 1H), 7.34 (m, 2H), 7.26 – 7.15 (m, 2H), 6.84 (d, $J = 12.4$ Hz, 1H), 6.46 (m, 2H), 4.79 (t, $J = 7.3$ Hz, 1H), 4.10 (s, 0H), 3.99 (dd, $J = 8.6, 6.5$ Hz, 2H), 3.58 (dd, $J = 16.3, 8.7$ Hz, 1H), 2.88 (d, $J = 16.2$ Hz, 1H), 2.42 (s, 3H), 1.66 – 1.54 (m, 2H), 1.48 (d, $J = 6.5$ Hz, 3H), 1.36 (h, $J = 7.4$ Hz, 2H), 0.93 (t, $J = 7.3$ Hz, 3H).

5.4 References

- (1) Helmy, S.; Leibfarth, F. A.; Oh, S.; Poelma, J. E.; Hawker, C. J.; Read De Alaniz, J. J. *Am. Chem. Soc.* **2014**, *136* (23), 8169.
- (2) Helmy, S.; Oh, S.; Leibfarth, F. A.; Hawker, C. J.; Read De Alaniz, J. J. *Org. Chem.* **2014**, *79* (23), 11316.
- (3) Hemmer, J. R.; Poelma, S. O.; Treat, N.; Page, Z. A.; Dolinski, N. D.; Diaz, Y. J.; Tomlinson, W.; Clark, K. D.; Hooper, J. P.; Hawker, C.; Read De Alaniz, J. J. *Am. Chem. Soc.* **2016**, *138* (42), 13960.
- (4) Yang, Y.; Hughes, R. P.; Aprahamian, I. *J. Am. Chem. Soc.* **2014**, *136* (38), 13190.
- (5) Dong, M.; Babalhavaeji, A.; Samanta, S.; Beharry, A. A.; Woolley, G. A. *Acc. Chem. Res.* **2015**, *48* (10), 2662.
- (6) Beharry, A. A.; Sadovski, O.; Woolley, G. A. *J. Am. Chem. Soc.* **2011**, *133* (49), 19684.
- (7) Davidson, D.; Bernhard, S. A. *J. Am. Chem. Soc.* **1948**, *70* (10), 3426.
- (8) Arnett, E. M.; Maroldo, S. G.; Schilling, S. L.; Harrelson, J. A. *J. Am. Chem. Soc.* **1984**, *106* (22), 6759.
- (9) Constants, T. I.; Acid, B. **1955**, 3.
- (10) Bordwell, F. G. *Acc. Chem. Res.* **1988**, *21* (12), 456.
- (11) Bordwell, F. G.; Van Der Puy, M.; Vanier, N. R. *J. Org. Chem.* **1976**, *41* (10), 1883.
- (12) Boothe, J. H.; Wilkinson, R. G.; Kushner, S.; Williams, J. H. *J. Am. Chem. Soc.* **1953**, *75* (7), 1732.
- (13) Goumont, R.; Magnier, E.; Kizilian, E.; Terrier, F. *J. Org. Chem.* **2003**, *68* (17), 6566.
- (14) Lehnert, W. *Tetrahedron* **1973**, *29* (4), 635.

- (15) Goswami, P.; Das, B. *Tetrahedron Lett.* **2009**, 50 (8), 897.
- (16) Nazir, R.; Thorsted, B.; Balčiūnas, E.; Mazur, L.; Deperasińska, I.; Samoć, M.; Brewer, J.; Farsari, M.; Gryko, D. T. *J. Mater. Chem. C* **2016**, 4 (1), 167.